Flying-V Family Design

W.J. Oosterom

Delft University of Technology

TU Delft

Flying-V Family Design

by

W.J. Oosterom

to obtain the degree of Master of Science
at the Delft University of Technology.
to be defended publicly on Friday April 9, 2021 at 8:45 AM.

Student number:	4463250	
Project duration:	August 24, 2020 – April 9, 2021	
Thesis committee:	Dr. ir. R. Vos,	TU Delft, supervisor
	Dr. ir. G. la Rocca,	TU Delft
	Dr. ing. S.G.P. Castro,	TU Delft

TU Delft

Abstract

The Flying-V is a novel aircraft configuration that promises a large improvement in fuel burn performance compared to conventional aircraft, integrating the passenger cabin and cargo volume into the lifting surface. The Flying-V is a V-shaped flying wing with an oval cabin and engines over the trailing edge. The aircraft does not have high-lift devices, and fins and elevons provide stability and control. The Flying-V has been studied on several aspects such as aerodynamics and structures, confirming its large potential fuel burn reduction.

This study focuses on the feasibility of developing a family of Flying-V aircraft, which is a crucial step in passenger aircraft development offering multiple aircraft variants at limited development and production cost. The ability to design a family of Flying-V aircraft can be a large advantage with respect to blended wing body designs, of which earlier research suggests that developing a family is difficult due to its lack of a constant cross-section. On a higher level, this research is one of the few focusing on family design of an unconventional aircraft configuration in the conceptual design phase.

The Flying-V family is optimised for minimal fuel burn, ensuring commonality in terms of common variables and common components between family members. Fuel burn is calculated using fuel fractions and the Breguet range equation. A vortex-lattice method is employed to study the aerodynamic characteristics of the aircraft, enhanced with a viscous module to estimate its lift-to-drag ratio. The weight of the aircraft is estimated using empirical relations, a semi-analytical oval fuselage weight estimation method and a quasi-analytical conventional aircraft wing weight estimation method. The fuel burn model is validated using the reference aircraft family, resulting in a fuel burn within 0.9% of the data provided by the aircraft manufacturer. Feasibility of the Flying-V family design is ensured by including a range of top-level aircraft requirements on payload, range, cruise speed and altitude, low-speed performance, stability and control and airport regulations. The complete model is built within a ParaPy framework, which is a Knowledge-Based Engineering environment programmed in Python. Optimisation of the Flying-V aircraft family is performed using an iterative procedure, optimising variables that describe the planform and cross-section of the aircraft. The only unique variable for each aircraft variant is the length of the untapered part of the cabin, maximising commonality in the aircraft family.

The optimised Flying-V (FV) family consists of three aircraft with a passenger capacity of 293, 328 and 361 for the FV-800, FV-900 and FV-1000 respectively. The design ranges of the Flying-V family members at maximum passenger capacity are $11.2 \cdot 10^3$ km, $14.8 \cdot 10^3$ km and $15.4 \cdot 10^3$ km. The range of the FV-800 is smaller than the other two aircraft family members because no requirement was imposed on this range, determining the range implicitly from the available fuel volume resulting from optimisation of a two-member aircraft family. The optimised design suggests a 20% and 22% lower fuel burn than the modelled reference aircraft family for the FV-900 and FV-1000 on the design mission, proving the feasibility in terms of fuel burn of a Flying-V aircraft family. The penalty in fuel burn compared to individually optimised aircraft is 8.9%, 7.1% and 4.2% for the FV-800, FV-900 and FV-1000 respectively. The takeoff mass of the Flying-V family members is $185 \cdot 10^3$ kg, $234 \cdot 10^3$ kg and $266 \cdot 10^3$ kg respectively. With respect to the modelled A350 family, this is a reduction of 17% and 15% for the -900 and -1000 variant. The approach speed of the FV-900 and FV-1000 is estimated at 136 and 137 kts, much lower than the specified approach speed of the reference aircraft of 140 and 147 kts. Besides constraints on payload and commonality, driving requirements in Flying-V family design are the shift in centre of gravity during flight, the wingspan and the fuel tank volume. Feasibility of the design is ensured by drawing a floor plan of the aircraft fitting its payload and furnishing. Additionally, a sensitivity analysis on the obtained design vector confirms its optimality.

Preface

Dear reader,

This thesis has been written in light of the final graduation project of Aerospace Engineering at Delft University of Technology. It has been exciting to work on this research on family design of the Flying-V. During my study, I have always had an interest in novel aircraft configurations, of which the Flying-V is the flagship of the aerospace department at Delft University of Technology. Aircraft family design has been a very interesting subject, integrating a variety of disciplines into one complex design problem. It was interesting to find how little is known about aircraft family design, especially for unconventional aircraft configurations, despite its rather large importance as a potential make-or-break factor for any aircraft configuration. This research is one of the few focusing on family design of an unconventional aircraft configuration in the conceptual design phase, and might be the start of more research into this interesting and crucial aspect of aircraft design. Please note that the front page image is an adapted version of a figure by Delft University of Technology[1].

I would like to thank Dr. Roelof Vos for his great support during the project, quickly understanding any challenges encountered and regularly meeting to discuss progress and difficulties. I have always enjoyed our meetings, both personally and intellectually.

Lastly, I would like to thank my roommates. De Roos van Suyd has been a very motivating working place, especially during the COVID-19 pandemic.

W.J. Oosterom
Delft, March 2021

[1] https://www.tudelft.nl/lr/flying-v/ [cited on 23-9-2020]

Contents

List of Figures

List of Tables

Nomenclature

Latin Symbols

A	area (m^2)
b	wing span (m)
b_{outer}	outer wing span (m)
c	chord length (m)
c'	normalised planform chord length (-)
C_D	drag coefficient (-)
C_f	skin friction coefficient (-)
C_L	lift coefficient (-)
C_M	pitching moment coefficient (-)
c_T	specific fuel consumption (N/N/s)
C_{L_α}	lift coefficient slope (1/rad)
C_{l_β}	lateral stability coefficient (1/rad)
$C_{L_{\alpha_v}}$	vertical surface lift slope (1/rad)
C_{n_β}	directional stability coefficient (1/rad)
D	drag force (N)
E	Young's modulus (Pa)
E	endurance (s)
f	form factor (-)
G	shear modulus (Pa)
H_1	oval crown height (m)
H_2	cabin height (m)
H_3	oval keel height (m)
I	area moment of inertia (m^4)
L	lift force (N)
L	cabin length (m)
M	Mach number (-)
M	moment (Nm)
M	pitching moment (Nm)
N	normal force (N)
q	dynamic pressure (Pa)
q	shear flow (N/m)
R	range (m)
S	wing (reference) area (m^2)
S_{wet}	wetted area (m^2)
T	thrust (N)
t	thickness (m)
V	velocity (m/s)
W	weight (N)

Greek Symbols

α	angle of attack (deg)
β	sideslip angle (rad)
λ	taper ratio (-)
ρ	density (kg/m^3)
σ	stress (Pa)

1

Introduction

Multiple sizes of one aircraft are often designed to offer a range of aircraft suitable for different missions and payloads: a family of aircraft. An example aircraft family is shown in Figure 1.1[1]. Such a family of aircraft is attractive to limit development and production costs for the manufacturer but also operational costs for an airline. Hence, the feasibility of developing a family should be studied for any new aircraft concept. One example of such a novel aircraft concept is the Flying-V, which promises a large improvement in fuel burn performance compared to conventional competitor aircraft [13]. Up till now, only one variant of the Flying-V has been studied and optimised, which is designed as a competitor to the A350-900 aircraft.

Liebeck states about the blended wing body (BWB), which is a somewhat similar aircraft configuration as the Flying-V, "commonality may be the key to provide the incentive and courage to proceed to develop this new airplane concept." ([14] p. 4) On the contrary, Mike Sinnett, at the time vice-president of Product Development and Future Airplane Development at Boeing, states that a BWB does not lend itself to a stretch or shrink. “You take the most expensive part of the airplane, the non-constant section, and growing it in a non-constant way, or shrinking it in a non-constant way. It’s really hard.”[2] Clearly, there is reason to study the feasibility of a family of Flying-V aircraft. When family design leads to unsatisfactory penalties in performance, the Flying-V concept might not be economically viable anymore.

In this study, the design of a Flying-V family is investigated and its performance is analysed and compared to the reference Airbus A350 family. A successful family design will make the Flying-V an even more promising concept with a stronger market prospect.

Figure 1.1: A350 family, figure adapted from Airbus.

1.1. Research Objective and Questions

This research aims to study the feasibility of a family of Flying-V aircraft. The main research objective is

[1] https://www.airbus.com/aircraft/passenger-aircraft/a350xwb-family [cited on 2-7-2020]

[2] https://leehamnews.com/2018/04/03/dont-look-for-commercial-bwb-airplane-any-time-soon-says-boeings-future-airplanes-head/ [cited on 12-5-2020]

to assess the fuel burn performance of a Flying-V aircraft family compared to a conventional aircraft family for a given set of top-level aircraft requirements, by designing a Flying-V aircraft family and modelling a reference conventional aircraft family.

The main research question to achieve this research objective is:

What is the fuel burn performance for a Flying-V aircraft family compared to a conventional tube-and-wing aircraft family, for a given set of top-level aircraft requirements?

The research question can be split into several sub-questions:

1. What is the fuel burn performance of a family of Flying-V aircraft with a certain level of commonality, compared to a reference conventional aircraft family?
   (a) What is the most suitable method to estimate fuel burn performance for a single Flying-V or conventional aircraft within a family design method in the conceptual design phase?
   (b) What is the level of commonality between the aircraft family members?
   (c) What is the most suitable method to design a family of Flying-V aircraft in the conceptual design phase?
2. What are the driving top-level requirements in the optimised aircraft family design?
   (a) What are the top-level requirements when optimising a family of aircraft for fuel burn performance?
   (b) What is the sensitivity of the family design optimisation to these top-level requirements?

1.2. Outline

In the following chapters, an answer to the research questions will be formed. To identify the knowledge gap filled by this research, the background and current state of the Flying-V project are described first in Chapter 2. The description of the state of the art also serves as an initial investigation of reusable research within the development of a fuel burn model. Furthermore, the motivation of developing a family of products is described, and different methods to design a family of aircraft are studied. Chapter 3 describes the experimental setup used within this research, including top-level aircraft requirements for the Flying-V family, its parametrisation and the optimisation architecture employed. Chapter 4 discussed the method to estimate fuel burn of an aircraft, including an aerodynamic analysis and weight estimation method. Verification of the described methods and validation of the results is discussed in Chapter 5. The resulting Flying-V family design is presented in Chapter 6, comparing its performance and driving requirements to the reference conventional aircraft. Chapter 7 concludes the research and discusses possible directions for future research.

2

Background

In this chapter, the state of the art of the subject of this research, the Flying-V, is investigated. The benefits and drawbacks of opting for a flying wing principle are discussed, followed by a description of the evolution of the Flying-V aircraft. Then, product family design and aircraft family design specifically are discussed in detail, identifying the knowledge gap in Flying-V family design. The ParaPy framework used in this study is shortly described, concluding with top-level requirements for the Flying-V aircraft family.

2.1. Flying Wing Principle

Since the early beginnings of powered flight, the idea of a tailless flying wing aircraft has been the subject of multiple studies. The first recorded version was the D-8 of Dunne in 1911 [15]. The Horten brothers developed a flying wing in the 1930s and 1940s, which led to the first turbojet-powered flying wing aircraft, named the Ho-IX [15]. Later, notional flying wings were developed by Northrop, such as the N-1M and N-9M small one-seaters or the later XB-35 and YB-35 heavy bomber aircraft. A well-known example of a flying wing is the B2-Spirit stealth bomber shown in Figure 2.1[1]. Probably the most influential researcher on flying wings and blended wing bodies (BWB) is Robert Liebeck. In 2004, Liebeck presented the design of a 250 and 450 passenger BWB, which has served as the starting point of many subsequent studies [1]. A notional figure of the 450 passenger version is shown in Figure 2.2.

Figure 2.1: B2-Spirit stealth bomber, obtained from XairForces.

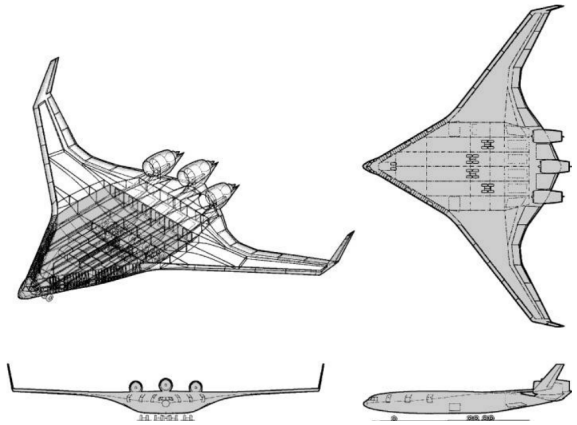

Figure 2.2: Layout of the BWB-450 concept by Liebeck [1].

Studies into the flying wing or BWB concept have revealed large potential benefits of the configuration, yet also identify large challenges. The main benefit of a BWB concept lies in the fact that one structure integrates both the structural function of accommodating the payload and the aerodynamic function of providing lift. In conventional tube-and-wing aircraft, a separate fuselage is required to accommodate the payload, resulting in a larger wetted area and increased friction drag compared to the BWB concept [15]. This also means that

[1] https://www.xairforces.com/ [cited on 20-5-2020]

the separate wing introduces large bending moments on the structure, whilst the payload can relieve this bending moment in a flying wing configuration [13]. In addition, a BWB suffers less from interference drag due to the smooth blending between its body and wing [16]. Furthermore, the shape of the BWB is more area-ruled, such that its wave drag at high velocities will also be lower than for a conventional configuration [16]. Another benefit mentioned by Chen et al. is the reduced wetted area per unit of useful volume for a BWB, such that zero-lift drag is reduced. In the end, this means that a BWB can provide a higher lift-to-drag ratio than conventional aircraft and hence has a reduced fuel burn and takeoff weight for a given amount of payload [1]. Due to a reduced fuel consumption, the BWB can also have a lower climate impact. In general, a BWB does not have a tailplane and high lift devices, such that corresponding noise is reduced. In addition, the BWB often features engines that are mounted above the wing, such that the wing will shield the engine noise from the ground. Finally, due to its simple configuration, a BWB might have a limited part count and hence reduced manufacturing costs [17]. Brown and Vos estimate a lower fuel burn per passenger kilometre of up to 30% for a long-range 250-passenger BWB compared to a conventional tube-and-wing aircraft. Although these results are provisional and may change with an increasing level of detail in the design, this potential improvement is still very promising.

Challenges that have been identified are related to stability and control, integration between the propulsion, airframe and aeroacoustic considerations and several other difficulties arising in a complex aircraft design. For instance, a difficulty in BWB design is to achieve the typical maximum of 3 deg deck angle during cruise, due to the relatively low lift curve slope [1]. The maximum lift coefficient required during landing and takeoff will therefore also impose challenges, e.g. requiring a large landing gear to allow for high angles of attack. Qin et al. find that an elliptic lift distribution is aerodynamically less efficient than an averaged elliptic-triangular lift distribution, whilst a triangular lift distribution results in the lowest structural weight [18]. This demonstrates the importance of fully studying the aerodynamic behaviour of the aircraft integrated into a multidisciplinary study. Due to the fact that the complete aircraft provides lift, the wing loading on a BWB is in general relatively low, such that takeoff and landing speeds are low and as a result the required field length is limited. However, a low wing loading means that an aircraft is more sensitive to gusts.

Structurally, the cabin of the BWB introduces large challenges. Since an aircraft cabin needs to be pressurised, a circular shape as found in conventional aircraft is beneficial. However, in a BWB design this is difficult to establish, since the blended configuration means that a laterally stretched cabin would match the outer shape better. A second challenge is that a BWB needs to be relatively large in order to have an airfoil-shaped cross-section and sufficient cabin height. This problem is recognised by Mike Sinnett, at the time vice-president of Product Development and Future Airplane Development at Boeing[2]. He states that a BWB in general has a larger wingspan and is therefore less airport compatible. He explains that span is an interesting choice for designers when there is a lot of range needed. A small span is not possible for a BWB design, since the cabin height should be sufficient. As such, BWB aircraft will only be efficient on long-range flights. Another potential setback of a BWB design mentioned by Sinnett is that it possibly cannot load and unload quickly enough, which is especially important for short flights.

Additional possible setbacks of a BWB design could be that passengers are located further away from the centre of gravity centre line of the aircraft, increasing the chances of motion sickness [19]. In addition, passengers generally like to sit at the windows, which is more difficult in a wide-cabin BWB design. Leaving the aircraft in a sufficiently short time in emergency situations might be difficult, as emergency exits are located further away from the passengers on average compared to conventional aircraft configurations.

Finally, the design of a family of BWB's could be challenging. As was already touched upon in Chapter 1, the design of a blended wing body family might mean that expensive parts of the fuselage need to be stretched, since the fuselage probably does not have a constant cross-section. Figure 2.3 visualises the common and unique components in a blended wing body design envisioned by Liebeck [14]. A T-shaped plug is used to form different blended wing body sizes, reusing the outer wing and part of the fuselage. Structurally, this is probably very challenging, especially in combination with a pressurised cabin. Unfortunately, Liebeck does not specifically address structural design challenges. Liebeck does mention an important benefit of a blended wing body family design, automatically adding wing area and span when the payload is increased. According to Liebeck, commonality in a family of two blended wing body designs can offer a 23% and 12% reduction in non-recurring and recurring cost respectively [14]. Fuel is placed by Liebeck in the outer wing, not scaling the fuel capacity with larger or smaller aircraft variants.

For a complete overview of the history and design of the BWB and its benefits and challenges, the inter-

[2] https://leehamnews.com/2018/04/03/dont-look-for-commercial-bwb-airplane-any-time-soon-says-boeings-future-airplanes-head/ [cited on 12-5-2020]

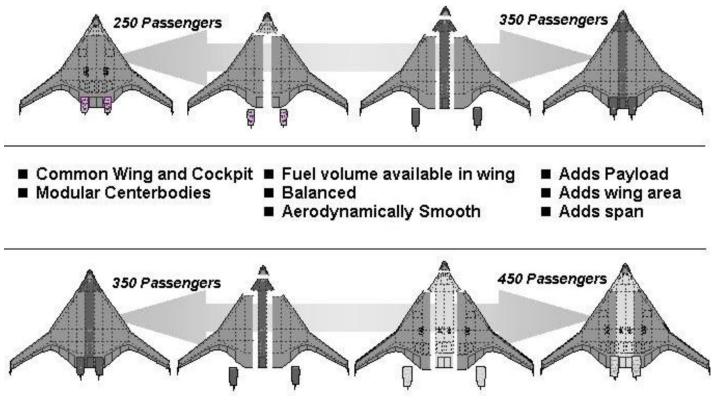

Figure 2.3: Common and unique components for a blended wing body aircraft, figure from Liebeck.

ested reader is referred to the articles by Okonkwo and Smith [15] and Chen et al. [16].

2.2. Evolution of the Flying-V

A potential solution to some of these challenges present in flying wing or blended wing body designs is the Flying-V. In this section, the chronological development of the Flying-V concept is discussed. The initial design and subsequent improvements on aerodynamic and structural design are discussed, followed by engine placement and interior design. Finally, a short overview of recent developments is presented, which is mostly focused on investigating the concept more thoroughly regarding high angle of attack performance and scaled testing.

2.2.1. Initial Design

The flying wing principle has been adopted by Benad in a joint study between the technical university of Berlin and Airbus, presented as the new aircraft configuration for commercial passenger transport [2]. In this study, the concept of a flying wing was studied by designing a competitor for the A350-900 aircraft, designing for the same cruise speed of Mach 0.85 and a payload capacity of 315 passengers and 36 LD3 containers. The result was named the Flying-V, featuring a 10% higher lift-to-drag ratio and a 2% lower operating empty weight than its direct competitor. The wingspan is comparable to the A350-900, but the aircraft is notably shorter as shown in Figure 2.4. A CAD model of the design is shown in Figure 2.5.

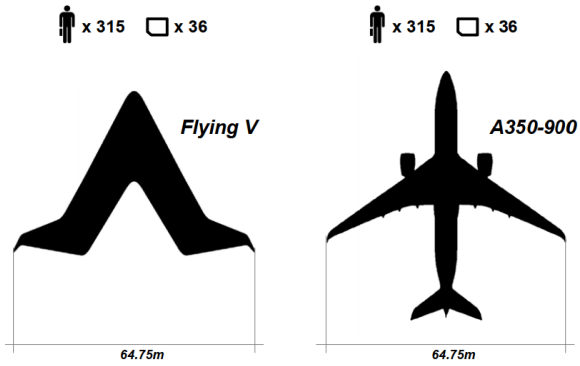

Figure 2.4: Planform of the Flying-V concept by Benad [2].

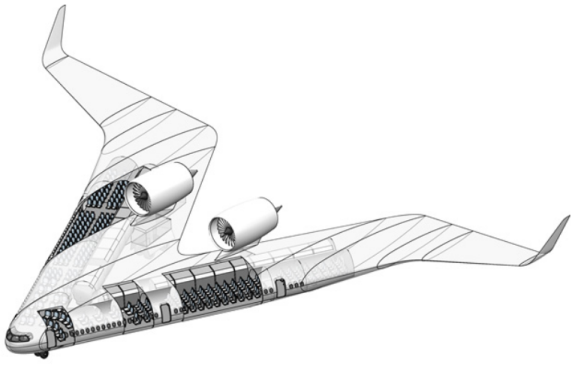

Figure 2.5: Layout of the Flying-V concept by Benad [2].

The Flying-V is a potential solution to some of the problems identified with flying wing designs as discussed in Section 2.1. One of the major problems with flying wing designs is finding an efficient way of using the volume within the wing. One solution is the blended wing body, of which was described earlier that finding a structural efficient cabin layout is hard, resulting in weight increases due to large oval or similar structures. The Flying-V copes with this by using two circular cabins, of which one is designated to cargo. By introducing sweep on these cabins, the effective cross-section in the direction of flight is oval. Achieving a

trimmed aircraft in flight for a BWB comes with a large induced drag penalty due to the short moment arm of the movables with respect to the centre of gravity. In the Flying-V configuration, this problem is solved due to the highly swept wing which has movables on the outer part of the main wing, transition wing and outer wing. Note that the centre of gravity of the Flying-V is also positioned more forward than for a BWB configuration by leaving out the 'triangle in the back' of the aircraft, effectively increasing the moment arm of the movables even more. Finally, the initial Flying-V design allows for emergency exits on both sides of the cabins, whereas the BWB does not.

The aircraft wing is designed to have an elliptical lift distribution whilst ensuring that the wing is longitudinally stable, by varying its reflexed camber lines and introducing a moderate twist [13]. Benad applies the principle of Prandtl, stating that an elliptical lift distribution is favourable to minimise induced drag [20]. Trimming is of smaller importance than on conventional aircraft, since no high lift devices are employed which in conventional aircraft create large nose-down pitching moments. The exclusion of lift devices is made possible by designing the wing to provide sufficient lift at takeoff. Benad argues that a flying wing with positive dihedral and sweep is directionally stable [13]. Lateral stability is not considered in this initial study.

The span of the passenger cabin of the Flying-V is limited to 26 m to ensure passenger comfort, which decreases towards higher spans due to larger accelerations when sitting further away from the aircraft's centre axis. This value was determined by measuring the wingspan of previous BWB concepts [13]. Benad notes that a higher aircraft efficiency is expected when this maximum span would be increased. Benad positions the neutral point and the centre of gravity halfway the passenger cabin to limit c.g. movement, by limiting the sweep of the outer wing.

Fuel is stored in the transition wing, outer wing and the centre part of the middle wing. As such, the centre of gravity should not change largely during flight. Benad notes that additional fuel tanks could be included in the outer part of the middle wing, noting that this might lead to integration difficulties with movables, cargo holds or emergency exits [13].

Additional advantages of the Flying-V layout proposed by Benad are the shielding of the engines by the wing, such that ground noise is reduced the absence of movables such as high-lift devices and the simplicity of the design regarding camber lines and twist.

Benad notes that a lot of investigations should still be performed, for example studying the nose-down pitching moment introduced by the engines during takeoff and landing or the angle of attack of the cabin floor during these flight segments, which might be significant due to the low lift coefficient of the Flying-V.

2.2.2. Aerodynamic Design

In 2016, Faggiano set off to investigate the aerodynamic design of the Flying-V aircraft more thoroughly [3]. By means of a multi-fidelity design space exploration optimising the design for its lift-to-drag ratio during cruise, the lift-to-drag ratio is found to be 25% higher than the NASA Common Research Model. The latter has been adopted as a reference aircraft since limited data is available on the A350-900 competitor. Faggiano has put effort into translating the model into a number of variables that describe its outer shape completely and uses the ParaPy framework[3] as the principal platform for his research. The airfoils are described using Class-Shape Transformation coefficients, a method to describe the complex shape of an airfoil with a limited number of variables [21]. The design strategy employs the Athena Vortex Lattice method to quickly estimate the aerodynamic properties of a design vector, which is further optimised using the Stanford University Unstructured (SU2) code when its initial estimation results are satisfactory. A single and a dual step optimisation procedure are adopted, varying planform and airfoil variables simultaneously or subsequently. In both methods, a fin sizing methodology is applied after the optimisation has converged, minimising for fin area whilst complying with different directional stability requirements. An empirical viscous model is added to estimate profile drag. Faggiano recognises the results of the study by Qin et al. [18] which demonstrated that a combination of an elliptical and triangular lift distribution results in the highest lift-to-drag ratio. During the optimisation the height of the cabin is fixed to be 2.1 m based on top-level requirements on the cabin dimensions, and the required floor area for the payload is calculated based on this fixed height and a certain required payload volume. An important assumption made by Faggiano is the location of the reference point required for calculating the pitching moment, assuming a static margin of 2.5% MAC.

Important changes have been made to the design in order to achieve its high aerodynamic efficiency. First of all, the sweep angle of the outer wing is increased from 15 deg to 38 deg as shown in Figure 2.6. The

[3] https://www.parapy.nl/ [cited on 12-5-2020]

outer wing was twisted down to alter the lift distribution of the wing, leading to a large reduction in induced drag and pitching moment coefficient. Furthermore, the two pressurised cylinders are replaced by one larger oval pressurised cabin, visualised in Figure 2.7. This allows for a 10 abreast seating instead of 6, placing the cargo mostly behind the passengers. This layout was first described by Vos et al. [22], connecting four arcs to form one oval structure which defines the cross-section of the fuselage. This allows for a large uninterrupted payload space and increases the flexibility of the interior layout. The oval structure is complemented by horizontal and vertical panels, which are loaded in tension and compression to maintain the oval pressurised structure.

2.2.3. Structural Design and Weight Estimation

Van der Schaft started on the structural design and weight estimation of the Flying-V in 2017 [23]. The oval fuselage concept which was also used by Faggiano in the aerodynamic design [3] was adopted. The geometry used by Faggiano served as a basis for the structural design. No conclusive results on weight were found due to difficulties in closing the automated design loop. However, it was shown that the oval fuselage design is indeed feasible. It is interesting to note that the static margin was determined to be 16.7% MAC, rather than 2.5% as assumed by Faggiano [3]. Research into structural design and weight estimation was continued by Claeys in a joint project with Airbus, of which the results are confidential [12].

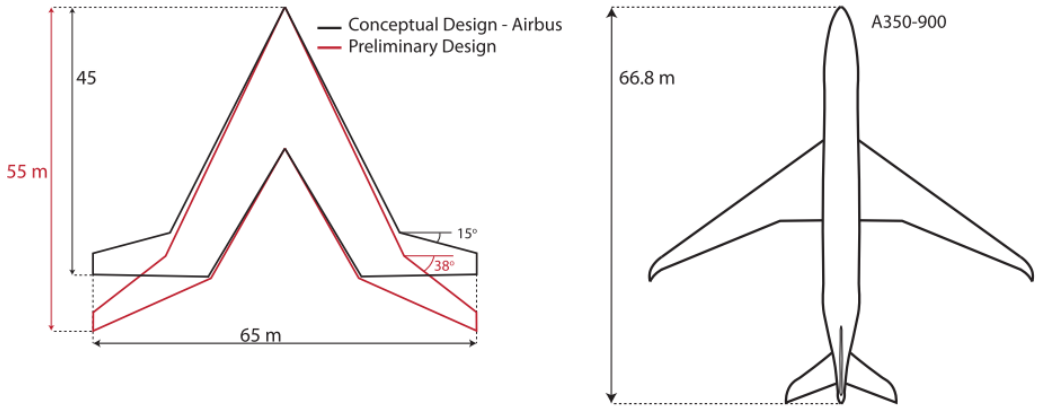

Figure 2.6: Planform of the Flying-V after Faggiano (in red), compared to Benad and the reference aircraft [3].

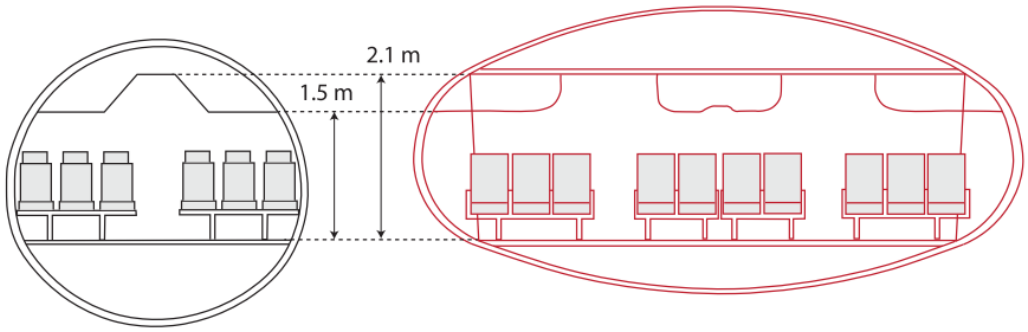

Figure 2.7: Cross-section of the Flying-V after Faggiano (in red), compared to Benad [3].

2.2.4. Engine Placement

Rubio Pascual studied the optimal position of the engines to minimise aerodynamic interference between the wing and the engines [24]. The engines have a significant effect on the aerodynamics of the aircraft as a whole. Rubio Pascual carried out simulations to model the flow around the flying wing and its engines at

cruise conditions, computing its viscous drag empirically. The difference between the worst position considered and the most optimal location is a lift-to-drag ratio loss of 55%. The resulting optimal location of the engines limits the reduction in lift-to-drag ratio due to the installed engine to 10%. Note that the objective of the optimisation was the lift-to-drag ratio and constraints were imposed upon the optimisation problem to make sure the result would be feasible regarding structures, controllability and regulations. The one-engine inoperative induced yawing moment is limited at this optimal engine location, and a thrust-induced pitching moment is small [24]. It is important to realise that the resulting engine position is optimal for cruise conditions at a fixed angle of attack.

2.2.5. Recent Developments

A study on interior design has been performed by Chung in 2018 [25], which mainly showed the versatility of the interior of the Flying-V. For instance, sleeping capsules with two beds each were introduced which could be placed towards the back of the aircraft. Part of these novel ideas would probably also fit in conventional configurations.

In 2019 a variety of studies have been performed on the Flying-V. These studies mainly analyse the Flying-V design on different aspects rather than redesigning parts of the aircraft. First, Palermo studied the aerodynamic characteristics of a 4.6% scaled model of the Flying-V [26]. Additionally, the longitudinal stability and control of the Flying-V were investigated, focusing on finding the location of the neutral point and determining the control surface effectiveness. In the meantime, Viet studied vortex formation on the Flying-V at higher angles of attack using wind tunnel experiments on the scaled model [27]. The wind tunnel results show vortex formation at an angle of attack of approximately 11 deg. Ruiz Garcia has constructed an aerodynamic model of the 4.6% Flying-V model based on wind tunnel experiments [28]. A joint project with Airbus led to a confidential study into handling qualities of the Flying-V by Cappuyns [29]. Santosh has studied the Flying-V in ground effect, assessing changes lift, drag and pitching moment coefficients when the aircraft is in ground proximity [30]. CFD analyses were performed on the 4.6% scaled model of the Flying-V, showing that the lift-to-drag ratio was only slightly affected in ground proximity. Finally, Bourget has studied the landing gear design [31] and Van der Pluijm investigated the cockpit design [32].

To conclude, studies on a variety of disciplines suggest that the Flying-V is a promising concept for the next generation aircraft. It has yet to be shown that the Flying-V concept allows for the development of an aircraft family to fully compete with modern conventional aircraft. Apart from the initial study by Benad [2], no integrated conceptual design of the Flying-V has been performed. Studies focused either on aerodynamics, weight, stability and control, handling qualities, or some other aspect of the aircraft. Naturally, these studies acknowledged the fact that only part of the larger picture was studied and incorporated necessary constraints of other disciplines. However, especially a fast aerodynamic analysis and weight estimation require further attention to construct a complete and computationally efficient fuel burn performance model for the Flying-V.

2.3. Product Family Design and Commonality

In order to fully grasp the idea of commonality and product family design, this section describes the idea of a product family and defines commonality. Then, the benefits of commonality are investigated, especially focused on aircraft families. The section concludes with a short discussion on commonality metrics.

2.3.1. Product Family Design

A definition of a product family is given by Simpson et al.: "A product family is a set of products that share common components/functions, while each variant has its unique specifications to meet demands of certain customers" ([33], p. 1). In an earlier article by Simpson et al., a product family is defined to be "a group of related products that is derived from a product platform to satisfy a variety of market niches" ([34], p. 3). A product platform is about a design, a set of components or elements which are shared by multiple products.

Within product family design there are two main branches in which all family design methods can be divided: module-based and scale-based design [34]. An alternative way to describe these two approaches is by configurable and parametric product family design [34]. Studying these two methods gives a more clear idea about different types of product families.

Module-based or configurable design is about modularity, which for instance could lead to an aircraft design in which several different wings can be attached to some fuselage, defining the wing and the fuselage

as separate modules which can be combined in multiple ways to fulfil certain missions. Scale-based design means that part of the design is scaled, keeping large parts of the design equal between product variants. Scale-based or parametric design is well-known from the aerospace industry, in which aircraft fuselages are stretched to offer a different passenger capacity, re-using large parts of the aircraft design such as the wing structure or the nose cone.

In both design methods, common and exclusive components are defined. The goal of family design is to achieve a certain degree of commonality, which is elaborated upon in the following sections. Defining the common and exclusive components is regarded as the first step in family design according to Jiao et al. [35]. In module-based design, this would be mainly about dividing the product into clear modules. Scale-based design also requires some form of modularity, defining common modules and scalable modules. The second step Jiao et al. describe is the determination of the optimal values of all variables, both common and exclusive. In this light, Section 2.4 discusses different family design optimisation methods in depth.

2.3.2. The Concept of Commonality

Within the broad area of evolvability, commonality, changeability and other terms describing similar concepts, it is important to get a clear definition of commonality within the scope of this research.

Changeability or evolvability is to be distinguished from commonality. According to Van Heerden, evolvability is a specific form of changeability. Van Heerden argues that evolvability and commonality are not the same concepts [36]. Product platforms and product families are mainly focused on enlarging the variety of products with only limited extra cost and effort; often, these families are pre-planned. However, evolvability is about reusing designs over time, not necessarily in a planned way. When designing an aircraft, future scenarios could be taken into account, such as the chances that in the future due to some technique the engines are required to be fuselage-mounted instead of wing-mounted. This could mean that a design that already employs fuselage-mounted engines scores higher on evolvability, since it requires less effort to convert it into this future design later on.

Naturally, evolvability and changeability are closely related to family design. Not all family design is planned for, thinking for example about the Boeing 747 aircraft which was first delivered in 1969 and of which the 747-8 version was first delivered in 2011[4]. Each 747 generation could be seen as a family, but also the complete 747 series could be regarded as one large family. As such, commonality can be described as one of several enablers for evolvability.

Bador et al. describe two types of commonality: transverse and temporal commonality [37]. Transverse commonality is commonality between various products in a family. Temporal commonality is commonality between products that change over time, such as cockpits which are upgraded periodically. Transverse commonality is about standardisation between different product variants, whilst temporal commonality deals with the reusability of a design. Both types of commonality are related to modularity. The concept of temporal commonality is closely linked to the concept of evolvability described by Van Heerden [36].

Within this research, a family of products is considered of which all family members are known beforehand. It is not impossible that later variants of the same product would reuse parts of the design of this initial family, but the scope of this research is limited to the known variants of the Flying-V family. This means that the broad concept of evolvability is not employed to study the benefits of the Flying-V family, but that the concept of commonality is used throughout this research. Commonality is employed in terms of transverse commonality rather than temporal commonality. Commonality is used as a concept to describe the degree or amount of similarity and equal components between the members of the Flying-V family. The probable benefits of the Flying-V family as an enabler for future aircraft configurations or derivatives are interesting, but not the scope of this research.

Commonality is closely connected to modularity. "Modularity decomposes functions into independent groups, while commonality clusters the components and functions based on similarity or other criteria" ([33], p. 2). As such, defining different modules within a product aids the designer in increasing commonality, as common modules can easily be recognised and defined. Clearly, module-based design is built upon the principle of modularity, decomposing a product into several modules. However, also for scale-based design methods modularity is an important concept, since some modules of the product are shared and others are scaled. A distinction between different modules in a system is of paramount importance, especially when

[4]http : / / active . boeing . com / commercial / orders / displaystandardreport . cfm ? cboCurrentModel = 747&optReportType = AllModels&cboAllModel=747&ViewReportF=View+Report [cited on 25-9-2020]

part of the modules are scaled whilst others are to remain the same and should therefore be able to cope with these scaled modules. For both design principles and as such in this research, it is an important step to define the different modules within the Flying-V and the reference aircraft.

According to Simpson et al., three types of parts can be distinguished: unique, variant and common parts [34]. A scaled part could be seen as a variant part, since it fulfils the same function in each product variant but has a slightly different design. In determining parts or modules, three types of modularity can be distinguished. Modularity can be done on a functional, technical and physical basis [35]. In the same way, functional, technical and physical commonality can be defined.

2.3.3. The Importance of Commonality

Simpson et al. describe the essence of commonality is to differentiate products for the customer whilst maximising its commonality for the manufacturer [34]. This section describes the costs benefits of commonality in more detail.

An interesting in-depth thesis on commonality is written by Boas [38]. Boas describes that commonality has potential benefits on development costs, production costs and operational costs.

Regarding development costs, the required development scope for the development of products reduces when commonality is increased, since designs or ideas can be reused. However, it should be noted that common modules could have a larger complexity than the individual modules that are replaced, such that this benefit is not as large as it at first glance seems. Often, this means that the initially developed variant has increased complexity and therefore high development costs, whereas later versions have lower development costs. At some point, a break-even point is reached at which family design is actually beneficial. Birrenbach states that manufacturers can adapt better to market needs since a fleet of aircraft is designed rather than a specific type [39]. In addition, the risk associated with development might reduce, since the chances that a module will be actually incorporated in a product could increase [40].

Production costs can be split into direct and indirect costs. The direct costs, such as material costs and labour, might be higher when the shared module is more complex than an individual module would be. However, due to a learning curve in production, the labour costs decrease when larger amounts of products are made. In addition, material costs might reduce when larger amounts of the same material are bought. In some way, this same principle holds for the suppliers which can possibly reduce their prices due to a larger production rate and their own learning curve. Indirect costs such as facility costs could also be reduced by commonality, although this benefit does not seem to be very large [38].

Finally, operational costs can be divided into maintenance and direct operating costs. Maintenance costs might reduce in a similar fashion as production costs, with the most important difference that these costs are made by the operator rather than by the manufacturer. The operator will also have a learning curve and reduced product costs due to the larger volume of the same products that is acquired. On the contrary, direct operating costs might increase. For instance, a family of aircraft might be somewhat less optimal than individually optimised aircraft, such that fuel consumption is increased. However, training costs for the crew can reduce when similar aircraft types are used rather than multiple different aircraft types. For example, Birrenbach mentions the common type rating which is often acquired for an aircraft family, such that pilots can operate each type within a fleet without additional training [39]. This would mean that only one flight simulator is required for a fleet of different aircraft. Additional benefits mentioned by Birrenbach are the reduced number of spares in storage, reduced administration costs and product identity for e.g. service items.

Something that is not explicitly mentioned by Boas but is recognised by Van Heerden is the benefit of commonality regarding certification [36]. Within the aircraft industry, certification is a time-consuming and expensive step in the development of an aircraft, such that a reduction in the need for certification is really interesting. Therefore, reusing designs by increasing commonality between aircraft is a large benefit, requiring only amendments to the certification of the baseline aircraft rather than requiring a completely new certification procedure.

Boas mainly focuses on platform divergence, describing the reduced benefit of commonality when the family members are not designed simultaneously. In this situation, a common platform might be mostly designed for the needs of product A, whilst a later product B requires the same platform [38]. According to Boas and Crawley, in reality a lot of product families are developed in a sequential rather than in a parallel way [40]. In sequential family design, the short-term product will be penalised with higher development costs and possibly production or operation costs, whilst in the long-term the development of later family members should counteract these initial penalties [40]. In this research, the effects of timing on the benefits

of commonality are not included. It is regarded primarily as the task of the manufacturer to fully obtain the benefits of commonality through careful planning of the development and manufacturing of a product family.

Commonality does come at a price. In the end, commonality is a constraint defining parts of a design to be equal to other designs [1] and hence the performance of individual products within a family will be less optimal than individually optimised products. For instance, in a conventional aircraft family the wing area might be based on the largest aircraft family member, such that smaller aircraft family members have an oversized wing resulting in fuel burn performance loss. Product family design is about the trade-off between the benefits and drawbacks of commonality, carefully balancing the economic benefits of commonality against the reduced performance of the individual products.

2.3.4. Commonality Metrics

Several methods to describe the degree of commonality in a product family exist, of which variable-based methods are deemed most applicable for this research. Variable-based methods define design variables to be common or unique between products. The approach of Messac et al. forms the basis of different variable-based commonality models in literature. Messac does not include commonality beforehand in the optimisation procedure, but includes it directly in the optimisation procedure by applying penalty functions to design variables that differ between the family members [41]. In this way, the optimisation will try to set all variables equal to each other, only scaling variables that should be different across family members in order to meet all constraints or when it results in a much better fulfilment of the objectives. The direct inclusion of the selection of common and exclusive design variables in the optimisation procedure means that the designers do not need to select them a priori, allowing for more design freedom and leading to potentially optimal designs. Variable-based methods do not require subdivision of the aircraft into several separate components, but can have a high level of detail when a large number of variables is included. Furthermore, these methods are rather flexible, requiring no re-definition of the aircraft to increase the level of detail; extra analysis or sizing procedures could easily be included. Moreover, variable-based methods do not require large assumptions on costs or production quantity, whereas several other commonality metrics such as the Degree of Commonality Index (DCI), Component part commonality Index ($CI^{(C)}$), Total Constant Commonality Index (TCCI), Product Line Commonality Index (PCI) or Percent Commonality Index (%C) require assumptions on part count or cost. As such, a method that depends only on design variables is deemed most useful in conceptual aircraft family design. A potential drawback of a variable-based method is that the exact benefit of commonality in terms of cost or development time is not really made visible by this method because it is difficult to establish a clear relation between cost and design variables. Hence, variable-based methods require further analysis of the results to study the actual benefit in terms of cost due to commonality.

2.4. Aircraft Family Design Methods

Within aircraft family design the same two main design principles discussed in Section 2.3.1 can be distinguished: module-based and scale-based design. In this section, these methods are discussed in-depth, specifically focusing on aircraft family design.

Module-based family design is a design paradigm to develop a family of products by adding or substituting different modules to some planform. Module-based aircraft family design is found mainly in small aircraft such as UAVs, whereas not much development appears to have been made on the topic of module-based family design in large transport aircraft.

Scale-based family design methods are the principal family design method for large transport aircraft. Scale-based family design methods are based upon the principle of scaling a design to construct multiple family members. An example of a scaled design is shown in Figure 2.8, in which the fuselage of the aircraft is the principal scaled component. Within scale-based family design methods, two major design principles can be distinguished: sequential and simultaneous methods [42]. Set-based design is also shortly discussed.

Sequential family design methods have been the method to design families of aircraft for multiple decades. A baseline aircraft is designed, followed by expected or unexpected derivative versions. During the design of the baseline aircraft, margins might be incorporated deliberately to account for derivative designs, but in principle, the design method is not optimising for multiple aircraft at once from the start of the program. One of the papers at the root of family design methods and serving as a basis for many later papers is written by Willcox and Wakayama [42] in 2003. In this paper, a method to optimise multiple aircraft simultaneously

is presented. The method is applied on a family of two blended wing body (BWB) aircraft, seating 272 and 475 passengers having both a range of 8550 nm. In this paper, a comparison is made between sequential and simultaneous optimisation. The sequential optimisation was performed by optimising the larger variant of the aircraft family, minimising takeoff weight. Then, the smaller version was optimised for minimum takeoff weight, utilising the exact same wing as the larger version. This is an example version of sequential family design, in which part of the aircraft is re-used on subsequent versions without optimising this common part for both variants, such that derivative aircraft are probably sub-optimal. The general idea of leaving margins in either the design phase or in the actual baseline aircraft appears to be a sub-optimal solution to the problem of designing a family of aircraft. After all, including margins in a product means it is not performing at its optimal point with its maximum performance. For this reason, simultaneous family design methods are rather promising.

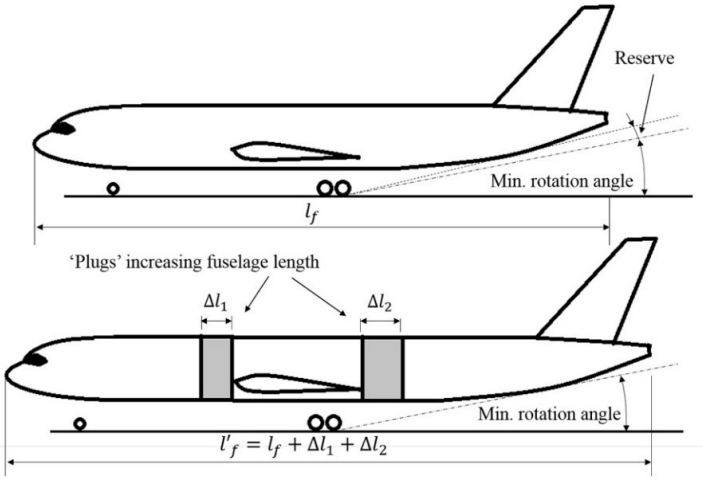

Figure 2.8: Sequential scale-based design, leaving margins in landing gear length to allow stretching of the fuselage [4].

Simultaneous family design was already touched upon when discussing the paper by Willcox and Wakayama on sequential family design [42]. A small reduction in takeoff weight of 0.2% was achieved for a simultaneously designed aircraft family compared to a sequential design procedure. Due to a relatively small increase in takeoff weight of the smallest aircraft, the larger aircraft's takeoff weight was reduced much more leading to a net reduction of the weights of both aircraft.

Simultaneous optimisation is rather promising, but conclusive results on the optimal optimisation architecture are not easy to find. The majority of the articles on family design methods show the general principle of the applied family design method on a certain case, comparing it to a limited number of different family design routines. The results are considered rather dependent on the number of variables and constraints included in the specific family design case. Furthermore, virtually all discussed studies have a limited level of detail in terms of aircraft parameters and constraints. Many of the discussed studies have conventional aircraft as a subject, leaving only a few studies that focus on unconventional configurations.

The final aircraft family design procedure that needs attention is the set-based method worked on by a group at Cranfield University. The set-based design (SBD) paradigm was first described by Riaz [43], and has since then been used in several other studies by Cranfield University such as the PhD thesis of Van Heerden [36]. The fundamental idea of SBD is to keep all design options in the design space, only discarding infeasible options based on careful requirement selection. The effect of changing or adding a requirement is immediately clear, aided by the interactive interface AirCADia of Guenov et al. [44]. The main incentive to develop this set-based design principle for conceptual aircraft design was the observation that both sequential and simultaneous optimisation methods "have the tendency to exploit assumptions present in the computational models and to drive the design towards a solution which (...) may be infeasible".

Set-based design is mainly focused on keeping all design options open for as long as possible, which is considered to be mainly applicable to the early stages of conceptual design. However, in this research the Flying-V family is not to change conceptually; rather, a family of aircraft of the Flying-V concept is compared to a family of aircraft of the conventional configuration. The Flying-V concept is moving towards later design phases, and as such this research is on family design with a predetermined configuration. Therefore, the

set-based design paradigm is not considered suitable for this study.

There appears to be a knowledge gap regarding a more detailed yet conceptual simultaneous family design, studying an unconventional configuration. Further research into optimal optimisation routines in aircraft family design is therefore recommended. This research into family design of the Flying-V can form the start of more research into this interesting and important area.

Within large passenger aircraft design, no examples of module-based design have been found and the author does not foresee any changes in this on short notice. Only the study of Van Keymeulen needs to be mentioned, which concluded that the application of a modular fuselage is not beneficial [45]. Aircraft families are a well-known example of scale-based family design, which is considered most applicable for this research. To fully compare the effect on performance by designing a family of Flying-V aircraft to designing a family of conventional aircraft, the design paradigm of a family of conventional aircraft should not be altered.

As has been explained in the discussion on set based-design, this method is not considered applicable in the current design phase of the Flying-V. Simultaneous family design has been proven to yield better results than sequential design, for example regarding takeoff weight in the described study by Willcox and Wakayama [42]. In addition, sequential design methods for unconventional aircraft are hard to define, since most sequential design principles are tailored to conventional tube-and-wing aircraft. Many recent studies have been performed into simultaneous optimisation, whilst only limited development can be observed within sequential family design methods. The reference aircraft for the Flying-V, the Airbus A350, has also largely been designed simultaneously [46]. Hence, simultaneous scale-based family design is selected as the family design method in this research.

2.5. Design of Modern Conventional Passenger Aircraft Families

The A350 family was the reaction of Airbus on the Boeing 787 after customers reacted negatively to the initial idea to counteract the Boeing 787 with an improved version of the Airbus A330[5]. Both aircraft are exemplary modern passenger aircraft, of which large numbers have been sold [47]. In this section, both aircraft families are discussed, focusing on the reference Airbus A350 family.

2.5.1. Airbus A350

Large parts of the design have benefited from the development of the A380 aircraft. The fuselage is extra wide compared to the A330 and B787, such that it was called the A350XWB (eXtra Wide Body). Initially, three variants were proposed: the -800, -900 and -1000. However, due to limited interest in the -800 variant, its development has been stopped and the only remaining customer has ordered -900 variants instead in 2018[6]. The principal difference between the -900 and -1000 variant is the increased takeoff weight of the latter. Payload capacity is increased by inserting a total of 11 extra frames into the fuselage, increasing the fuselage length with 7 m [7]. An improved version of the Trent XWB engine has been used on the -1000 variant, and the wing area has been increased by 4% which meant a modification of 90% of the wing parts[5]. A modification of 90% of the wing parts seems to result in a very low commonality, but this figure was not confirmed by any other sources and as such no large conclusions should be tied to this figure. Additionally, it should be noted that the most expensive wing parts might not have been changed, such that the effect of a limited commonality in terms of part count is not directly related to a similar increase in cost. Differences include a trailing edge extension and an increase in chord length of 0.4 m. According to chief engineer McConnell, the flap lift performance was increased and also "cruise performance" was enhanced by these changes[7]. Unfortunately, McConnell does not elaborate on the specific improvements in cruise performance. Due to the increase in takeoff weight the landing gear had to be altered, using six-wheel-bogies instead of four and extending the landing gear bay[7]. An Ultra-Long Range (ULR) version of the A350-900 has also been introduced, which has additional fuel capacity to increase its range from 15001 km to 17964 km. Interestingly enough, this does not require additional fuel tanks but only additional venting and piping, according to Marisa Lucas-Ugena, Airbus' A350 marketing director. "The only thing that is really specific for the ULR is the additional fuel. And even on that, we are using the space we already have. It's really just a minor evolution of that system with

[5] https://janes.ihs.com/Janes/Display/jawaa054-jawa [cited on 6-9-2020]

[6] https://luchtvaartnieuws.nl/nieuws/categorie/2/airlines/laatste-order-voor-airbus-a350-800-geschrapt [cited on 9-9-2020]

[7] https://www.flightglobal.com/airbus-opts-for-larger-wing-on-a350-1000-through-trailing-edge-extension/93107.article [cited on 9-9-2020]

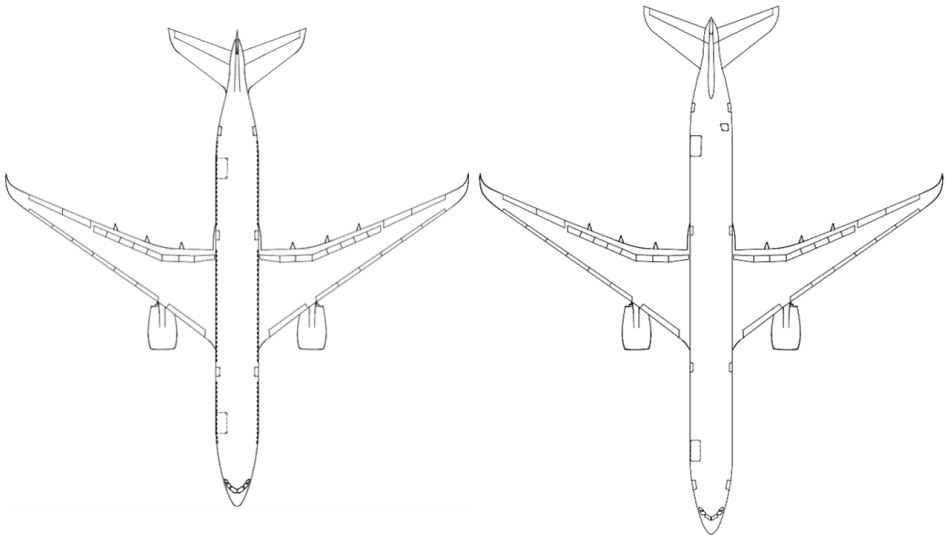

Figure 2.9: Planform view of the A350-900 (left) and -1000 (right), CAD drawings obtained from Airbus.

additional piping and additional venting."[8] The top-view of the A350 variants is shown in Figure 2.9[9].

Regarding the A350-800, the initial idea was to redesign several parts of the aircraft to increase its performance at the cost of a lower commonality with the A350-900. According to Van Heerden, "developing a smaller derivative is often more difficult than a larger one." ([47], p. 152). This is probably illustrated by the A350-800, which required this redesign to have competitive performance. However, at the start of the detailed design phase of the -800 variant the company decided to choose for commonality such that the performance slightly reduced. A350 chief engineer Gordon McConnell states that they are "chasing economics to provide the lightest possible aircraft." This was mainly due to pressure of the airlines, which stated that the optimisation would mean that their cost of ownership would increase. As such, its wing is completely the same as the wing of the A350-900. The fuselage is shortened with a total of 10 frames, of which 6 frames are forward of the wing and 4 frames aft of the wing. All systems are kept the same where possible [48].

Commonality between the A350-1000 and -900/800 version is estimated to be 70%, whilst commonality between the -900 and -800 versions should have been even higher [10]. Unfortunately, it is unclear whether this commonality is in terms of part count or in terms of another metric. Limiting commonality on the -1000 variant to increase performance was a design decision, and even the customers were involved. The customers "all understood" this decision according to the A350 programme manager Didier Evrard. An important aspect of the A350 family is its Common Type Rating; the A350 family retains fly-by-wire pilot commonality with the A320, A330, A340 and A380 aircraft families[5]. According to Airbus, this leads to a 65% reduction in pilot training time. "This achievement is a fine example of our ability to combine innovation with commonality" [11]. Airbus states that the A350-1000 has 95% common part numbers compared with the A350-900[12].

The A350 family is an exemplary case of modern passenger aircraft development. Despite its almost simultaneous development, the -900 variant serves as the principal baseline aircraft to which changes are made for the -800 and -1000 variant. The A350 family shows that modern aircraft manufacturers are really focused on commonality, being a recurring theme in many interviews with leading Airbus employees. In the end, this led to 95% common part numbers between the -900 and -1000 variant. Note that the economic benefit is not necessarily as large, since the 5% exclusive parts might be expensive or large components in terms of development or production.

[8] https://www.traveller.com.au/airbus-a350900ulr-why-only-seven-of-the-worlds-longest-range-airline-are-being-built-h10tuq [cited on 10-9-2020]

[9] https://www.airbus.com/aircraft/support-services/airport-operations-and-technical-data/autocad-3-view-aircraft-drawings.html [cited 6-9-2021]

[10] https://search.proquest.com/docview/896355989?accountid=27026 [cited on 6-9-2020]

[11] https://www.airbus.com/en/newsroom/news/en/2014/10/the-common-type-rating-is-approved-for-a350-xwb-and-a330-pilot-training.html [cited on 11-9-2020]

[12] https://www.airbus.com/content/dam/corporate-topics/publications/backgrounders/Backgrounder-Airbus-Commercial-Aircraft-A350-XWB-Facts-and-Figures-EN.pdf [cited on 11-9-2020]

2.5.2. Boeing 787

The Boeing 787 has been launched as the Boeing 7E7 in 2004, focusing on efficiency, economics and environmental performance, exceptional comfort and convenience and e-enabled systems[13]. The 787-8 was first introduced in 2009, followed by the 787-9 in 2013 and the 787-10 in 2017. The 787-8 can be regarded as the baseline variant, which was the starting point for the later two variants[47]. Large design changes were made between the 787-8 and the 787-9. The 787-9 has a larger undercarriage in terms of brakes, tires and trucks, in order to withstand its higher maximum takeoff weight. Additionally, the thickness of the fuselage structure was altered, removing thickness in over-designed parts on the 787-8 and adding thickness at more critical locations. The wseight of the wing was optimised in order to lift the larger takeoff weight with the same planform and wing area. In the end, both range and payload of the 787-9 were increased with respect to the 787-8, enabled by the aforementioned design changes and the addition of a hybrid laminar-flow control systems on the leading edge of the fin and horizontal stabiliser. The 787-10 has been largely designed based on the 787-9, and the 787-8 design has been updated with design changes of the 787-9. During the development of the 787 family the engines have also been improved by Rolls-Royce and General Electric, such that later 787 aircraft have more powerful engines than the initial 787-8 aircraft. Finally, an interesting change on the 787-10 with respect to the smaller 787 aircraft is the introduction of a semi-levered main landing gear, which essentially enables a larger pitch angle during takeoff or landing having the aircraft load on one of the two main gear wheel axes before the other wheel axis touches the ground, increasing the effective length of the landing gear. A tail skid is added to prevent damage on the tail resulting from high angles during takeoff or landing.

Naturally, the large number of changes between the aircraft family members has no positive effect on commonality. For instance, the new hybrid laminar-flow control system on the 787-9 has not been introduced on the 787-8, whilst it has been introduced on the later 787-10. The wing of the 787-9 is used on the 787-10, whereas there are differences with respect to the 787-8 wing. Boeing expects the market potential of the 787-9 and 787-10 to be larger than the potential of the 787-8, such that similarity between the 787-9 and 787-10 is very beneficial. According to Jenks, vice-president of the 787 development, the 787-10 has not been designed with an increased range to retain a high level of commonality with the 787-9, not requiring changes such as a larger wing [49]. Some locations on the wing required strengthening due to the longer fuselage of the 787-10, which were also applied on the wing of the 787-9 to retain commonality, which is a very clear example of a trade-off between commonality and individual aircraft performance. As such, at the same maximum takeoff weight, the 787-10 has a larger payload capacity and shorter range. As a result, the 787-10 has an extreme degree of commonality with the 787-9, with approximately 95% common part numbers with the 787-9 [50].

Comparing the 787 family to the A350 family, commonality appears to be higher between the 787-9 and 787-10 than within the A350 family, whereas commonality with the 787-8 is probably less. However, no clear metrics have been provided by both manufacturers, such that commonality is difficult to assess. Changes in the maximum takeoff weight required changes in the landing gear in both aircraft families. Design of the 787 and A350 family appears to have taken place not completely in a simultaneous way, with the A350-900 being the starting point for the A350 family and the 787-8 and later the 787-9 for the 787 family. A potential benefit of this approach is that the experience obtained from designing the first variant can aid in the development of the second or third variant, even resulting in an updated first aircraft variant such as in the 787 family.

[13] http://www.boeing.com/history/products/787.page [cited on 26-3-2021]

3

Experimental Setup

In this chapter, the experimental setup is described. First, the use of the Knowledge-Based Engineering ParaPy environment is explained, followed by top-level aircraft requirements the aircraft family should fulfil. Then, the parametrisation of the Flying-V family and the design principle to form a family of aircraft are explained. Finally, the optimisation architecture which is applied to optimise a family of aircraft is introduced.

3.1. ParaPy Framework

Previous studies on the Flying-V have been using the ParaPy framework programmed in Python[1]. ParaPy is a Knowledge-Based Engineering (KBE) environment, of which the characteristics are extensively discussed by La Rocca [51]. In short, KBE is a technology that is aimed at reducing development time and costs by capturing knowledge and making it easily reusable. As such, repetitive design can be automated. In addition, KBE and Multidisciplinary Design Optimisation (MDO) are intimately coupled, such that MDO features are easily integrated into a KBE environment. This feature is beneficial since both single aircraft optimisation and family of aircraft optimisation require a form of multidisciplinary optimisation. Furthermore, most KBE systems have an object-oriented programming paradigm. This aids in defining modularity, which is a key step in family design optimisation. Finally, KBE systems specifically provide dependency tracking, runtime caching and demand-driven evaluation. The first two principles ensure that computed values are up to date when required and are easily reused. Demand-driven evaluation ensures that values are only computed when they are required, such that no computational resources are wasted. In a family design routine, a large number of function evaluations are required, such that minimising usage of computational resources is of paramount importance.

For all these reasons, a KBE framework is employed in this research. Since previous studies on the Flying-V led to a fully defined conceptual design of the Flying-V in ParaPy, this specific KBE environment is reused. ParaPy is programmed in Python, hence additional analyses and methods are written in Python to ensure smooth coupling with the existing tools and to gain access to large resources of publicly available libraries.

3.2. Top-level Aircraft Requirements

The Flying-V aircraft family needs to be designed for certain top-level aircraft requirements to ensure the competitiveness of the Flying-V aircraft, being introduced as a competitor to the A350 aircraft family. As such, the performance of the A350 family should be met. A summary of all constraints is provided in Table 3.3.

3.2.1. Payload and Range

The Flying-V aircraft family members should be able to fly a certain combination of payload and range, represented by a payload-range diagram as in Figure 3.1. The design mission is the maximum range at the maximum number of passengers without any cargo. For the A350-900 reference aircraft, this is approximately 14800 km at a payload weight of $31 \cdot 10^3$ kg as shown in Figure 3.1. Similarly, the A350-1000 design mission is defined as 15350 km at a payload weight of $34 \cdot 10^3$ kg. For all aircraft, a diversion of 200 nm and a loiter phase of 30 minutes is included.

[1] https://www.parapy.nl/ [cited on 23-9-2020]

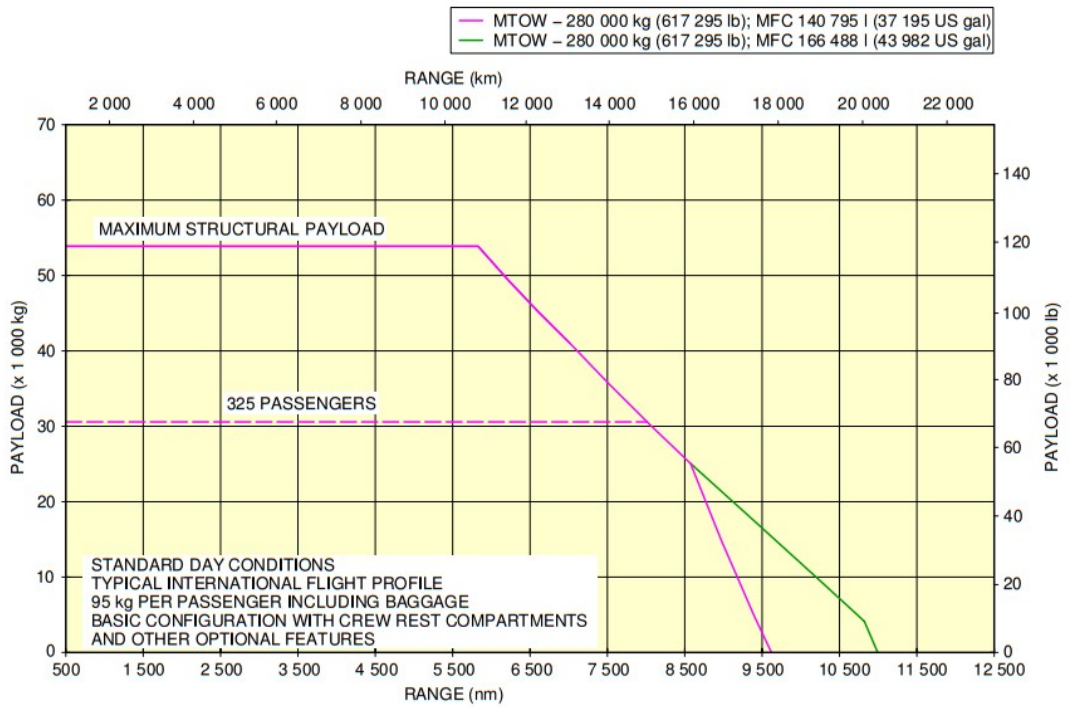

Figure 3.1: Payload-range diagram for the A350-900 reference aircraft [5].

Not only the weight of the payload should be incorporated as a requirement, but also its size. This means that the payload is translated into cargo of a certain size and weight, and a passenger cabin with a certain capacity. Top-level requirements on the payload, cabin furnishing and cargo volume are presented in Table 3.2 [5]. Regarding the -800 variant, a lot of data is unavailable or unsure and as such assumptions had to be made on cabin furnishing and emergency exits. The floor area of the payload is determined using Table 3.1, resulting in the required cabin floor area and required total floor area, $S_{\text{paxcabin}_{\text{req}}}$ and $S_{\text{totalcabin}_{\text{req}}}$. In these equations, w_{floor} is the width of the cabin floor, $S_{\text{constainers}}$ the floor area of the containers.

Table 3.1: Formulas used to calculate total floor area of the payload.

	Formula	Notes or source
Passengers	$0.487 \cdot n_{\text{pax}_{\text{ec}}} + 1.397 \cdot n_{\text{pax}_{\text{ec}}}$	Based on seat pitch and 10 pax per row, 6 m wide cabin
Lavatories	$n_{\text{lavatories}} \cdot 1.0$	Raymer[6]
Galleys	$1.5 \cdot 0.3048^2 \cdot n_{\text{pax}}$	Raymer[6]
Emergency exits, aisles	$L_{\text{cabin}} \cdot 0.5$	Based on aisle width and initial floor plan study
Cargo	$2 \cdot 1.0 \cdot w_{\text{floor}} + 1.1 \cdot S_{\text{containers}}$	1 m between passengers and cargo, 10% margin on container area

Cabin dimensions are constrained by Benad to equal the A350-900 reference aircraft [13]. The minimum head clearance over the seat closest to the wall is 1.6 m, head clearance in the aisle is 2.1 m and seat pitch, seat width and aisle width of the economy class are constrained at 81.3 cm, 50.8 cm and 46.0 cm respectively. Seat pitch, seat width and aisle width of the business class are constrained at 152.4 cm, 75.0 cm and 54.6 cm. The height of the cabin reduces when moving into the tapered part of the fuselage, with the minimum cabin height set at 1.9 m. The differential pressure in the cabin is taken from earlier research on the Flying-V at 57,500 Pa [12], which is close to a cabin pressure of 6000 ft and a cruise altitude of 11,500 m.

Finally, the fuel weight and size are a requirement. The required fuel capacity for the Flying-V aircraft family is calculated based on the design mission, calculating the ferry and harmonic range following from this fuel capacity. The method to calculate fuel consumption of these aircraft is discussed in detail in Chapter 4.1.

Emergency evacuation regulations are found in subpart D of CS and FAR 25. CS25.807 states the maximum number of passengers per specified door type. For the reference aircraft, a combination of type-A and type-C doors is used, which have a maximum of 110 and 55 passengers respectively. For this reason, most variants of the A350-900 aircraft have two doors of both types, such that its maximum passenger capacity is up to 330 passengers depending on the seating arrangement [52]. Versions with four type-A doors have a maximum seating capacity of 440 passengers. The A350-1000 aircraft with 385 passengers normally has a C-A-A-A emergency exit configuration, allowing 385 passengers. The -800 variant is assumed to have the same door configuration as the -900 variant, since only one type-A and three type-C doors would not suffice for 276 passengers. An additional requirement regarding emergency exits is found in CS25.807, which specifies that emergency exits may not be more than 18.3 m (60 ft) apart along the longitudinal axis of the aircraft. 2 cargo doors are used on the Flying-V, one per cargo compartment. The size of the cargo door is based on LD-9 containers with a 10% margin on width and height.

Table 3.2: Top-level requirements for the Flying-V aircraft family. Passenger weight is discussed in Section 4.3.3. *The range of the Flying-V -800 is not a constraint but follows implicitly from the family optimisation procedure based on its available fuel tank volume.

		Variable	Unit	-800	-900	-1000
Cabin furnishing	Large galley carts	$n_{\text{large carts}}$	-	35	35	44
	Small galley carts	$n_{\text{small carts}}$	-	0	10	10
	Attendant seats	$n_{\text{attendants}}$	-	8	8	8
	Lavatories	n_{lav}	-	7	9	11
	Closets	n_{closets}	-	2	2	2
Emergency exits	Type-A doors per side	$n_{\text{type-A doors}}$	-	2	2	3
	Type-C doors per side	$n_{\text{type-C doors}}$	-	2	2	1
Design range		R_{des}	km	11160*	14800	15350
Design number of passengers	Business class	$n_{\text{pax}_{\text{bc}}}$	# pax	36	48	52
	Economy class	$n_{\text{pax}_{\text{ec}}}$	# pax	257	280	309
Additional harmonic payload	Cargo	W_{cargo}	10^3 kg	8.1	22.9	33.1
	LD9 (LD4) containers	n_{LD9} (n_{LD4})	-	10 (18)	14 (24)	18 (30)
Total payload weight		-	10^3 kg	35.7	53.8	67.1
Cruise Mach number		M_{cr}	-	0.85	0.85	0.85

3.2.2. Airport Requirements

The airports which the aircraft family serves impose several requirements. The Flying-V design is to be categorised in the same category as the A350-900 reference aircraft, which is the Code E/Group V category of the FAA and ICAO[2]. This means that the reference field length is more than 1800 m and the wingspan b should be between 52 m and 65 m. Furthermore, its outer main gear wheel span y_{mlg} is limited to 14 m and its tail height h_{tail} to 20.1 m [13], which is easily met by the baseline Flying-V design with a height of 17 m. The fin height of Faggiano is 5.5 m which means that this constraint on tail height is met for all fins with an equal or lower height on aircraft with similar dimensions. The wingspan is a design variable that can easily be constrained. The engines should not be less than 5 m apart as suggested by Rubio Pascual [24], to satisfy disk failure requirements. Hence, the minimum engines lateral distance, $y_{\text{eng}_{\text{min}}}$, is 5.0 m. The reference field length is determined to be outside the scope of this research, requiring a detailed low-speed performance analysis.

A constraint on approach speed, $V_{\text{app}_{\text{max}}}$, is included to ensure that the wing loading of the Flying-V is sufficient to achieve an approach within the C/D category of the ICAO. The reference A350-900 aircraft falls into the Aircraft Approach Category C with an approach speed of 140 kts, whilst the A350-1000 falls into the D category with an approach speed of 147 kts [5]. Both values are at maximum landing weight. The approach speed is constrained at 140 kts for the FV-800. The approach speed is calculated using Equation 3.1.

$$V_{\text{app}} = \sqrt{\frac{W_{\text{MLW}}}{S}\frac{2}{\rho_0}\frac{1}{C_{L_{app}}}} \tag{3.1}$$

In this equation, the density ρ_0 is at sea-level since the approach speed is defined in terms of indicated airspeed. The landing weight W_{MLW} is set at 76% of the takeoff weight, which is on average the case for the

[2]https://www.skybrary.aero/index.php/ICAO_Aerodrome_Reference_Code [cited on 10-9-2020]

reference aircraft according to Airbus specifications [5]. For the Flying-V, the maximum lift coefficient in approach configuration $C_{L_{\text{app}}}$ is set at 0.73 for all aircraft family members. This value originates from the Flying-V configuration which was studied in more detail by earlier studies, such as the study on the landing gear of Bourget [31]. In reality, the maximum lift coefficient might change for a larger or smaller aircraft variant, but since the wing area of the aircraft changes with a change in payload this effect is assumed to be limited. The design used by Bourget is a combination of the -900 and -1000 aircraft envisioned in this study, having a wingspan of 65 m and a payload capacity comparable to the -900 aircraft.

3.2.3. Stability and Control

CS25 and FAR25 specify a lot of requirements on stability and control of transport aircraft. Both the Flying-V and the reference aircraft are to be certified abiding by these regulations. CS25.171 on stability in general and parts 173, 175 and 177 on longitudinal, directional and lateral stability and control should be complied with.

Anderson states that an aircraft is longitudinally stable when Equation 3.2 holds, a relation which is valid for a positive lift curve slope [53]. As such, he argues that the neutral point of the aircraft, which only depends on the planform of the aircraft, should be behind the centre of gravity. In this way, an aircraft will return to its stable position whenever a disturbance in lift is encountered.

$$\frac{\partial C_M}{\partial C_L} < 0 \tag{3.2}$$

As such, the location of the centre of gravity is an important parameter to be determined. As explained by Raymer [6] the centre of gravity location should remain within the forward and aft centre of gravity limits determined in a stability and control analysis. The allowed location of the centre of gravity with respect to the neutral point generally includes a margin, the so-called static margin. Faggiano applies a static margin of 2.5% MAC. The minimum static margin, $x_{\text{sm}_{\text{min}}}$, is set at 0.0 to ensure longitudinal static stability.

CS25.27 states that the "extreme forward and the extreme aft centre of gravity limitations must be established for each practicably separable operating condition." Figure 3.2 visualises an example of the change in centre of gravity location during flight due to the burning of fuel. A similar process takes place when the aircraft is being loaded at the airport. An early estimation of the centre of gravity during loading of the aircraft was made by Benad [13]. The centre of gravity was also determined by Cappuyns [29] using the component weights obtained by Claeys [12]. Note that the results of the latter studies are confidential. During aircraft development, the centre of gravity for ground operations and in-flight should be studied for various mission scenarios. In this research, only the most forward and aft centre of gravity locations during the cruise phase are considered. Explicitly defining a maximum centre of gravity shift would have a large impact on the optimisation results since this requirement would be driving, but a proper value is hard to define. As such, the centre of gravity shift was included in the optimisation procedure differently, opting for a small increase in fuel burn to limit the shift in centre of gravity where applicable. The 10% most promising design vectors in terms of fuel burn of an optimisation step were selected, followed by a selection of the design vector with the smallest centre of gravity shift during flight.

Regarding directional stability, Benad states that a positively swept wing with a moderately positive dihedral angle will be directionally stable, and that vertical surfaces behind the centre of gravity will increase this directional stability. Faggiano takes this one step further and determines the minimum yawing moment derivative, $C_{n_{\beta_{\text{min}}}}$, to be 0.0005 1/deg as in Equation 3.3 [3].

$$C_{n_\beta} \geq 0.0005 \tag{3.3}$$

Lateral stability is present when Equation 3.4 holds [54].

$$C_{l_\beta} \leq 0 \tag{3.4}$$

3.2.4. Noise, Emissions and Operator Requirements

Requirements for noise and emissions are often included. However, noise and emissions are not expected to vary significantly between individually optimised aircraft and aircraft family members. In addition, emissions are largely related to fuel burn which is included as the principal objective of the optimisation procedure. As such, noise and emissions are not be included as requirements in the family design optimisation process.

The operator might include several requirements on reliability, utilisation rate, lifetime or turnaround time. Despite the significance of these figures on the viability of the aircraft concept, it is considered outside

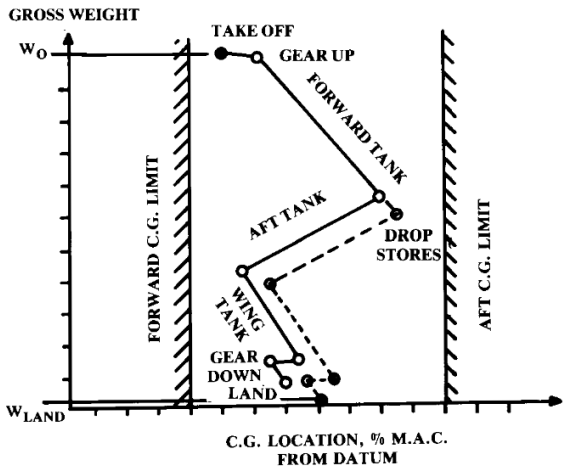

Figure 3.2: The location of the centre of gravity changes during flight, figure from Raymer [6].

the scope of this research to include it in a family design process. In addition, the results between individually optimised aircraft and aircraft family members are not expected to differ significantly.

Table 3.3: Constraints on the Flying-V (FV) aircraft family.

Description	Constraint			Value			Unit
				FV-800	FV-900	FV-1000	
Approach speed	V_{app}	$\leq$	$V_{app_{max}}$	140	140	147	kts
Passenger cabin floor	$S_{paxcabin}$	$\geq$	$S_{paxcabin_{req}}$	242	283	315	m^2
Total cabin floor	$S_{totalcabin}$	$\geq$	$S_{totalcabin_{req}}$	332	405	468	m^2
wingspan	b	$\leq$	b_{max}		65.0		m
Outer main gear wheel span	y_{mlg}	$\leq$	$y_{mlg_{max}}$		14.0		m
Engines lateral distance	y_{eng}	$\geq$	$y_{eng_{min}}$		5.0		m
Tail height	h_{tail}	$\leq$	$h_{tail_{max}}$		20.1		m
Longitudinal static stability	x_{sm}	$\geq$	$x_{sm_{min}}$		0.0		m
Directional static stability	C_{n_β}	$\geq$	$C_{n_{\beta_{min}}}$		0.0005		1/deg
Lateral static stability	C_{l_β}	$\leq$	$C_{l_{\beta_{max}}}$		0.0		1/rad

3.3. Parametrisation and Family Design Principle

In this section, the parametrisation of the Flying-V is presented, followed by a short description of the parametrisation of the reference aircraft. Then, the principle to design a family of aircraft is explained.

3.3.1. Flying-V Parametrisation

Research by Hillen provided a new parametrisation of the Flying-V, which is the basis to build upon in this research [55]. The parametrisation used in this research is visualised in Figure 3.3 and Figure 3.4. During optimisation of a single aircraft or a family of aircraft, variables indicated in green and red are varied whereas variables indicated in black are fixed. Fixed variables, such as the width of the cabin w_H, are not varied to limit the scope of this research and to enable comparison of the results with earlier Flying-V studies. Sections 4 and 5 on the Flying-V planform are airfoils described by CST coefficients.

3.3.2. Reference Aircraft Parametrisation

For the reference aircraft, no optimisation is performed, such that an elaborate parametrisation is not provided in this research. All dimensions follow from drawings by Airbus [5], except for the airfoils. The wing is described by three airfoils, using the NACA 0020 airfoil at the root, the NACA 2415 at the end of the yehudi and the 9% thick NASA/Langley Withcomb supercritical airfoil described by Faggiano [3] at the tip, of which the CST coefficients are provided in Table 3.4. The location of the airfoils is visualised in Figure 3.5, in which

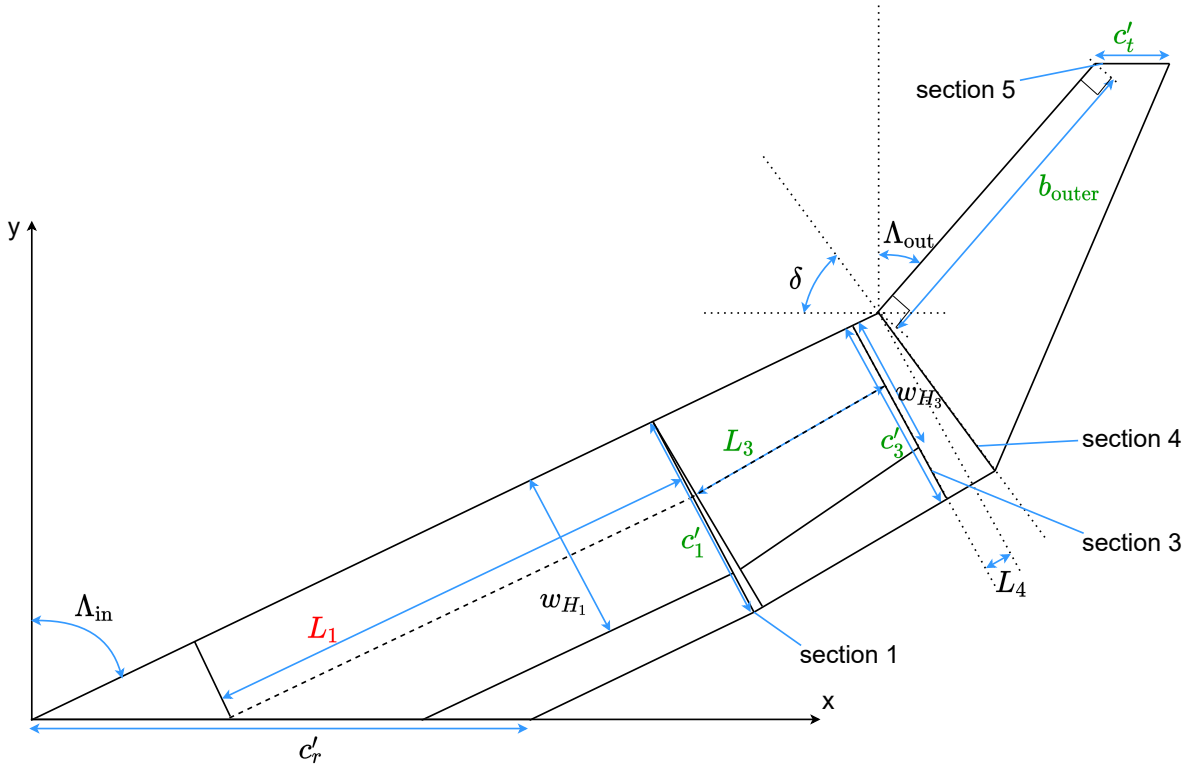

Figure 3.3: Parametrisation of the Flying-V planform. Fixed variables are shown in black and design variables in green. The unique variable between family members, L_1, is indicated in red. Fixed variables are explained in Table 3.8.

the dimensions are applicable to the Airbus A350-1000 [5]. Both the horizontal and vertical tail are modelled with the symmetrical NACA 0012 airfoil from root to tip.

This figure also indicates the fuselage beam of length L_{beam} for the reference aircraft, starting just aft of the nose of the aircraft and ending halfway the root chord of the vertical tail. The location with respect to the nose of the aircraft for the fuselage beam and component weight groups is provided in Table 3.5.

Table 3.4: CST coefficients for the tip airfoil of the reference aircraft wing.

	Bernstein coefficients
Upper	[0.1557, 0.0533, 0.1783, 0.0599, 0.1853, 0.2543]
Lower	[-0.1502, -0.1091, -0.0309, -0.3185, 0.0493, 0.2168]

3.3.3. Family Design Principle

The design of an aircraft family aims at a high level of commonality between aircraft family members. In Section 2.3.4 variable-based commonality metrics are described as the most efficient choice to ensure commonality in conceptual aircraft design. However, investigating the application of a variable-based commonality model to the specific problem at hand, its application is found rather limited. The only variable that can actually be scaled such that the benefits of commonality can be captured is the length of the untapered part of the fuselage L_1. Other variables, such as the width of the cabin or the outer wingspan, change a large number of structural components of the aircraft such that cost savings in development and production will probably be very limited. Variable-based commonality models do not include any information on cost or complexity of changing one variable instead of another, such that this manual selection of the scaling variable is considered the most viable option for this research.

As such, all variables indicated in green in Figure 3.3 and Figure 3.4 are set equal between aircraft family members, whereas only the length of the untapered cabin L_1 is allowed to be unique for each aircraft family

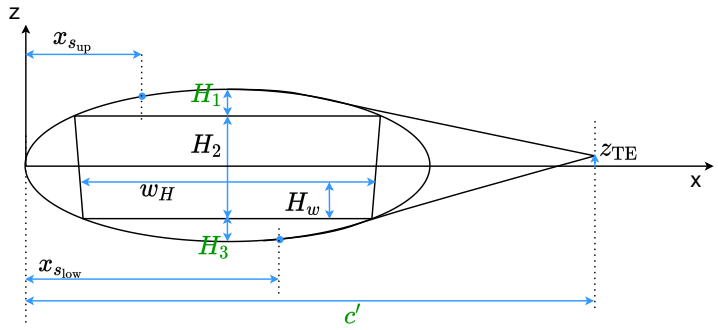

Figure 3.4: Parametrisation of a Flying-V cross-section, applicable to sections 1 and 3 on the Flying-V planform. Fixed variables are shown in black and design variables in green. Fixed variables are explained in Table 3.8.

Description	Variable	A350-900	A350-1000	Unit
Fuselage beam start	$x_{\text{fusbeam}_{\text{start}}}$	1.7	1.7	m
Fuselage beam end	$x_{\text{fusbeam}_{\text{end}}}$	58.4	65.4	m
Cockpit	x_{cockpit}	3.4	3.4	m
Passenger cabin start	$x_{\text{paxcabin}_{\text{start}}}$	5.0	5.0	m
Passenger cabin end	$x_{\text{paxcabin}_{\text{end}}}$	53.1	60.1	m
Front spar main wing	$x_{\text{spar}_{\text{front}}}$	23.0	27.5	m
Aft spar main wing	$x_{\text{spar}_{\text{aft}}}$	29.5	33.9	m
Landing gear nose	$x_{\text{LG}_{\text{nose}}}$	4.6	4.6	m
Landing gear main	$x_{\text{LG}_{\text{main}}}$	33.3	37.7	m
Horizontal tail half-chord	$x_{\text{HT}_{\text{c/2}}}$	56.2	63.2	m
Vertical tail half-chord	$x_{\text{VT}_{\text{c/2}}}$	58.4	65.4	m

Table 3.5: Dimensions of the reference aircraft, all in x-direction with respect to the nose of the aircraft as indicated in Figure 3.5.

member, indicated in red. However, this does not mean that the complete untapered part of the cabin is unique for every aircraft, since plugs are used to lengthen the cabin where required. As such, the thickness of all common fuselage structural members should be sufficient to carry the loads of the most heavily loaded aircraft family member. This is ensured by selecting the thickest structural member for every section of the fuselage from all aircraft variants.

The length of the fuselage plugs for the different aircraft variants is based on the difference in the total length of the fuselage of the aircraft as well as on the difference in engine and landing gear location. The landing gear location is determined as described in Section 4.3.4 and determines the location of the entire fuselage component it is connected to. Figure 3.6 visualises the common components between the aircraft variants, as well as plugs to lengthen the untapered part of the aircraft wing and the fuselage structure with the engine and landing gear attached. The smallest variant of the Flying-V imposes a constraint on the length of the tapered cabin part, since the engine should be attached to the untapered cabin to allow the insertion of frames aft of the engine for larger aircraft. Hence, the tapered cabin length L_3 is constrained at a maximum of 11 m.

The heaviest variants for the fin, landing gear, APU and outer wing are used on all aircraft family members. The weight of the systems, furniture and operational items is assumed to scale with input parameters such as the takeoff weight and cabin length and is therefore unique for each family member. The location of the nose gear and the size of the elevons are defined to be the same for all aircraft.

Commonality comes at the cost of decreased individual product performance with respect to an individually optimised product. For the aircraft family problem in this study, this penalty comprises two parts.

1. Penalty due to the selection of the heaviest variant or thickest structural member for the complete aircraft family.
2. Penalty due to the selection of common variables for the aircraft family, optimising design variables for a family of aircraft rather than for an individual aircraft.

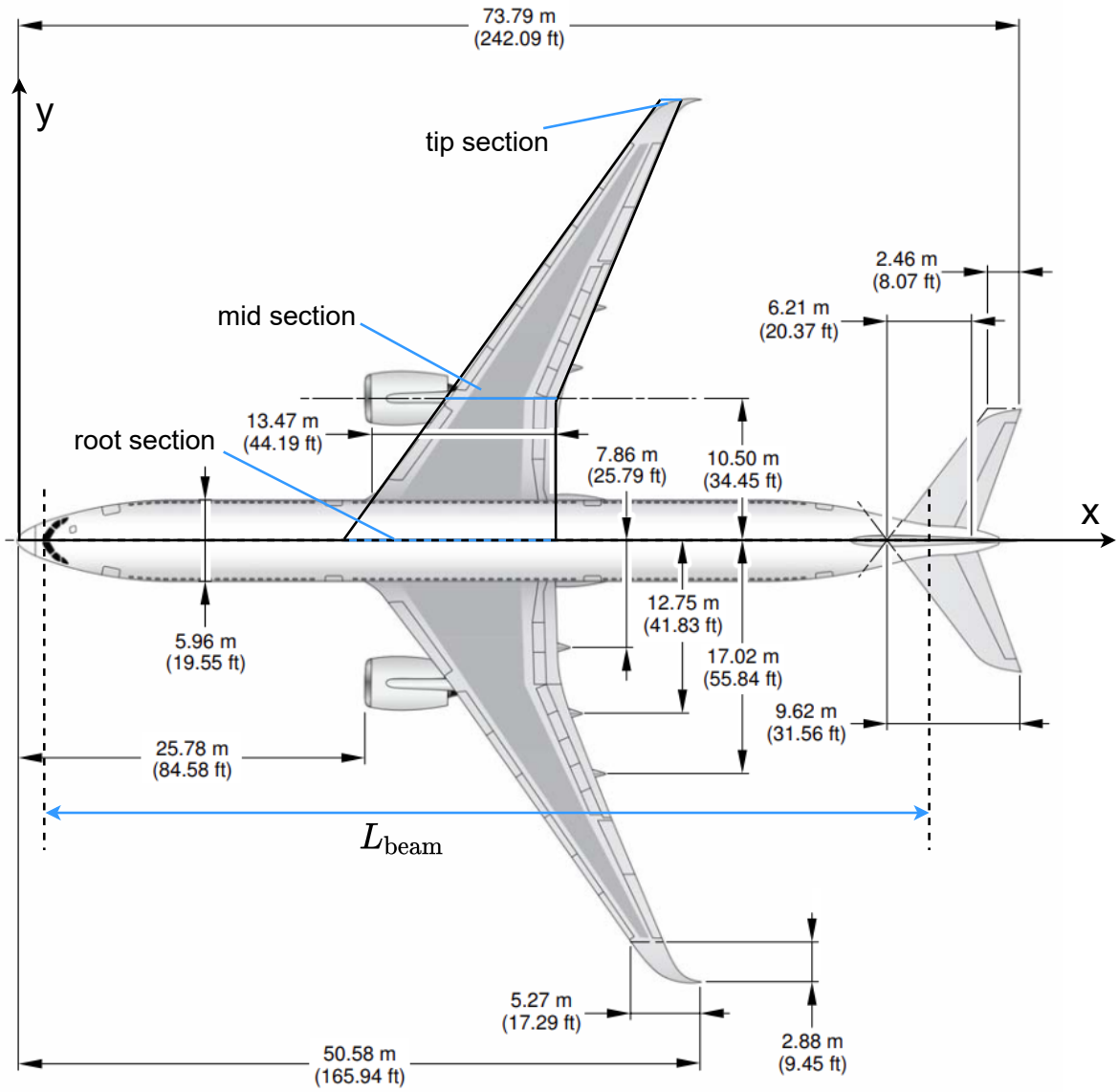

Figure 3.5: Parametrisation of the A350 reference aircraft. Adapted from Airbus.

The first penalty can be easily quantified by comparing equal aircraft designs with and without the constraint of using the heaviest component or thickest structural member. The second penalty is more difficult to assess, since this requires optimisation of individual aircraft to compare the aircraft family with. For the Flying-V aircraft family, both penalties are assessed in this research.

3.4. Optimisation Architecture

The optimisation architecture to optimise a single aircraft is visualised in Figure 3.7.

The inner loop is a multidisciplinary analysis (MDA) that converges towards the fuel burn of the aircraft. The MDA is assumed to be converged when the fuselage weight does not change with more than 1% between two iterations. Convergence is ensured by performing one extra iteration step after this condition is first reached, making sure that the difference between two subsequent iterations is still less than 1%. The aerodynamic analysis, weight estimation method and fuel burn analysis are described in Chapter 4. The outer loop optimises the different variables describing the aircraft as discussed in Section 3.3.3. In practice, optimising a family of aircraft is done in an iterative process consisting of two steps, as shown in Figure 3.8. The objective is to minimise the weighted fuel burn performance of the aircraft family members including a penalty p for

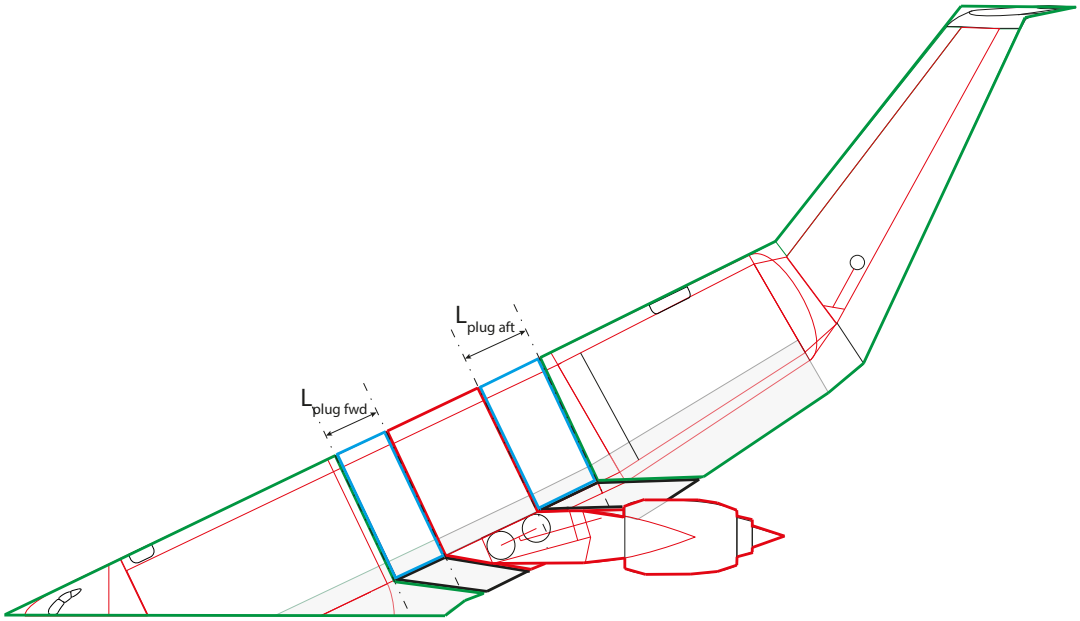

Figure 3.6: Components of each aircraft family member. Similar components (green), fuselage plugs (blue) and the moving section with the engine and landing gear (red). The floor plan and component locations are only indicative.

any violated constraint, as defined in Equation 3.5. For clarity, the constraints are separately shown on the XDSM. Please note that only the optimisation process is visualised, whereas in reality a variety of outputs is obtained from a converged optimisation process to study the characteristics of the optimised aircraft.

$$\min f(x) = \min_{x} \sum_{i}^{N} \frac{W_{\text{fuel}_i}(x)}{W_{\text{fuel}_{i_0}}} + p(x) \tag{3.5}$$

In this equation, the design vector x consists of all design variables of which the initial values are provided in Table 3.6.

Table 3.6: Initial values for the design variables of the aircraft family. The only unique variable for every aircraft variant is the length of the untapered cabin L_1.

	L_1	L_3	b_{outer}	λ	c_1'	c_3'	H_{1_1}	H_{1_3}	H_{3_1}	H_{3_3}
FV-800	18.75									
FV-900	23.75	11.1	15.33	0.15	1.16	1.21	0.6	0.6	0.7	0.6
FV-1000	28.75									

In each iteration, the principal design variables roughly describing the aircraft's planform are optimised, having a large impact on the aircraft's performance. This step is followed by an optimisation of the remaining design variables which describe the cross-section of the cabin or the chord length of the wing, having a smaller impact on the performance of the aircraft. Iterating between these two steps is done manually, limiting total computational time and ensuring feasibility of the design after each step. Note that both single aircraft and family of aircraft can be optimised during the process, to get a feeling of the impact of design variables on the performance of aircraft and to assess the cost of enforcing commonality between the aircraft family members.

The optimisation for the Flying-V aircraft family is performed for a family of two aircraft, consisting of the -900 and -1000 variant as competitors to the reference Airbus A350 family. No clear constraint on the range of the -800 has been defined since it lacks a reference aircraft, such that the range of the -800 follows implicitly from its available fuel tank volume.

The optimisation algorithm used to perform the smaller optimisation steps within the larger optimisation procedure is the Differential Evolution (DE) algorithm, implemented in SciPy [3] and described by Storn and

[3] https://docs.scipy.org/doc/scipy/reference/generated/scipy.optimize.differential_evolution.html [cited on 26-11-2020]

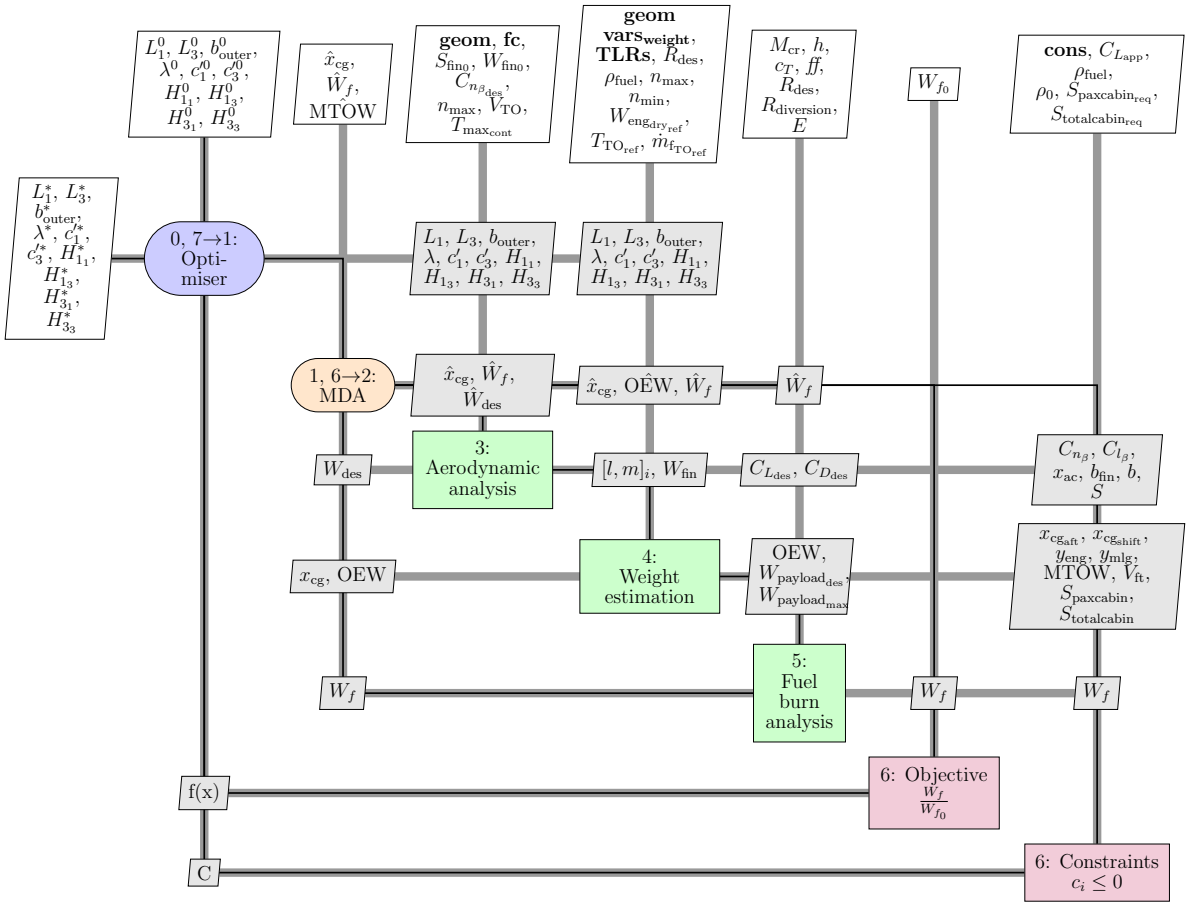

Figure 3.7: XDSM of the single aircraft optimisation method. **TLRs** are top-level requirements provided in Table 3.2, **cons** are constraint values provided in Table 3.3, **geom** are fixed variables describing the Flying-V shape provided in Table 3.8, **vars$_{\text{weight}}$** are inputs to the weight estimation model provided in Table 3.7 and **fc** are standard atmospheric conditions provided in Table 3.9.

Price [56]. This algorithm is expected to be the most efficient choice for the optimisation problem at hand, which is highly complex and does probably not respond to inputs in a way that would allow gradient-based optimisation. The differential evolution algorithm constructs a variety of design vectors and selects the most promising design vectors to be the seed of a new generation. This algorithm is capable of finding the global optimum. The SciPy implementation of the algorithm allows different mutation and crossover schemes, of which the default *best/1/bin* scheme is used. This scheme uses the *best* design vector of a generation and uses *one* vector difference to form the next generation of design vectors, as described in Equation 3.6. In this equation, F is a constant scalar setting, g is the generation index, i the vector index and r_1 and r_2 random indices between 0 and $p-1$. A *binomial* crossover scheme is used, instead of an exponential crossover operator. This binomial distribution means that a uniform crossover is employed.

$$x_{\text{i,g}} = x_{\text{best,g}} + F(x_{\text{r1,g}} - x_{\text{r2,g}}) \tag{3.6}$$

The SciPy implementation of the DE algorithm allows parallelisation of the optimisation, employing different workers to evaluate the objective. This largely speeds up the process on multi-core computers.

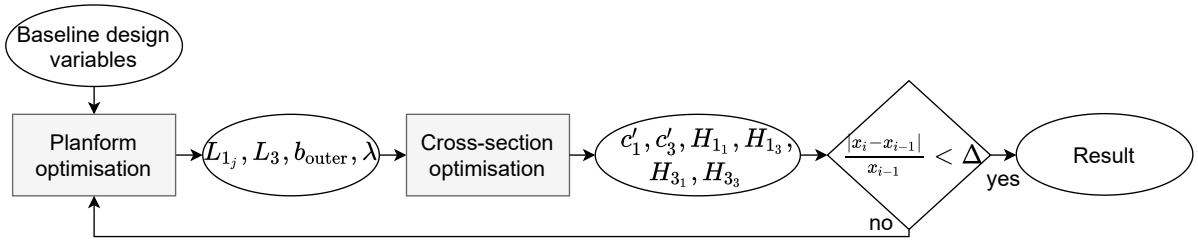

Figure 3.8: Family design optimisation procedure. j denotes the aircraft variant, indicating that only L_1 is a unique variable for family variants. i denotes the iteration number. The subscripts $_1$ and $_3$ refer to the untapered and tapered cabin part respectively.

Table 3.7: Input parameters for the weight estimation method applied in this research, including a reference to a section providing more information on the respective parameter and value.

	Parameter	Unit	Value	Explanation
Cargo doors	$n_{\text{cargo doors}}$	-	2	Section 3.2
Windscreen area	S_{ws}	m^2	2.3	Section 4.3.2
Minimum cabin height	$h_{\text{cabin}_{\text{min}}}$	m	1.9	Section 3.2
Number of cycles	n_{flights}	-	100000	Section 4.3.2
Cabin pressure differential	Δp_{cruise}	kPa	57.5	Section 3.2
Frame pitch	L_{frame}	m	0.635	Section 4.3.2
Minimum gage thickness	t_{gage}	m	$1.2 \cdot 10^{-3}$	Section 4.3.2
Modelled to actual weight factor	k_{MA}	-	1.2	Section 4.3.5
Safety factor	n_{safety}	-	1.5	Section 4.3.2
Weight reduction metal to composites	k_{MC}	-	0.2	Section 4.3.5
Front spar location outer wing	$\bar{x}_{\text{spar}_{\text{front}}}$	-	0.15	Section 4.3.3
Front spar location outer wing	$\bar{x}_{\text{spar}_{\text{aft}}}$	-	0.60	Section 4.3.3
Spanwise start location fuel tank outer wing	$\bar{y}_{\text{ft}_{\text{start}}}$	-	0.0	Section 4.3.3
Spanwise end location fuel tank outer wing	$\bar{y}_{\text{ft}_{\text{end}}}$	-	0.3	Section 4.3.3
Outer wing rib pitch	s_{rib}	m	0.6	Section 4.3.3
Dive velocity	V_{dive}	m/s	300	Section 4.3.2
Landing gear pitch angle	θ_{LG}	deg	17	Section 4.3.4
Landing gear strut length	$L_{\text{LG}_{\text{strut}}}$	m	5.5	Section 4.3.4
Landing gear wheel radius	$r_{\text{LG}_{\text{wheel}}}$	m	0.635	Section 4.3.4
Number of fuel tanks	n_{ft}	-	4	Appendix A
APU dry weight	W_{apu}	kg	417	Appendix A

Table 3.8: Fixed variables describing the geometry of the Flying-V. All variables are the same for all aircraft variants.

Description	Variable	Value	Unit
Length between inner and outer wing	L_4	1.0	m
Width at input height of section 1	w_{H_1}	6.2	m
Width at input height of section 3	w_{H_3}	5.8	m
Leading edge sweep of inboard wing	Λ_{in}	64.5	deg
Leading edge sweep of outboard wing	Λ_{out}	40.7	deg
Dihedral angle of trunk 4	Γ_4	-0.1785	deg
Dihedral angle of trunk 5	Γ_5	5.825	deg
Incidence angle of section 4	i_4	0.4	deg
Incidence angle of tip section	i_{tip}	-4.37	deg
Orientation angle of section 4	δ	52.6	deg
Cabin height at section 1	H_{2_1}	2.25	m
Cabin height at section 3	H_{2_3}	1.75	m
Arm-rest height at section 1	H_{arm_1}	0.6	m
Arm-rest height at section 3	H_{arm_3}	0.6	m
Vertical trailing edge position at section 1	z_{TE_1}	-0.3	m
Vertical trailing edge position at section 3	z_{TE_3}	-0.04	m
Upper curve starting location at section 1	$\bar{x}_{s_{up_1}}$	0.4	-
Upper curve starting location at section 3	$\bar{x}_{s_{up_3}}$	0.3	-
Lower curve starting location at section 1	$\bar{x}_{s_{low_1}}$	0.4	-
Lower curve starting location at section 3	$\bar{x}_{s_{low_3}}$	0.3	-
Upper curve coefficient at section 1	c_{up_1}	$1e^{-5}$	m^{-3}
Upper curve coefficient at section 3	c_{up_3}	$1e^{-5}$	m^{-3}
Lower curve coefficient at section 1	c_{low_1}	$2e^{-3}$	m^{-3}
Lower curve coefficient at section 3	c_{low_3}	$1e^{-4}$	m^{-3}
Upper Bernstein coefficients section 4	A_{u_4}	[0.088, 0.066, 0.21, 0.079, 0.24, 0.23]	-
Lower Bernstein coefficients section 4	A_{l_4}	[-0.13, -0.084, -0.031, -0.31, 0.069, 0.20]	-
Upper Bernstein coefficients section 5	A_{u_5}	[0.14, 0.068, 0.20, 0.078, 0.14, 0.29]	-
Lower Bernstein coefficients section 5	A_{l_5}	[-0.099, -0.084, -0.025, -0.39, 0.061, 0.17]	-

Table 3.9: Standard atmospheric conditions.

Parameter	Unit	Value
p_0	Pa	101,325
ρ_0	kg/m^3	1.225
T_0	K	288.15

4

Single Aircraft Performance Analysis

This chapter describes the method to analyse single aircraft performance, culminating in the fuel weight of a Flying-V or conventional aircraft for a given range and payload. First, the fuel burn analysis is described, followed by the aerodynamic analysis and weight estimation method. Finally, any differences within the method between the reference aircraft and the Flying-V will be discussed.

4.1. Fuel Burn Analysis

In this section, the fuel burn method and low-speed performance are discussed in detail. The fuel burn method integrates the aerodynamic and structural disciplines in order to determine the fuel burn for a given mission profile, following the model setup visualised in Figure 3.7. A fuel burn performance model requires an idea of engine performance, such that a short discussion on the applied engine model is provided first. Then, the to be flown mission is discussed, followed by the procedure to calculate mission fuel burn.

4.1.1. Engine Model

Determining the fuel burn for an aircraft for a given mission is largely dependent on engine performance. This section shortly describes the engine model used in this study.

The reference aircraft family uses the Trent XWB engine, using the -84 version on the A350-900 and the -97 version on the A350-1000. Engines with similar performance are placed on the Flying-V family, scaling down the dry weight of the engines proportionally to the takeoff weight with respect to the A350 family to account for the reduced takeoff weight of the Flying-V aircraft. The thrust-to-weight ratio of both reference aircraft is not exactly equal, such that the average ratio is used to calculate the dry engine weight for the Flying-V aircraft variants. Note that a fundamental assumption of this scaling is a similar thrust-to-weight ratio between the reference aircraft and Flying-V. A study into the conceptual design of the Flying-V including a thrust-to-weight ratio versus wing loading diagram is required to fully validate this assumption.

Table 4.1 summarises the most important characteristics of both reference engines, in which $\dot{m}_f$ is the fuel flow in kg/s. The specifications of the engines are obtained from the ICAO engine database [57]. The specific fuel consumption $c_{T_{\text{cruise}}}$ is hard to find since engine manufacturers often do not specify these figures publicly. As such, it assumed to be 14.0 N/N/s, which is slightly higher than 13.5 N/N/s claimed on Wikipedia[1] to account for non-ideal conditions during cruise, since engines often not continuously operate at their optimal design condition. Since this value is used both for the reference aircraft and the Flying-V, the exact accuracy of this coefficient is of limited importance when comparing fuel burn of both aircraft configurations.

4.1.2. Mission and Flight Profile

The Flying-V and reference aircraft are designed to perform a certain mission, transporting a certain amount of payload over some range. The mission requirements were presented in Table 3.2. An exemplary payload-range diagram is shown in Figure 4.1. In this study, aircraft are designed for point D, with design payload DPL and design range R_D. Some of the payload can be traded for range to achieve the maximum range R_M, or some range can be traded for payload to reach point H with maximum payload MPL. Note that these three

[1] https://en.wikipedia.org/wiki/Rolls-Royce_Trent [cited on 24-3-2021]

Table 4.1: Specifications of the Trent XWB engine variants, with TO indicating takeoff conditions.

		-84	-97
$T_{\max_{\text{con}}}$	kN	317.6	370
$T_{\max_{\text{TO}}}$	kN	374.5	430
$c_{T_{\text{cruise}}}$	N/N/s	14.0	14.0
W_{dry}	kg	7277	7550
$\dot{m}_{\text{fTO}}$	kg/s	2.819	3.498

points H, D and M are all at maximum takeoff weight, whilst ultimately the ferry range can be reached with a lower takeoff weight and filled fuel tanks.

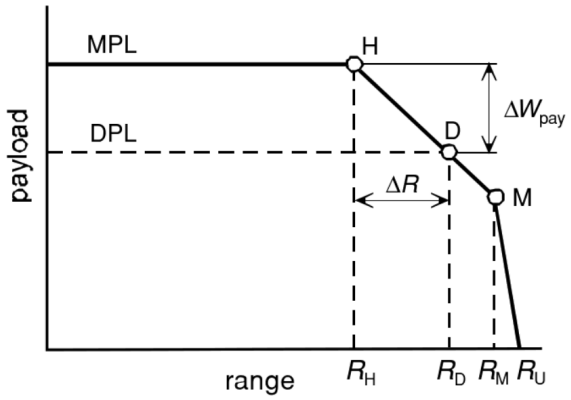

Figure 4.1: Notional payload-range diagram from Torenbeek [7].

For a given range, a flight profile can be constructed which specifies the distance flown and the altitude during flight. Figure 4.2 visualises a notional flight profile, including a diversion to an alternate airport and a loiter phase. Since the reserve fuel which is required to perform this diversion is a significant part of the MTOW and varies with MTOW, it cannot be neglected. The aircraft structure is sized for the maximum fuel weight, including the fuel weight from the diversion. In addition, the fuel volume is included as a constraint to make sure that the required fuel fits. After sizing the aircraft for the design mission, the harmonic range and ferry range are also assessed by assuming the same fuel capacity and adding or removing payload.

In this research, the aircraft is assumed to fly at a constant altitude during the complete cruise phase. In reality, the aircraft will not fly at a constant altitude, often applying a step-climb procedure, climbing in steps as the aircraft gets lighter during flight.

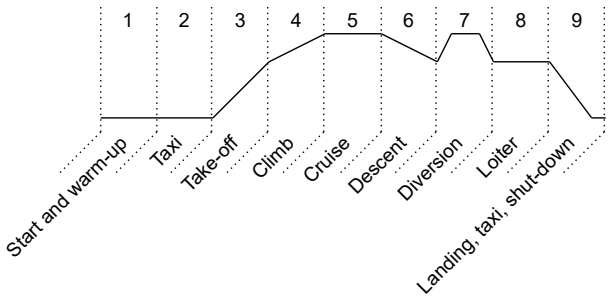

Figure 4.2: Generic flight profile for the Flying-V and reference aircraft.

4.1.3. Fuel Burn Model

The fuel weight is estimated using the so-called fuel fraction method. Fuel fractions describe the ratio between the start and end weight of the aircraft per mission segment. For most flight segments, the values for

transport jets provided by Roskam are used as described in Table 4.2 [11]. The distance flown during the take-off and climb segments is neglected. Since parts of the climb and descent segment will not be in the correct direction, e.g. climbing out or approaching an airport in a different direction than towards the departure or destination, this assumption seems fair. Torenbeek states that the descent and landing segment of a flight do not require any additional fuel compared to cruising the distance covered during these segments [7]. 5% reserve fuel is included to account for the diversion and loiter phases [3]. Taxiing and shutdown can be done using the reserve fuel. As such, the fuel fractions of these flight segments are not included in the total mission fuel weight.

For the cruise segment the Breguet range equation is used to calculate the fuel fraction, described in Equation 4.1 [58]. In this equation, the flight velocity V follows from the cruise Mach number as in Equation 4.2. The specific fuel consumption c_T is discussed in Section 4.1.1. The lift-to-drag ratio $\frac{L}{D}$ is determined using the aerodynamic model described in Chapter 4.2.

$$R = \frac{V}{c_T}\frac{L}{D}\ln\left(\frac{W_{5_{\text{start}}}}{W_{5_{\text{final}}}}\right) \tag{4.1}$$

$$V = M \cdot a = M \cdot \sqrt{\gamma RT} \tag{4.2}$$

The static temperature T follows from the cruise altitude, the atmospheric temperature lapse rate and the atmospheric temperature of 288.15 K at zero altitude. The atmospheric temperature lapse rate is $6.5 \cdot 10^{-3}$ K/m until an altitude of 11,000 m and above this altitude the temperature is constant until an altitude of 20,000 m. γ is the heat capacity ratio, which is 1.4 in dry air, and R is the specific gas constant which is 287 J/kg/K in air.

Table 4.2: Fuel fractions for all flight segments of a Flying-V or reference aircraft mission, taken from Roskam [11].

Mission segment	Fuel weight fraction
(1) Start and warm-up	0.990
(2) Taxi	0.990
(3) takeoff	0.995
(4) Climb	0.970
(5) Cruise	Breguet range equation
(6) Descent	0.990 (not included)
(7) Diversion	Included in reserve fuel
(8) Loiter	Included in reserve fuel
(9) Landing, taxi, shut-down	0.992

Once all fuel fractions have been determined, the takeoff weight of the aircraft is calculated using Equation 4.4. M_{ff} is the overall fuel fraction which is determined by multiplying all fractions of the individual flight phases.

$$M_{\text{ff}} = \prod_{n=1}^{9}\left(\frac{W_{n+1}}{W_n}\right) \tag{4.3}$$

$$W_{\text{TO}} = W_{\text{OEW}} + W_{\text{payload}} + (1 - M_{\text{ff}})W_{\text{TO}} \tag{4.4}$$

Equation 4.1 is used to determine the harmonic or ferry range of an aircraft, assuming the same velocity, specific fuel consumption and lift-to-drag ratio as were determined for the design range. In reality, a different payload weight could result in a different centre of gravity location, such that the static margin of the aircraft is changed resulting in a different lift-to-drag ratio.

4.2. Aerodynamic Analysis

This section describes the aerodynamic analysis. First of all, an applicable model type is selected based on several requirements. Then, the aerodynamic analysis procedure is described, including the sizing of the fins of the Flying-V and the viscous module to augment an inviscid aerodynamic model.

4.2.1. Aerodynamic Model Selection

Desired characteristics of the aerodynamic model employed in this family design study are the following.

- **Low computational cost**: the computational cost should be limited to allow a family design optimisation routine with many iterations using limited computational power.
- **Provide accurate lift-to-drag ratio**: the lift-to-drag ratio is one of the principal parameters in calculating fuel burn, which is the main objective of single aircraft optimisation within the family design routine.
- **Provide lift and moment distribution**: an important input to the structural weight estimation method is the lift and moment distribution over the wing.
- **Allow high Mach numbers**: the Flying-V and reference aircraft fly at approximately Mach 0.85 in cruise, such that the aerodynamic model preferably would be used in the transonic regime.
- **Provide stability derivatives**: in order to incorporate constraints on the stability of the aircraft, stability derivatives should be obtained.

As is the case in any model, the selection of a flow solver is a trade-off between accurate results and computational cost. The aerodynamic model should be sensitive to the design variables which are varied between aircraft family members, but does not need to be completely accurate in e.g. the drag distribution over the wing. Regarding drag, the lift-to-drag ratio during cruise is the only parameter that should be accurately estimated. Note that the Flying-V model is approximated by estimating only the contributions to lift of the wing-fuselage structure and the contributions to drag of the wing-fuselage structure, pylons and engines, neglecting the contribution of the fins. Inclusion of the fins would yield both a higher lift coefficient and an increased viscous drag, such that this assumption has little effect on the total lift-to-drag ratio. Reference studies such as by Faggiano et al. or Rubio Pascual and Vos also neglect the fins [9, 59].

A variety of aerodynamic models is available, ranging from very simple lifting-line models converging in a few seconds to complete computational fluid dynamic models taking multiple days to reach a solution. In the following, different types of aerodynamic model types are discussed shortly, which are all considered to be fast enough for use in an optimisation procedure. In Section 3.1 the ParaPy framework has been discussed which is used throughout this research. As such, within the optimisation procedure only models available within this framework are considered and their applicability is discussed.

Lifting Line Methods

Lifting line methods use the Prandtl lifting line theory, using horseshoe-shaped vortices to represent a lifting surface. The interested reader is referred to Anderson introducing the underlying principles as well as the method itself [53]. The lifting line method has low accuracy and as such comes at a limited computational cost. A well-known solver which includes the lifting line method is XFLR5[2], which is discussed later under quasi three-dimensional solvers in more detail. Within the ParaPy framework, no lifting line methods are readily available.

Vortex Lattice Methods

Vortex lattice methods (VLMs) are essentially an extension of the lifting line method by using a series of lifting lines. VLMs model a lifting surface as a sheet of horseshoe vortices and employ the principle that the normal component of the induced velocity on any point of this surface should be zero, since no flow crosses the lifting surface. Figure 4.3 visualises this method, placing vortices on the quarter-chord length of each panel and defining control points at 75% chord length of each panel. Note that several chordwise panels can be used at every spanwise position. The Biot-Savart law is applied to find the induced velocity on the control points, leading to a system of equations that can be solved for the strengths of all vortices [53]. Note that VLMs are inviscid, such that a separate analysis is required to account for viscous effects. VLMs work under the assumption of thin surfaces and small angles of attack.

The Athena Vortex Lattice (AVL) method is an example of such a vortex lattice method, developed at MIT by Drela and Youngren[3] [60]. AVL is supported by the ParaPy framework. AVL can be used to find the lift and moment distribution over lifting surfaces and is limited to low Mach numbers and thin surfaces. Furthermore, the method allows trimming of the aircraft by defining its control surfaces and the trim condition to be

[2] http://www.xflr5.tech/xflr5.htm [cited on 22-9-2020]
[3] http://web.mit.edu/drela/Public/web/avl/ [cited on 22-9-2020]

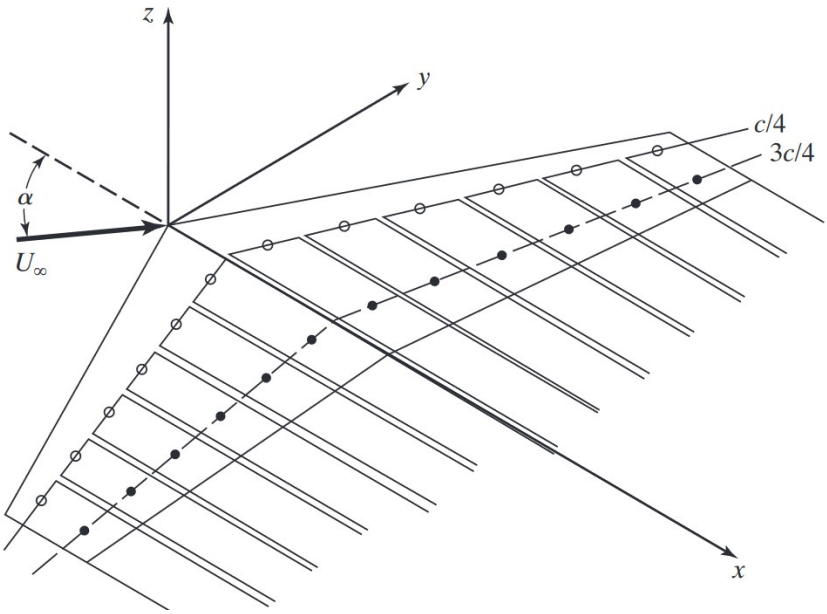

Figure 4.3: Distribution of horseshoe vortices over a thin surface in a vortex lattice method ([8], p.391).

fulfilled. AVL allows computation of stability derivatives when the mass distribution of the vehicle is provided. Unfortunately, both the original article by Drela and the user guide of the program do not discuss the way AVL performs this calculation, which is probably done using a finite-difference scheme or a direct method. Drela discusses both methods in a section on VLMs in his book, but does not discuss which is used by AVL [61]. The direct approach means that the force and moment equations are implicitly differentiated with respect to the various parameters using the chain rule. This is possible because both the vorticity and induced velocity have a simple dependency on these parameters. Examples of studies employing AVL to perform stability analyses do not mention the way AVL computes these derivatives either [62–65]. Personal correspondence with Drela learns that the direct method is used in AVL. Being an inviscid solver, AVL is more accurate on derivatives that are not largely influenced by viscous effects such as C_{l_p} and C_{n_p} [62]. Since AVL is a VLM, it costs only a few seconds to run. Note that earlier Flying-V research by Faggiano et al. uses AVL to quickly investigate whether a certain design vector is feasible, and uses SU2 to optimise feasible design vectors further and to confirm the design vector is indeed promising.

Quasi Three-Dimensional Solver

Building upon the vortex lattice method AVL, Q3D has been developed at Delft University of Technology by Mariens, Elham and Van Tooren [66]. Q3D is supported by the ParaPy framework. Q3D is a so-called quasi three-dimensional solver. Its main principle is combining a three-dimensional vortex lattice method (AVL) with a 2D airfoil model (e.g. XFoil[4]) to augment the inviscid three-dimensional results of AVL with the viscous drag approximation of the 2D airfoil model. The main incentive to develop this solver was the need for a quick aerodynamic model in an MDO environment providing not only lift and moment but also drag. According to the authors, a designer "would like to have a tool that is fast, accurate, design sensitive, suitable to support optimisation, and can evaluate a wide range of different wing shapes" ([66], p. 547). The model is mainly developed for clean wings in cruise conditions without any high lift devices deployed. The 2D airfoil analysis models included in Q3D are XFoil, VGK and MSES. XFoil is used for the low-speed regime, whereas VGK and MSES are used for the higher speed regimes. Note that XFoil is the fastest tool amongst these models, whereas MSES is the slowest since it solves the Euler equations. Q3D was validated using MATRICS-V, a higher-fidelity solver using a full potential flow model and a viscous unsteady integral boundary layer formulation. Unfortunately, Mariens et al. do not discuss the accuracy of MATRICS-V. On a 3.16 GHz processor and 4GB RAM computer, Q3D takes approximately 20 seconds to evaluate one lift coefficient value for the Fokker 50 wing in the subsonic regime and 30 seconds using VGK or 100 seconds using MSES in the transonic regime [66]. Note that MATRICS-V takes 180 and 300 seconds respectively for these cases. Q3D has been developed in

[4]https://web.mit.edu/drela/Public/web/xfoil/ [cited on 22-9-2020]

conjunction with EMWET, which was discussed in Section 4.3.3. Interestingly enough, results obtained with VGK were found to be more accurate than MSES in the transonic regime. Q3D was found to overestimate the lift coefficient in transonic flow (regardless of the 2D solver used). The overall error is no more than 2% compared to MATRICS-V (for a free-stream Mach number smaller than the drag divergence Mach number), which is considered really accurate given the large reduction in computational time.

XFLR5, another hybrid solver allowing usage of several 3D models coupled to XFoil, is limited to Mach numbers below 0.7 given the fact that XFoil is limited to the subsonic regime [67]. It is not supported by the ParaPy framework, but is discussed as a reference for Q3D. XFLR5 offers a lifting line model, a vortex lattice method and a 3D panel method. XFLR5 was found to be most accurate when using the vortex lattice method[5], making it largely comparable to Q3D with the latter being more suitable for the transonic regime. As such, XFLR5 is deemed less suitable for application in studying the transonic Flying-V family.

Selecting a Flow Solver

Since computational cost and ease of integration within the existing ParaPy framework are deemed very important characteristics of the chosen flow solver, only relatively fast and ParaPy-integrated models are considered. Of these models, AVL is considered the best choice. Regarding the described desired characteristics of the aerodynamic model, the only characteristic it lacks is the allowance of high Mach numbers. Being a comparative study between different aircraft designs and requiring mainly a lift and moment distribution and lift-to-drag ratio, this aspect is considered less relevant than computational cost, on which AVL scores best. Adopting AVL as aerodynamic model requires a separate viscous module, which is discussed in Section 4.2.2.

4.2.2. Aerodynamic Analysis Procedure

Within this research, AVL is evaluated in the incompressible regime at Mach 0.3. The wing is described by five spanwise airfoils located at the root, tip and at intermediate sections including the trailing edge and leading edge kink of the Flying-V wing. The elevons described by Cappuyns on the outer wing are used to trim the aircraft [29]. The winglets of the Flying-V are neglected, as shortly described in Section 4.2.1. By including a wingspan up to the limit of 65 m for the largest aircraft variant and neglecting the engines, this assumption is assumed fair.

In the following, the procedure to find the maximum lift-to-drag ratio is described, followed by a discussion on the viscous module and the fin sizing procedure.

Maximising the Lift-to-drag Ratio

The maximum lift-to-drag ratio of the aircraft is determined based on its lift-drag polar. The drag coefficient and lift coefficient are related as in Equation 4.5, in which A is the aspect ratio which is calculated using Equation 4.6. The zero-lift drag coefficient C_{D_0} is determined using the viscous module resulting in Equation 4.9.

$$C_D = C_{D_0} + \frac{C_L^2}{\pi A e} \tag{4.5}$$

$$A = \frac{b^2}{S} \tag{4.6}$$

The Oswald efficiency factor e is found by running AVL at an estimated design lift coefficient $C_{L_{\text{des}}}$ and solving Equation 4.5 for this condition. As shown in Figure 3.7, the design cruise weight W_{des} is iteratively determined within the MDA loop. g is the gravitational acceleration which is 9.80665 m/s^2.

$$C_{L_{\text{des}}} = \frac{W_{\text{des}} g}{\frac{1}{2}\rho V^2 S} \tag{4.7}$$

The maximum lift-to-drag ratio can be determined by taking the derivative of the lift-to-drag ratio and equating this to zero, resulting in Equation 4.8.

$$\left(\frac{C_L}{C_D}\right)_{\text{max}} = \frac{1}{2}\sqrt{\frac{\pi A e}{C_{D_0}}} \tag{4.8}$$

[5] http://www.xflr5.tech/docs/Results_vs_Prediction.pdf [cited on 22-9-2020]

Viscous Module

In order to account for viscous effects in a non-viscous aerodynamic model, a viscous module can be added to augment a fast computational inviscid method. Faggiano et al. developed such a viscous module for the Flying-V, neglecting lift-related profile drag but accounting for skin friction and pressure drag [9]. Note that the assumption to neglect lift-related profile drag has been validated by Faggiano et al. The principle idea of this viscous module is to address both the skin friction and pressure drag, C_{D0}, by Equation 4.9, in which C_f is the flat-plate skin-friction coefficient, f the form factor of a given component, S the reference area and S_{wet} the wetted area. For every component, C_f and f need to be determined.

$$C_{D0} = C_f \cdot f \cdot \frac{S_{\text{wet}}}{S} \tag{4.9}$$

For the Flying-V, the total zero-lift drag coefficient is estimated by summing the contributions of the wing, engine nacelles and pylons resulting in Equation 4.10. Lift and drag of the fins are neglected as explained in Section 4.2.1.

$$C_{D_0} = C_{D_{0_{\text{wing}}}} + C_{D_{0_{\text{pylons}}}} + C_{D_{0_{\text{nacelles}}}} \tag{4.10}$$

The zero-lift drag coefficient of the pylons $C_{D_{0_{\text{pylons}}}}$ is estimated to be $3 \cdot 10^{-4}$ based on the study by Bourget [31]. For the nacelles of the engines, the form factor is provided by Raymer [6] in which d is the diameter of the nacelle and l its length.

$$f_{\text{nacelle}} = 1 + 0.35\frac{d}{l} \tag{4.11}$$

For the wing, the form factor is calculated using Equation 4.12. $\Lambda_{0.5h}$ is the half-chord sweep angle of the lifting surface.

$$f_{\text{wing}} = 1 + \left(2.7 \cdot \frac{t}{c} + 100 \cdot \left(\frac{t}{c}\right)^4 \cos^2(\Lambda_{0.5})\right) \tag{4.12}$$

The skin friction coefficient C_f for turbulent flow, which is used due to the transonic conditions the Flying-V flies at, is given in Equation 4.13 in which Re is the Reynolds number.

$$C_f = \frac{0.455}{(\log_{10} Re)^{2.58}(1 + 0.144M^2)^{0.65}} \tag{4.13}$$

Fin Sizing

Considering aircraft family design optimised for individual fuel burn performance and family commonality, driving factors are expected to be the weight, size and location of the main components of the aircraft. Estimation of the fin size is therefore considered rather important, whereas control surface sizing is deemed outside the scope of this research. As such, static stability is imposed as a requirement and the fin sizing procedure of Faggiano [3] is adopted. Faggiano sizes the fins to meet three requirements which follow from the three main functions every tail surface should fulfil according to Obert [68]. These requirements are the following:

- **Directional static stability**: this means that C_{n_β} should be positive.
- **One engine inoperative condition at takeoff**: in this condition, the required rudder deflection should not exceed 20 degrees.
- **Landing in maximum crosswind condition**: in this condition, the required rudder deflection should not exceed 20 degrees.

The yawing moment derivative for the fin-less aircraft C_{n_β} is estimated using AVL. The contribution of the fins to this coefficient can be found in any handbook, such as in Torenbeek [69].

$$C_{n_{\beta_v}} = C_{L_{\alpha v}} \left(1 + \frac{d\sigma}{d\beta}\right) \frac{q_v}{q} K_{FV} \frac{S_v l_{x_v}}{Sb} \tag{4.14}$$

In this equation, $\frac{d\sigma}{dv}$, $\frac{q_v}{q}$ and K_{FV} are to account for different flow conditions at a tail surface due to the presence of the wing. These are neglected for the Flying-V fins, which are assumed to be free of these effects. S_v is the area of the vertical surface and l_{x_v} is the moment arm of the surface. The empirical relation

by Raymer is used to determine $C_{L_{\alpha_v}}$. The required rudder deflection δ_r for the asymmetric thrust case is provided by Sadraey as in Equation 4.15 [70].

$$\delta_r = \frac{T_{max} \cdot l_{engine}}{C_{n_{\delta_r}} qSb} < 20^\circ \tag{4.15}$$

In which the rudder deflection derivative is described in Equation 4.16.

$$C_{n_{\delta_r}} = -C_{L_{\alpha_v}} \frac{S_v l_{x_v}}{Sb} \frac{q_v}{q} \tau_r \frac{b_r}{b_v} \tag{4.16}$$

The rudder angle of attack effectiveness parameter τ_r is dependent on the ratio between the chord of the rudder and the chord of the fin, which is e.g. 0.52 for a ratio of 0.3.

$$\delta_r = -\frac{C_{n_\beta} \beta}{C_{n_{\delta_r}}} < 20^\circ \tag{4.17}$$

The fin surface area is minimised with its aspect ratio, taper ratio and sweep angle as design variables and given the constraints on rudder deflection and yawing moment derivative. The optimisation tends to converge to a very high sweep angle and a low taper ratio, since this is beneficial for the described constraints. However, this does not necessarily result in an optimal weight. As such, Faggiano includes tight bounds on these variables to make sure that the design is feasible in non-aerodynamic disciplines.

Since this research is not a pure aerodynamic optimisation, the objective is improved with respect to Faggiano by including the fin weight in the objective function. The fin weight and wing area are equally weighted in the objective function, normalising both parameters by an initial estimation of the respective parameter and adding the two normalised results, as in Equation 4.18. The fin weight is estimated using the approach described in Section 4.3.3.

$$\text{objective} = \frac{S_{\text{fin}}}{S_{\text{fin}_0}} + \frac{W_{\text{fin}}}{W_{\text{fin}_0}} \tag{4.18}$$

4.3. Weight Estimation Method

In this section, the method to estimate aircraft weight is explained. A generic description of the setup of the method is provided, followed by detailed explanations of the various parts within the method.

4.3.1. Weight Estimation Method Setup

A weight estimation method should have multiple characteristics for application in a conceptual aircraft family design methodology.

- **Low computational cost**: as for all disciplines, its computational cost should be low. The time to estimate the weight of an aircraft should be in the order of seconds, preferably less.
- **Estimate weight per component or module**: the weight of different components should be known, to allow estimation of the centre of gravity and subsequent analyses on stability or control.
- **Sensitivity to family design variables**: the results should vary between the different members of an aircraft family to allow distinction between them.

To estimate weight per component or module requires at least a Class II weight estimation method. Class I weight estimation methods estimate the weight on the level of operating empty weight (OEW), maximum takeoff weight (MTOW) and maximum zero-fuel weight (MZFW), which is a too coarse level, especially considering the requirement on the estimation of weight per component or module to determine the centre of gravity and perform subsequent stability analyses.

Weight estimation methods vary from simple empirical relations to detailed FEM analyses. FEM analyses are considered too detailed and have a too high computational cost for this research, not complying with the first requirement on the weight estimation method. Several empirical methods exist, of which the GD (General Dynamics) method and the methods of Raymer, Torenbeek and Roskam are well known and applied often. These methods are known as Class II weight estimation methods, which is most suitable for the level of detail of this research. Several studies into Class II weight estimation methods have been performed and many studies using a weight estimation method shortly discuss the differences between the different

options available. For instance, Decloedt has studied the effect of relaxed static stability using the Initiator model developed at Delft University of Technology [71]. Comparing different Class II weight estimation methods, Decloedt concludes that "overall Torenbeek's method delivers the most consistent results." ([71], p. 48) The GD-method and Raymer's method were found to underestimate the MTOW, whereas the method of Torenbeek slightly overestimates the MTOW. The margin of error of Torenbeek's method was determined to be approximately 5%, which is considered acceptable for preliminary design studies. Several studies into BWB designs and oval fuselages use the Torenbeek method as well, such as research by Vos and Hoogreef or Vos and Roelofs [72, 73]. These studies, amongst others, augment the Torenbeek method by the method of Howe for BWB aircraft as described by Howe in 2001 [74]. For BWB designs, the method of Howe is used by several studies such as by Okonkwo [75] and Brown and Vos [76].

A hybrid approach combining structural analysis of a component and empirical relationships is the so-called semi-analytical approach. For instance, at Delft University of Technology a series of studies has been performed into oval fuselages, following a semi-analytical approach. The oval fuselage has been first introduced by Vos et al. in 2012, who used very simple analytical equations to estimate the weight of such an oval fuselage [22]. In 2013, this was taken a step further by Hoogreef and Vos introducing a semi-analytical method to estimate the weight of oval fuselages. This method was further enhanced by Schmidt and Vos in 2014 [77]. Later, this research was continued by Elmendorp et al. and Roelofs and Vos, mainly increasing the complexity of the model and incorporating composites as a possible material [73, 78]. The research culminated in a surrogate model for composite structures.

The principal difference between the Flying-V and conventional aircraft is the application of an oval fuselage which also fulfils the wing function providing a significant amount of the total aircraft lift. The systems, operational items, landing gear, engine, cabin provisions and payload items do not differ much from conventional aircraft configurations. To limit computational effort and to ensure simplicity of the weight estimation method, the weight of these elements is estimated using empirical relations. The Class II weight estimation method of Torenbeek is augmented by the method of Howe to account for BWB-like structures in the Flying-V. Since no simple empirical relation exists for the complex oval fuselage structure of the Flying-V, a more detailed approach such as the semi-analytical approach is used. The complexity of Elmendorp and Roelofs is not considered necessary for this conceptual research, selecting Schmidt as the principal model to build upon. The model of Schmidt allows sizing of all primary structural members and offers great flexibility in changing loads on all members and altering any component's sizing procedure. It has a much higher level of detail than the initial oval fuselage weight estimation studies by Vos et al., but still has a very limited computational cost.

The outer wing of the Flying-V can be seen as a generic aircraft wing, not including a fuselage structure. As such, conventional methods can be used to estimate the weight of the outer wing of the Flying-V as well as the weight of the wing of the conventional reference aircraft. Since the wing weight forms a large part of the total weight of an aircraft and is largely influenced by the weight and location of the fuel and engine it possibly holds, a more sophisticated method than a simple empirical relation is used. EMWET is a method that allows a quick calculation of an aircraft's wing weight based on the loads acting on the wing, including both aerodynamic loads and loads resulting from fuel or engines. It was developed at Delft University of Technology by Elham [79]. EMWET is a quasi-analytical method that sizes the wing box at spanwise sections to ensure it is able to withstand all loads, and augments this analytical method with empirical relations to estimate secondary weights. The total wing weight of several aircraft has been assessed and shows consistently a smaller error than 2%. EMWET has a very high computational efficiency, taking only a few seconds to run on a standard computer.

The actual geometry of a Flying-V is hence modelled as a combination of simplified components. The validity of this approximation needs to be checked in later design stages, for example by performing a complete FEM analysis of the structure. Figure 4.4 visualises the different weight estimation methods employed on the planform of the Flying-V. The outer wing is investigated using EMWET, whereas the inner wing weight is estimated using the semi-analytical oval fuselage weight estimation method, using an empirical relation for the inboard wing parts which are not part of the fuselage. The so-called symmetry parts are not modelled, since a part of equal dimensions is included double in the oval fuselage weight estimation method, as indicated by overlapping parts. Note that the spars of the outer wing do not align with the oval fuselage structure of the inner wing, which is a direct result of the assumption to model the geometry of the Flying-V as a combination of simplified and separate components.

The takeoff weight W_{TO} of the aircraft is described in Equation 4.19. The operating empty weight W_{OEW}

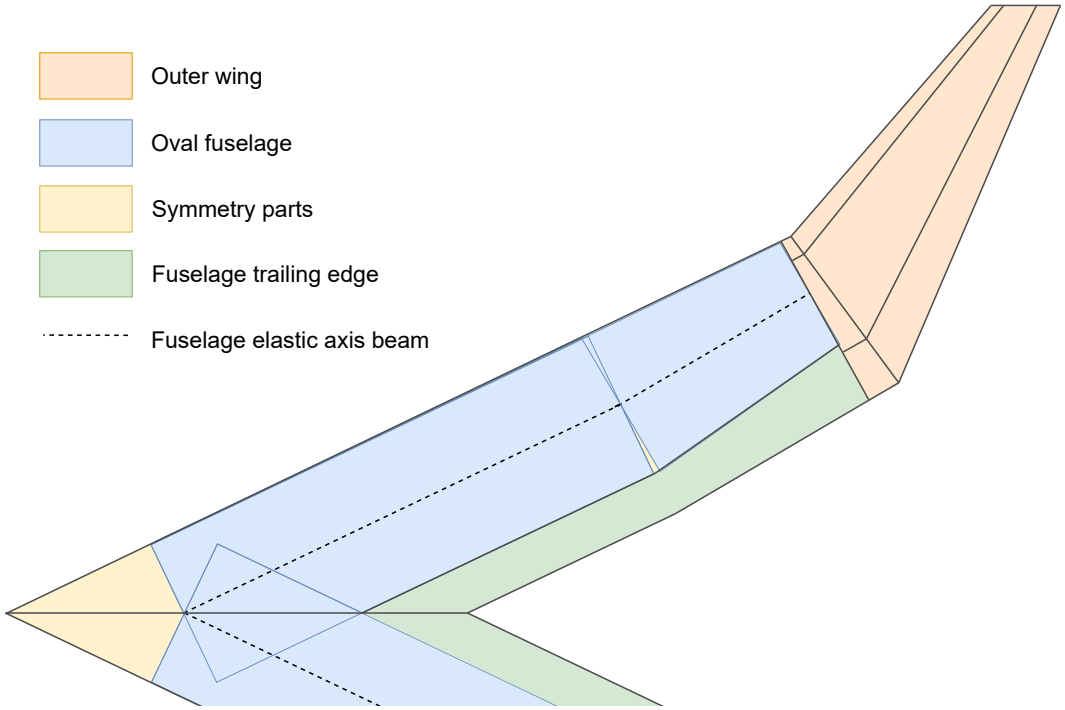

Figure 4.4: Weight estimation methods applied to estimate the wing and fuselage weight of the Flying-V.

is the sum of many component weight groups as described in Equation 4.20, in which the structure weight $W_{\text{structure}}$ is calculated using Equation 4.21.

$$W_{\text{TO}} = W_{\text{OEW}} + W_{\text{payload}} + W_{\text{fuel}} \tag{4.19}$$

$$W_{\text{OEW}} = W_{\text{structure}} + W_{\text{LG}} + W_{\text{propulsion}} + W_{\text{oper items}} + W_{\text{furniture}} + W_{\text{systems}} \tag{4.20}$$

$$W_{\text{structure}} = W_{\text{fuselage}} + W_{\text{outer wing}} + W_{\text{fins}} \tag{4.21}$$

The following sections describe the methods and empirical relations applied to estimate these weight groups in more detail.

4.3.2. Fuselage and Inner Wing Weight Estimation

To estimate the weight of the oval fuselage of the Flying-V the oval fuselage weight estimation of Schmidt et al. is taken as a basis [77]. However, this weight estimation method requires significant changes in order to make it suited for the weight estimation of the Flying-V fuselage. Principal differences between the oval fuselage of Schmidt et al. and this study are the fact that the fuselage also performs the wing function, providing the major part of the lift of the aircraft, its sweep angle and the fact that there are two fuselages. The sweep angle of the fuselage means that the aerodynamic moment does not only translate into a bending moment, but also into torsion around the elastic axis of the fuselage. Furthermore, the fact that there are two fuselages means that the bending moment at the start or root of the fuselage is non-zero, whereas in the BWB configuration of Schmidt et al. the bending moment of the fuselage should be zero both at the first and last section of the fuselage.

The principal idea of the oval fuselage weight estimation method is to model the fuselage as a beam through the elastic axis of the fuselage. This beam has already been shown in Figure 4.4. Along this beam, the fuselage is discretised into perpendicular sections such as the section shown in Figure 4.5. Possible moments introduced within the beam due to the slight kink at the start of the tapered cabin section are neglected; only the bending moment, torsion and shear force are considered. For each section, the longitudinal, lateral, transverse and pressure loads are calculated for ten load cases. Finally, the thickness of the various components is estimated based on several criteria. In the following sections, these steps are explained in detail.

Loads

First of all, the loads acting on the various structural members should be determined. In the following sections, the load cases and loads in longitudinal, lateral, transverse and hoop direction are discussed.

When sizing the primary structure, a variety of load cases should be considered. In the preliminary design phase of this research, a total of ten load cases is considered as described in Table 4.3. In detailed design, the number of load cases will be much higher. The load cases studied in this research comprise combinations of the maximum and minimum load factor, pressurisation and fuel mass during the cruise condition. In all these cases, the aircraft is assumed to be fully loaded with passengers. The maximum and minimum load factor are 2.5 and -1.0 respectively. For both landing load cases, the landing gears exert a high point load on the aircraft resulting from a hard landing. The landing gear is assumed to provide a certain fraction of the upward force. Schmidt sets this fraction to 0.5 [80]. As such, at a load factor of 2.5 this would mean that the landing gear has to withstand 125% of the takeoff weight, with the remaining 125% of the upward force provided by the aerodynamic forces. In all cases, a safety factor of 1.5 is applied. Pressurisation is explained in Section 3.2.

Table 4.3: Load cases for the Flying-V and reference aircraft.

Load case	Fuel mass	Pressurisation	Load factor
1	Max	Max	Max
2	Min	Max	Max
3	Max	Max	Min
4	Min	Max	Min
5	Max	0	Max
6	Min	0	Max
7	Max	0	Min
8	Min	0	Min
9	Min	0	Min, landing
10	Min	0	Max, landing

As has been shown in Figure 4.4, the fuselage is modelled as a beam along its symmetry axis. The fuselage beam is assumed to be clamped at its root at its connection to its symmetrical counterpart. Since the aircraft is symmetric along its longitudinal axis, the shear force is zero at the root of both fuselage beams when the aircraft is in steady symmetric flight. The bending moment and torsion are zero at the clamped root of both fuselage beams. Examples of point loads are the weight of the engine and the resultant of the lift and weight of the outer wing. Examples of moments are the bending moment component of the aerodynamic moment and the moment stemming from the resultant force of the outer wing around the inner wing tip section.

Aerodynamic loads are calculated by AVL as described in Chapter 4.2. The results are the sectional lift and moment in streamwise direction. The aerodynamic forces are converted to the fuselage beam in two steps. First, the aerodynamic moment is calculated around the elastic axis of the fuselage for each respective streamwise section. Then, the aerodynamic moment is decomposed into the bending moment and torsion around the fuselage elastic axis as shown in Figure 4.5.

The lift and weight of the outer wing are also contributing to the bending moment and torsion of the fuselage and are applied at the last section of the fuselage. Figure 4.5 visualises an indicative position for both the lift and weight and their respective moment arm to the elastic axis and to the last section of the fuselage. Note that the kink in the fuselage beam is neglected; no moment or force resulting from this kink is included in the model.

Once the bending moment is known along the fuselage beam, the maximum stress in the different structural members can be determined using Equation 4.22. In this equation, Δz_{max} is the maximum distance of the member with respect to the centroid of the section and I is the members moment of inertia. $\bar{t}$ is the smeared thickness of the member. Since this thickness is not known at the start of the fuselage mass estimation procedure, an educated estimate is used initially.

$$N = \frac{M \Delta z_{max}}{I} \bar{t} \tag{4.22}$$

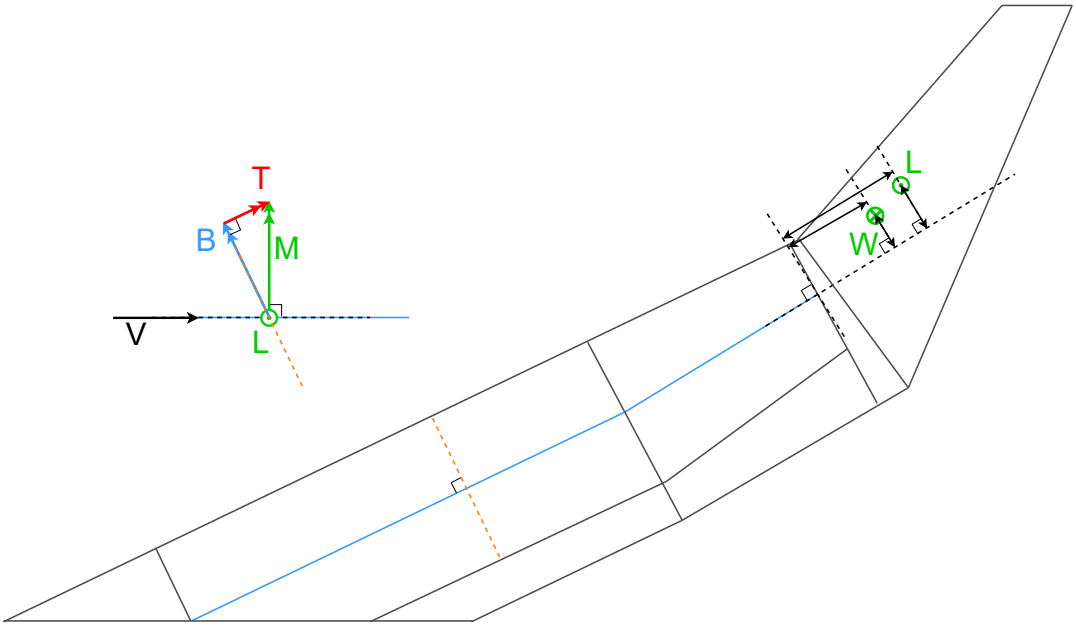

Figure 4.5: Aerodynamic lift (L) and the aerodynamic moment (M) converted to bending moment (B) and torsion (T) on the fuselage elastic axis indicated in blue. The outer wing lift and weight are introduced on the last section of the fuselage beam.

Note that the position of a structural member in the z-direction requires an idea of the section's position in the global reference frame. The position of all members has been related to half the section height, such that the floor position in the z-direction is described in Equation 4.23.

$$z_{\text{floor}} = -\frac{H_1 + H_2 + H_3}{2} + H_3 \tag{4.23}$$

Looking at the cross-section of the fuselage, there is a distributed load on the fuselage floor resulting from the weight of the payload, furnishing, operational items and systems. It is assumed that there are no lateral loads acting on the fuselage. Possible lateral loads on a fuselage floor in a conventional aircraft configuration with an oval fuselage could be due to the wing bending moment introduced on both the floor and ceiling panel when the fuselage is used as a carry-through structure for the wing box. In reality, the drag force acting on the Flying-V wing-fuselage structure could be a possible lateral load, but this load is neglected for the sake of simplicity. Additionally, the computationally efficient aerodynamic analysis does not yield the drag distribution.

Naturally, a pressurised fuselage means that the skin of the fuselage structure has to withstand pressure forces. For circular structures, the stress due to a pressure difference can be written as a function of the radius r of the cylinder. The hoop and longitudinal stress are calculated using Equations 4.24 and 4.25 respectively, in which Δp represents the pressure differential between the pressurised fuselage and the ambient.

$$\sigma_{hoop} = \frac{\Delta p r}{t} \tag{4.24}$$

$$\sigma_{long} = \frac{\Delta p r}{2t} \tag{4.25}$$

Using these relations, the stress in all three arcs making up a fuselage half-section can be determined. Since the fuselage cross-section is not perfectly circular, the trapezoid has to withstand the resultant of the pressure loads of the skin. Solving for the equilibrium of forces at the connecting nodes, the in-plane stress for the trapezoid members is determined. This results in the following equations, the derivation is described in more detail by e.g. Vos et al. [72]. α and r are the radius and angle of the three arcs describing the oval fuselage cross-section. β describes the angle of the vertical wall of the trapezoidal structure.

$$N_{\text{p, ceiling}} = -\Delta p(r_1 - r_2)(\cos\alpha_1 + \sin\alpha_1 \tan(-\beta)) \tag{4.26}$$

$$N_{\text{p, wall}} = \Delta p(r_1 - r_2)\frac{\sin\alpha_1}{\cos\beta} \tag{4.27}$$

$$N_{\text{p, floor}} = -\Delta p(r_3 - r_2)(\cos\alpha_3 + \sin\alpha_3\tan\beta) \tag{4.28}$$

Looking at the cross-sections along the length of the fuselage beam, these sections are loaded both in torsion and in shear. All weights are assumed to be on the longitudinal axis of the fuselage, such that torsion only results from the aerodynamic loads on the aircraft and from the resultant load of the outer wing. To find the shear flow through these cross-sections, thin-walled methods are applied. For clarity, this method is explained separately in the following section. Once all shear flows are determined, the shear stress τ in a member is determined using Equation 4.29.

$$\tau_{\text{hoop,long}} = \frac{q}{t} \tag{4.29}$$

Oval Fuselage Shear Flow

This section describes the model to calculate shear flows resulting from torque and shear forces on the oval fuselage. To find the shear flow through these cross-sections, thin-walled methods are applied.

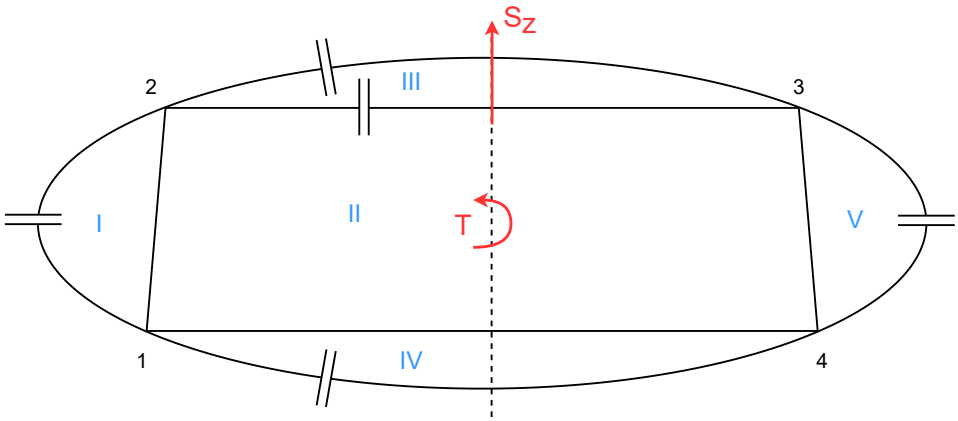

Figure 4.6: Oval fuselage cross-section with numbered cells and vertices. Cuts to determine the open-section shear flow are indicated.

First, the cross-section cells are cut open to calculate the open-section shear flow resulting from the shear force acting on the section. For the described fuselage cross-section, the cuts are shown in the figure, such that only the walls and the floor remain. For a pure vertical shear force and given the symmetric nature of the cross-section, the floor open-section shear flow will also be zero. Hence, only the walls have a non-zero open-section shear flow, which is positive upwards for a positive shear force and will be equal for a symmetrical cross-section. For a given thin-walled cell, the rate of twist is given in Equation 4.30 [81], in which A_i denotes the area of the cell.

$$\frac{\mathrm{d}\theta}{\mathrm{d}z} = \frac{1}{2A_\text{i}G}\oint_R q\frac{\mathrm{d}s}{t} \tag{4.30}$$

The shear flow can be described as the summation of the open-section shear flow and the shear flow at the cuts, which yields a constant shear-flow over the complete cell. As such, Equation 4.30 can be rewritten into Equation 4.31 in which the open-section shear flow is denoted by q_b and the constant cell shear flow by $q_{\text{s,0,R}}$.

$$\frac{\mathrm{d}\theta}{\mathrm{d}z} = \frac{1}{2A_\text{i}G}\oint_R \left(q_\text{b} + q_{\text{s,0,R}}\right)\frac{\mathrm{d}s}{t} \tag{4.31}$$

This leads to the following equations for the described fuselage cross-section cells. All shear flows are assumed positive counter-clockwise.

$$\frac{\mathrm{d}\theta}{\mathrm{d}z} = \frac{1}{2A_\text{I}G}\left[q_{\text{b}_\text{wall}}\delta_{12\text{r}} + q_{\text{s,0,I}}(\delta_{12\text{l}} + \delta_{12\text{r}}) - q_{\text{s,0,II}}\delta_{12\text{r}}\right] \tag{4.32}$$

$$\frac{\mathrm{d}\theta}{\mathrm{d}z} = \frac{1}{2A_{\mathrm{II}}G}[q_{\mathrm{b_{wall}}}(\delta_{34\mathrm{l}} - \delta_{12\mathrm{r}}) - q_{\mathrm{s,0,I}}\delta_{12\mathrm{r}} + q_{\mathrm{s,0,II}}(\delta_{12\mathrm{r}} + \delta_{14\mathrm{u}} + \delta_{34\mathrm{l}} + \delta_{23\mathrm{l}}) - q_{\mathrm{s,0,III}}\delta_{23\mathrm{l}} - q_{\mathrm{s,0,IV}}\delta_{14\mathrm{u}} - q_{\mathrm{s,0,V}}\delta_{34\mathrm{l}}] \tag{4.33}$$

$$\frac{\mathrm{d}\theta}{\mathrm{d}z} = \frac{1}{2A_{\mathrm{III}}G}\left[-q_{\mathrm{s,0,II}}\delta_{23\mathrm{l}} + q_{\mathrm{s,0,III}}(\delta_{23\mathrm{u}} + \delta_{23\mathrm{l}})\right] \tag{4.34}$$

$$\frac{\mathrm{d}\theta}{\mathrm{d}z} = \frac{1}{2A_{\mathrm{IV}}G}\left[-q_{\mathrm{s,0,II}}\delta_{14\mathrm{u}} + q_{\mathrm{s,0,IV}}(\delta_{14\mathrm{u}} + \delta_{14\mathrm{l}})\right] \tag{4.35}$$

$$\frac{\mathrm{d}\theta}{\mathrm{d}z} = \frac{1}{2A_{\mathrm{V}}G}\left[-q_{\mathrm{b_{wall}}}\delta_{34\mathrm{l}} - q_{\mathrm{s,0,II}}\delta_{34\mathrm{l}} + q_{\mathrm{s,0,V}}(\delta_{34\mathrm{l}} + \delta_{34\mathrm{r}})\right] \tag{4.36}$$

Finally, equating the moments at the symmetry axis of the section yields the required sixth equation. Note that the open-section shear flows cancel each other out when the moment is taken around this point, and that the shear force does not contribute either.

$$T = \sum_{R=1}^{\mathrm{N}} 2A_R q_{\mathrm{s,0,R}} \tag{4.37}$$

Which results in the following system of equations.

$$\begin{bmatrix} \delta_{12\mathrm{l}} + \delta_{12\mathrm{r}} & -\delta_{12\mathrm{r}} & 0 & 0 & 0 & -2A_{\mathrm{I}}G \\ -\delta_{12\mathrm{r}} & \delta_{12\mathrm{r}} + \delta_{14\mathrm{u}} + \delta_{34\mathrm{l}} + \delta_{23\mathrm{l}} & -\delta_{23\mathrm{l}} & -\delta_{14\mathrm{u}} & -\delta_{34\mathrm{l}} & -2A_{\mathrm{II}}G \\ 0 & -\delta_{23\mathrm{l}} & \delta_{23\mathrm{u}} + \delta_{23\mathrm{l}} & 0 & 0 & -2A_{\mathrm{III}}G \\ 0 & -\delta_{14\mathrm{u}} & 0 & \delta_{14\mathrm{u}} + \delta_{14\mathrm{l}} & 0 & -2A_{\mathrm{IV}}G \\ 0 & -\delta_{34\mathrm{l}} & 0 & 0 & \delta_{34\mathrm{l}} + \delta_{34\mathrm{r}} & -2A_{\mathrm{V}}G \\ 2A_{\mathrm{I}} & 2A_{\mathrm{II}} & 2A_{\mathrm{III}} & 2A_{\mathrm{IV}} & 2A_{\mathrm{V}} & 0 \end{bmatrix} \begin{bmatrix} q_{\mathrm{s,0,I}} \\ q_{\mathrm{s,0,II}} \\ q_{\mathrm{s,0,III}} \\ q_{\mathrm{s,0,IV}} \\ q_{\mathrm{s,0,V}} \\ \frac{\mathrm{d}\theta}{\mathrm{d}z} \end{bmatrix} = \begin{bmatrix} -q_{\mathrm{b_{wall}}}\delta_{12\mathrm{r}} \\ q_{\mathrm{b_{wall}}}(\delta_{12\mathrm{r}} - \delta_{34\mathrm{l}}) \\ 0 \\ 0 \\ q_{\mathrm{b_{wall}}}\delta_{34\mathrm{l}} \\ T \end{bmatrix}$$

Note that G is a reference value, which can be used when the δ of each section is recalculated based on this reference modulus as in Equation 4.38.

$$\delta = \int \frac{\mathrm{d}s}{t_i^*} \tag{4.38}$$

In which

$$t_i^* = \frac{G_i}{G_{\mathrm{ref}}} \cdot t_i \tag{4.39}$$

Solving for the shear flows in the section walls, this means that the shear flow through the respective walls results from Equation 4.40.

$$\begin{aligned} q_{12\mathrm{l}} &= -q_{\mathrm{s,0,I}} \\ q_{12\mathrm{r}} &= q_{\mathrm{s,0,I}} - q_{\mathrm{s,0,II}} + q_{\mathrm{b_{wall}}} \\ q_{23\mathrm{l}} &= -q_{\mathrm{s,0,II}} + q_{\mathrm{s,0,III}} \\ q_{23\mathrm{u}} &= -q_{\mathrm{s,0,III}} \\ q_{14\mathrm{u}} &= q_{\mathrm{s,0,II}} - q_{\mathrm{s,0,IV}} \\ q_{14\mathrm{l}} &= q_{\mathrm{s,0,IV}} \\ q_{34\mathrm{l}} &= -q_{\mathrm{s,0,II}} + q_{\mathrm{s,0,V}} - q_{\mathrm{b_{wall}}} \\ q_{34\mathrm{r}} &= -q_{\mathrm{s,0,V}} \end{aligned} \tag{4.40}$$

Naturally, this means that the shear flow for the front and aft arc and through the walls will not be equal between the front and aft side of the cross-section of the cabin. Since the fuselage weight estimation method assumes a symmetrical cross-section, these loads are averaged between the front and aft side. In reality, this might mean that the front wall needs to have different dimensions than the rear spar.

Structural Member Sizing

Once all loads on the structural members have been determined, the members are sized to make sure these loads can be withstood by the structure. The fuselage is assumed to consist of frames that strengthen the structure in the hoop direction and longitudinal stringers on a skin that prevent buckling in the longitudinal direction, also known as the semi-monocoque structure. The trapezoidal structure within the fuselage structure is made from sandwich panels.

In the weight estimation method built upon the method of Schmidt, isotropic materials are used for the structural members. The core of the sandwich panels is made from THPP80FN[6] and both the facings of the panels and the skin of the fuselage are made from AL2024T3. The frames are made from AL7075T3. To account for the effect that modern aircraft are to a large extent constructed using composites, a correction factor for the resulting weight is used as described in Section 4.3.5.

The strength of materials changes over the lifespan of the aircraft. The total number of cycles the aircraft is designed for is set at 100,000, following the design of Schmidt et al. [77]. The simplified model of a Z-shaped stiffener of Schmidt is used [80].

For a beam of length L as part of the trapezoidal structure, the following relation holds.

$$M + N_{\text{lat}}(v + e) - \frac{qL}{2} + \frac{qx^2}{2} \tag{4.41}$$

In this equation, v is the deflection of the beam, x is a location along the length of the beam and e its eccentricity. Note that the lateral force for the Flying-V floor structure is zero except for the pressure force. Solving the differential equation for the maximum deflection of the beam, Schmidt arrives at Equation 4.42, in which λ is a characteristic parameter of the differential equation [80].

$$v_{\text{max}} = \frac{q}{EI\lambda^4}\left(\sec\frac{\lambda L}{2} - 1\right) - \frac{qL^2}{8EI\lambda^2} \tag{4.42}$$

Filling this in in Equation 4.41 yields the maximum moment in the beam. Then, the maximum stress is found using Equation 4.43.

$$\sigma_{\text{lat}} = \frac{N_{\text{lat}}}{2t_{\text{face}}} + \frac{Mz}{I} \tag{4.43}$$

Regarding the longitudinal stress Equation 4.44 can be used, in which the longitudinal load in a member is the summation of the load resulting from the bending moment as in Equation 4.22 and pressure as in Equation 4.26.

$$\sigma_{\text{long}} = \frac{N_b}{2t_{\text{face}}} \tag{4.44}$$

The shear stress through each member has been determined in Equation 4.40. The von Mises stress σ_v is calculated using Equation 4.45. This equation is valid for thin plates with no out-of-plane stress or shear in any other direction than the plane.

$$\sigma_v = \sqrt{\sigma_{\text{lat}}^2 - \sigma_{\text{long}}\sigma_{\text{lat}} + \sigma_{\text{long}}^2 + 3\tau_{\text{lat,long}}^2} \tag{4.45}$$

Local buckling of the face sheet can occur in different ways. Dimpling refers to local buckling of the face sheets, crimping to local buckling of the core. These failure modes occur at the following stresses, in which ν is the Poisson's ratio and s the core material's cell size.

$$N_{\text{dimpling}} = \frac{2E_{\text{face}}t_{\text{face}}^3}{1 - \nu_{12}\nu_{21}}\frac{1}{s^2} \tag{4.46}$$

$$N_{\text{crimping}} = t_{\text{core}}G_{\text{core}} \tag{4.47}$$

$$N_{\text{wrinkling}} = 0.79(E_{\text{face}}E_{\text{core}}G_{\text{core}})^{\frac{1}{3}} \tag{4.48}$$

Global buckling of the complete sandwich beam occurs at

[6] https://thermhex.com/thermhex-data-sheet-thpp80fn-eng2013 [cited on 17-2-2020]

$$N_{\text{global}} = N_E \frac{1 + \frac{N_{E_f}}{N_s} - \frac{N_{E_f}}{N_s}\frac{N_{E_f}}{N_E}}{1 + \frac{N_E}{N_s} - \frac{N_{E_f}}{N_s}} \tag{4.49}$$

In which

$$N_s = G_{\text{core}} \frac{(t_{\text{core}} + t_{\text{face}})^2}{t_{\text{core}}} \tag{4.50}$$

$$N_E = \frac{E_{\text{face}}\pi^2}{L^2}\left(\frac{t_{\text{face}}^3}{6} + t_{\text{face}}\frac{(t_{\text{core}} + t_{\text{face}})^2}{2}\right) \tag{4.51}$$

$$N_{E_f} = \frac{E_{\text{face}}\pi^2}{L^2}\frac{t_{\text{face}}^3}{6} \tag{4.52}$$

The total mass of the beam per unit length is minimised given the four constraints on buckling and one constraint on the von Mises stress being no larger than the yield stress of the material to find the thickness of the core and face of the beam.

For the skin panels a similar approach is followed, with the main difference that the lateral stress is called the hoop stress. The skin panels have a minimum gage thickness, t_{gage}, which is set at 1.2 mm as in the study of Schmidt [80].

$$\sigma_v = \sqrt{\sigma_{\text{hoop}}^2 - \sigma_{\text{long}}\sigma_{\text{hoop}} + \sigma_{\text{long}}^2 + 3\tau_{\text{hoop,long}}^2} \tag{4.53}$$

General buckling of the skin occurs at the critical load defined in Equation 4.54, with L_{frame} being the frame space of the fuselage and D the plate bending stiffness.

$$N_{\text{cr,shell}} = k_x \frac{\pi^2 D}{L_{\text{frame}}^2} \tag{4.54}$$

Local buckling occurs at the critical load calculated using Equation 4.55, where $N_{\text{cr,j}}$ is the critical buckling line load and b_j the width of a stiffened panel strip. The buckling coefficient k depends on the type of constraints on the edges of the skin strip.

$$N_{\text{cr,j}} = \frac{k_j \pi^2 E_{\text{shell}}}{12(1 - \nu_{\text{shell}}^2)}\left(\frac{t_j}{b_j}\right)^2 \tag{4.55}$$

For the frames, Schmidt derives the required frame stiffness $(EI)_{\text{fr,oval}}$ resulting in Equation 4.56 which is directly related to the largest radius of the upper and lower arc of the fuselage, r_{max}. C_f is the Shanley frame constant which is set to $\frac{1}{16000}$. The frame efficiency factor k_f is derived by Schmidt to be 5.4.

$$(EI)_{\text{fr,oval}} = C_f \frac{r_{\text{max}}^3 M}{8 h_{\text{oval}} L_{\text{frame}}} \tag{4.56}$$

The required frame area follows from the required frame stiffness, Young's modulus and the frame efficiency factor.

$$A_{\text{fr,oval}} = \sqrt{\frac{(EI)_{\text{fr,oval}}}{k_f E_{\text{fr,oval}}}} \tag{4.57}$$

The smeared frame thickness results from the frame area and the frame spacing L_{frame} which is set at 635 mm, which is the estimated frame spacing of the reference aircraft family [82].

$$\bar{t}_{\text{frame}} = \frac{A_{\text{fr,oval}}}{L_{\text{frame}}} \tag{4.58}$$

Mass Estimation

The mass of the fuselage and inner wing comprises the weight of the primary structure, secondary structure and non-structural elements, resulting in Equation 4.59. In this section, all components of this equation are further explained. The primary structural weight is based on the sizing methodology explained above, whereas the weight of the secondary structure and non-structural elements is determined using empirical relations.

$$W_{\text{fuselage}} = 1.2 \cdot W_{\text{primary}} + 0.8 \cdot W_{\text{fus}_{\text{TE}}} + W_{\text{pb}} + W_{\text{ws}} + W_{\text{doors,misc}} + W_{\text{windows}} + W_{\text{apt}} + W_{\text{fd}} + W_{\text{paint}} + W_{\text{radar}} \quad (4.59)$$

Having determined the minimum thickness for all structural members, the primary structural mass of the fuselage W_{primary} is easily determined by multiplying the length, width, thickness and density of all members. This mass is determined per section, such that the fuselage can be loaded by its own weight in an iterative manner accurately per longitudinal section. The obtained fuselage mass from a load analysis does not include secondary structure items such as fasteners, cutouts or welds. To account for these weights, the primary weight of the fuselage is multiplied by a constant 1.2 which also accounts for the composite structure the Flying-V will be largely constructed from. In this study, the primary structure weight is estimated for a metal structure, such that an extra 20% weight is added to account for secondary structure items which is further explained in Section 4.3.5. The reduction factor on the fuselage trailing edge weight is also described in Section 4.3.5.

The fuselage trailing edge weight is estimated using Equation 4.60, as provided by Torenbeek [83]. This relation has been used by e.g. Vos et al. to estimate the trailing edge weight which completes the aerodynamic shape of a BWB aircraft [72].

$$W_{\text{fus}_{\text{TE}}} = S_{\text{TE}} \left[60 \left(1 + 1.6 \cdot \sqrt{\frac{W_{\text{TO}}}{10^6}} \right) + \Delta \right] \quad (4.60)$$

In this equation, S_{TE} is the surface area of the estimated trailing edge and Δ can be used to account for control surfaces. For simple systems such as a single slotted flap or elevator, this parameter can be set to zero, which is as such done for the Flying-V.

Pressure bulkheads are included at the front and rear end of the fuselage. The weight of a pressure bulkhead is estimated using a relation of Howe as provided in Equation 4.61 [74].

$$W_{\text{pb}} = 6.5 \cdot \bar{h}_{\text{pb}} \cdot S_{\text{bp}} \cdot \Delta_p \cdot \rho_{\text{mat}} \cdot 10^{-3} \quad (4.61)$$

In this equation, $\bar{h}_{\text{pb}}$ accounts for the shape of the bulkhead, and is 1 for dome-shaped bulkheads and 1.25 for flat bulkheads. S_{pb} is the surface area of the bulkhead, Δ_p the pressure difference between the cabin and ambient and ρ_{mat} the density of the applied material. For all bulkheads a dome shape is used. The front pressure bulkhead is assumed to have a circular shape with its diameter being half the height of the cabin, since it is located below the windscreen. The aft pressure bulkhead size follows from the dimensions of the aft part of the cabin.

A relation for the weight of the windscreen is also provided by Howe. The area of the windscreen S_{ws} is approximately 2.3 m^2 [32]. The dive velocity V_{D} is set at 300 m/s.

$$W_{\text{ws}} = 0.75 S_{\text{ws}} V_D \Delta_P \quad (4.62)$$

The weight of doors and miscellaneous items in the nose, $W_{\text{doors,misc}}$, is assumed to be approximately 0.2% of the MTOW [74].

The weight of the windows is provided in Equation 4.63. The total window area, S_{windows}, is approximated by using one window per fuselage frame and a window area of 0.24x0.34 m^2. No reliable source on the exact window size of the A350 aircraft family has been found, but this size is deemed reasonable compared to the window size of 0.24x0.37 m^2 as in the Boeing 787 Dreamliner [80]. Only the leading edge side of the untapered part of the cabin is assumed to have windows. The fuselage frame pitch is assumed to be 635 mm [84].

$$W_{\text{windows}} = 90 \delta_P S_{\text{windows}} \quad (4.63)$$

The weight of apertures, such as doors, is estimated using Equation 4.64 in which S_{apt} is the total area of these apertures.

$$W_{apt} = 60 S_{apt} \tag{4.64}$$

The weight of a rear ramp-type freight door is given in Equation 4.65, with B_f being the floor width of the freight door. The door is assumed to have the width and height of an LD-9 container with a 10% margin for both dimensions, yielding its surface area S_{door}.

$$W_{fd} = 10(1 + 0.75 B_f) S_{door} \tag{4.65}$$

The weight of the weather radar, W_{radar}, is obtained from Vos et al., setting it at 20 kg [72]. This weight estimation is adopted since this system is not included in older Torenbeek relations. Paint weight W_{paint} is related to the surface area by Vos et al. by 0.3 kg per m^2 of total wetted area.

Several weight relations for BWB aircraft by Howe are not included. Howe includes a weight penalty for the area between the pressurised fuselage and the leading edge, which is not really present in a Flying-V configuration. Howe also describes a weight penalty for the nose landing gear attachment, which is assumed part of the landing gear weight estimation by Torenbeek. Furthermore, extra weight could be added for a nose outer shell, but due to the symmetrical parts visualised in Figure 4.4 this is not deemed applicable. Finally, the mass of the crew floor is assumed to be already present in the oval fuselage weight estimation due to the double inclusion of part of the cabin floor as shown in Figure 4.4.

4.3.3. Outer Wing, Non-Structural and Payload Weight Estimation

In this section, the weight estimation of the outer wing, non-structural elements and payload is described. The outer wing weight estimation is performed using a method called EMWET, and the non-structural and payload weight is estimated using empirical relations.

Outer Wing

The outer wing of the Flying-V is essentially a normal wing, without a trapezoid structure or oval fuselage but with two spars, ribs and a skin. As described in Section 4.3.1, EMWET is employed to estimate the weight of the outer wing, $W_{outer\,wing}$. The obtained weight is reduced by 20% as explained in Section 4.3.5 to account for the use of lightweight materials. As inputs, EMWET requires the aerodynamic loads and a description of the planform of the wing, as well as the shape and spanwise position of airfoils. The aerodynamic loads resulting from AVL are per streamwise section, such that there is not a one-on-one relation between the loads resulting from AVL and the outer wing planform. As such, all loads outboard of the outer wing root chord's midpoint are assumed to be carried by the outer wing. This means that part of the outer wing aerodynamic loads are not included, which is compensated for by the extra inner wing loads which are included. The selection of aerodynamic loads is indicated on the left of Figure 4.7.

Since EMWET requires a streamwise definition of airfoils, the planform is rotated around the midpoint of its root. Furthermore, the section is mirrored to ensure a positive sweep angle, resembling the sweep angle of the outer wing. The resulting planform is shown on the right of Figure 4.7. Four streamwise chords are used to define the planform, illustrated by dashed orange lines in this figure. Note that the tip section chord is defined to be very small at 0.01 m.

When flying at the maximum takeoff weight, the bending moment of the outer wing is relieved by the inclusion of fuel in the outer wing. Furthermore, the weight of the fin on the tip of the outer wing is included by using the EMWET option to define an engine weight and spanwise position. The fuel tank in the outer wing is assumed to be between the front and aft spar and between the root and 30% of the span. The front and aft spar are at 15% and 60% of the chord respectively. The rib pitch is assumed to be 0.6 m which is common in large passenger aircraft [85].

As described in Section 4.3.2, the weight of the outer wing is introduced as a moment on the last section of the oval fuselage. The centre of gravity location of the outer wing is not a direct result of EMWET and is determined based on the thickness distribution of the spars and skin resulting from EMWET. The underlying assumption in this method is that the secondary weights, which are included in the resulting EMWET weight as well, are distributed in a similar fashion. The fuel weight is added per spanwise position and is assumed to be linearly distributed between the front and aft spar by taking the average height of both spars at each spanwise section. The fin weight is placed at the tip of the wing.

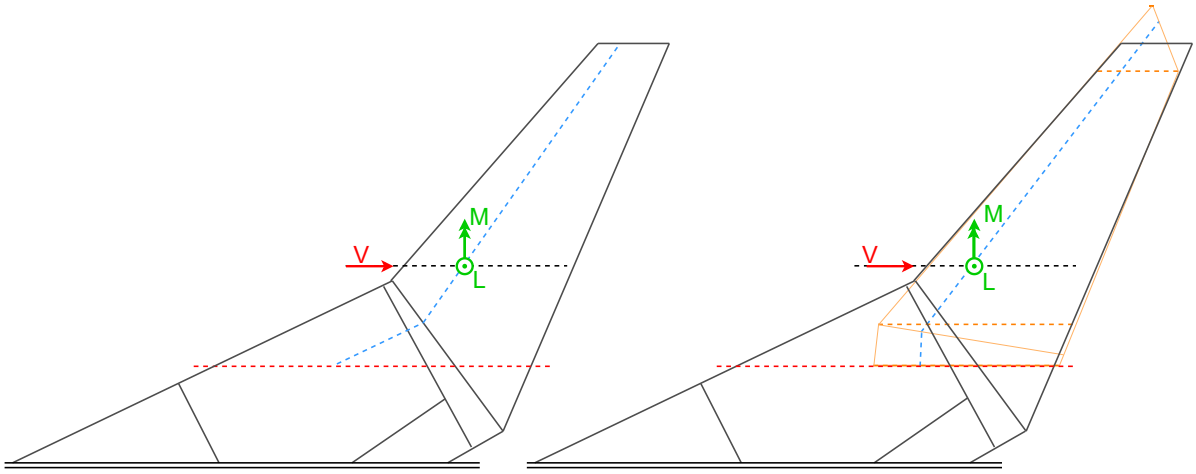

Figure 4.7: EMWET implementation of the outer wing. The left figure visualises the selection of stream-wise AVL results which are applied on the outer wing. The right figure visualises the EMWET implementation of the planform in orange.

Empirical Relations and Non-Structural Weight

As has been described in Section 4.3.1, empirical methods are applied to find the non-structural and payload weight of the aircraft. The empirical relations follow from Torenbeek's method [69]. The most important relations are provided in this section, whereas the remainder of the relations is provided in Appendix A.

The empennage weight is described in Equation 4.66 [10]. For a fixed horizontal tail, K_h is 1. Vertical tail weight is estimated by the same relation, substituting a v for all h. The Flying-V does not have a tail, but its relatively large fins are sized using the vertical tail equation, yielding W_{fins}. k_v is 1 for a fuselage-mounted horizontal tailplane configuration which is the case for the reference aircraft family. Note that this relation holds for imperial units. $\Lambda_{0.5h}$ is the half-chord sweep angle of the lifting surface. For both the reference aircraft and the Flying-V, a weight reduction of 20% is included as explained in Section 4.3.5. The dive velocity V_D is set at 300 m/s.

$$W_h = K_h S_h \left[\frac{3.81\{(S_h)^{0.2} V_D\}}{1000\sqrt{cos\Lambda_{0.5h}}} - 0.287 \right] \tag{4.66}$$

Fuel weight of the aircraft family members is a direct result of the flown mission and the performance of the aircraft and are discussed in depth in Chapter 4.1. Residual fuel weight $W_{resfuel}$ is a certain fraction of the total fuel tank capacity V_{ft} as in Equation 4.67 and is assumed part of the fuel weight in Equation 4.19.

$$W_{resfuel} = 0.151 V_{ft}^{2/3} \tag{4.67}$$

The fuel is assumed to be located both in the outer wing and in the trailing edge of the inner wing. Initially, the fuel is placed aft of the oval fuselage, whilst in later design phases this has been changed to aft of the wall of the trapezoid structure as visualised in Figure 4.8 to enlarge the inner fuel tanks of the aircraft limiting the centre of gravity shift during flight. No fuel can be placed at the location of the engine and landing gear as shown in Figure 3.6. The width of the engine and landing gear part of the fuselage is assumed to be 8 frames, which is with a frame pitch of 0.635 m a total length of 5.08 m. To limit the centre of gravity shift during flight the inner wing tanks are filled first, followed by the outer wing tank when required.

For the reference aircraft, the fuel is assumed to be in the wing including the part of the wing which penetrates the fuselage.

The Flying-V is designed for a certain cargo weight and number of passengers. The weight of the passengers is 75 kg per passenger, with 18 kg baggage per economy class passenger and 27 kg baggage per business class passenger. To determine the harmonic range of the aircraft, cargo weight is included as one unspecified weight. As such, the payload weight is calculated using Equation 4.68.

$$W_{payload} = 93 n_{pax_{ec}} + 102 n_{pax_{bc}} + W_{cargo} \tag{4.68}$$

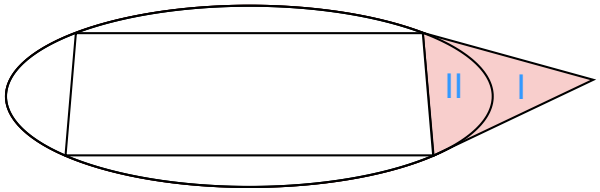

Figure 4.8: Fuel tank location shown on a cross-section of the fuselage, initial (I) and extra after the fuel tank enlargement (II).

4.3.4. Centre of Gravity, Landing Gear Positioning and Engine Placement

The centre of gravity is determined for the Flying-V aircraft, whereas for the reference aircraft it is deduced from aircraft dimensions and data provided by the manufacturer [5], as explained in Section 4.4.

For different situations occurring during missions with and without maximum payload or fuel, the centre of gravity is determined from the weight and location of all component weight groups. The weights are either point loads or distributed loads. Passengers, furnishing and operational items are assumed to be linearly distributed over the length of the passenger cabin. The passenger cabin starts at the root of the fuselage beam. Its end point is determined based on the total floor area the passengers and furnishing require, as explained in Table 3.1. The weight of the systems, secondary weights and fuselage trailing edge is linearly distributed over the length of the fuselage. The structural weight of the fuselage and inner wing is known per section and is distributed accordingly.

The longitudinal location of the main landing gear is determined based on the most aft centre of gravity location, placing the landing gear strut at an angle of 17 degrees. As such a maximum pitch angle of 17 degrees can be achieved at the most aft centre of gravity [31]. The length of the landing gear strut and the diameter of the landing gear tires are obtained from Bourget for a floor height of 5.5 m. Hence, $L_{\mathrm{LG_{strut}}}$ is 5.5 m and $r_{\mathrm{LG_{wheel}}}$ is 0.635 m. The longitudinal location of the nose landing gear is assumed to be fixed at the root of the fuselage beam which is for the baseline aircraft at 8.9 m from the nose. In reality, the nose landing gear can be placed at a different location to ensure a proper load on the nose gear for all centre of gravity positions. Note that the nose landing gear often takes up 5% to 10% of the weight of the aircraft since a lower nose gear load does not provide enough steering force [31]. The lateral position of the landing gear is taken from Bourget at 6.1 m from the aircraft centre axis for the FV-1000, shifting inboard for smaller aircraft variants with a change in the longitudinal centre of gravity position. As such, the track width of the FV-1000 is 12.2 m.

The engine is assumed to be connected to the same structural component as the landing gear, as visualised in Section 3.3.3. Placing both components at the same location is structurally efficient, requiring one structural component to introduce both loads into the rest of the fuselage and to combine the fairing structure of the engine pylon and landing gear bay. Based on the landing gear and fairing design of Bourget, the spanwise distance between the landing gear and the engine is fixed at 0.8 m.

4.3.5. Modelled Weight to Actual Weight

A finite element method (FEM) or semi-analytical method such as the method used in this study results in a weight estimation which is lower than the weight of the actual structure. Some parts of the structure are not modelled, such as stiffeners and fillets. Besides that, the joints, e.g. rivets, have to be added as well. All in all, the modelled weight is for metal structures approximately 40-80% of the actual weight [86].

The Flying-V, as well as the A350 reference aircraft, will be primarily built from composites. As such, the weight estimation methods for metal structures used in this study need a correction factor to estimate the actual weight of a composite structure. EMWET has not been validated for the use of composites, but has been verified [87]. The developers of EMWET had difficulty obtaining proper validation data for composite aircraft, which is one of the primary reasons to use metal sizing methods for this study as well. However, Elham mentions weight savings for composite wings for transonic aircraft of 15 to 21%, which only takes into account the use of composites for the primary structure [88]. Given the fact that the secondary weight of wings contributes significantly to the total wing weight, this saving could drastically increase for wings including composite secondary structures. A very well-cited article on composites in aircraft structures by Soutis mentions a weight saving from metal to composite structures of 40% for secondary structures and 20% for primary structures [89].

For the oval fuselage weight estimation method, the primary structure is assumed to contribute 60% to the total weight, which is the average of Droegkamp mentioning a contribution of 40% to 80% [86]. Combined

with a weight saving of 20% on primary structures and 40% on secondary structures, this means that the modelled weight is 83% of the actual weight. This means that the fuselage weight estimation result should be multiplied by a factor of 1.2. For the outer wing, it is unclear what the division in primary and secondary weight is for the result obtained using EMWET. It is assumed that the division between primary and secondary weight is equal to the average fraction of 60% provided by Droegkamp. As such, an overall saving due to the use of composite materials of 28% can be applied. The actual reduction factor is chosen to be 20% to make sure the weight estimation is on the conservative side.

The same weight reduction factor of 20% is used for the fuselage trailing edge and fins. The furniture weight is assumed to be mainly composed of secondary structures, and large weight savings on seats, soundproofing, galleys and flight deck furnishing are expected. Therefore, the weight reduction of 28% is applied to these parts of the furnishing weight. It should be noted that the actual factors chosen are not of paramount importance in a study on aircraft family design, which is primarily concerned about the sensitivity of the weight estimation method to input parameters and the comparison between a Flying-V and conventional aircraft.

4.4. Reference Aircraft

The fuel burn method of the reference aircraft follows largely the same principles as the method applied for the Flying-V.

Aerodynamically, the fuselage is assumed to generate no lift whereas the (negative) lift of the horizontal tail is added. The aircraft is trimmed assuming an all-moving horizontal tail. Following the study of Faggiano et al., the same nacelle and pylon drag are used on the reference aircraft as on the Flying-V [9]. Viscous drag of the horizontal and vertical tail is included in a similar fashion as for the main wing.

The fuselage beam used for the reference aircraft is visualised and explained in Section 3.3.2, including a description of the location of the different component weight groups. Key differences regarding the weight estimation are the inclusion of an empennage and the exclusion of fins and a fuselage trailing edge. Empennage weight is estimated using the relation of Torenbeek as in Equation 4.66. The weight and aerodynamic loads of the tail surfaces are introduced at their respective half-chord location. Regarding the fuselage weight estimation method, it is assumed that there is no torsion on the fuselage and that the fuselage is not used as a carry-through structure for the wing, meaning that the wing forces are only introduced as a longitudinal load and bending moment on the fuselage beam. The bending moment from the wing structure results from the wing weight (including engine and fuel weight) and aerodynamic loads. The bending moment is calculated with respect to the centre of the two wing spars. The weight of the complete wing is estimated using EMWET, which for the Flying-V is only used for the outer wing. The fuel is placed between the spars of the wing, which are placed at 15% and 65% of the chord. For the largest aircraft variant, the tank is enlarged for the part of the wing that penetrates the fuselage, linearly distributing additional fuel of the A350-1000 with respect to the A350-900 over the fuselage beam at this location.

The centre of gravity of the reference aircraft is determined from the position of the landing gears as shown on drawings provided by Airbus [5]. The longitudinal centre of gravity location is determined based on the load division between the nose and main landing gear. Aircraft design books such as the books of Raymer and Torenbeek advise a minimum nose gear load of 8% of the maximum takeoff weight to allow steering of the aircraft [6, 69]. Since a more aft centre of gravity location reduces the static margin and hence the trim drag and corresponding fuel burn, the most aft centre of gravity location is most beneficial in terms of fuel burn. The most aft centre of gravity location is found for the smallest possible nose gear loading, such that the 8% limit load on the nose gear is adopted. Hence, the longitudinal centre of gravity location measured from the nose of the aircraft for the A350-900 and A350-1000 is at 31.0 and 35.1 m respectively.

5

Verification and Validation

In this chapter, a verification of the described methods is performed and the results are validated. The aerodynamic analysis and weight estimation method will be verified and validated first, followed by a validation of the resulting fuel burn performance.

5.1. Aerodynamic Analysis

In this section, verification and validation of the aerodynamic analysis are described. First, a suitable validation method is selected, followed by the results with respect to lift-to-drag ratio, spanwise lift distribution and static stability derivatives.

5.1.1. Validation Method

A more sophisticated model is used to validate the coarse aerodynamic model used within the optimisation procedure. Both 3D panel methods and Euler or RANS solvers potentially have a higher accuracy than the aerodynamic models described in Section 4.2.1. In this section, both models are shortly discussed and the choice for FlightStream as validation model is explained.

Euler and RANS Methods

The motion of a fluid can be described using Navier-Stoke equations. These non-linear equations, or simplified models based on these equations, can be approximated with different types of flow solvers. DNS, LES and RANS are the most accurate and require a significant computational time. Linearised potential equations are of lower accuracy and hence have a lower computational cost. An aerodynamic optimisation of the Flying-V was performed by Faggiano using SU2, which is an example of a solver that can solve the full (laminar), Euler and RANS equations using finite-volume or finite-element methods. Since this method is also supported by the ParaPy framework, this solver is considered for validation.

Stanford University Unstructured (SU2) is an open-source CFD package, specifically designed keeping aerodynamic shape optimisation in mind [90]. It offers a variety of solvers, both Reynolds-Averaged Navier-Stokes (RANS) and Euler equations. SU2 offers the possibility to output derivatives based on an adjoint method, which is interesting for a stability analysis. SU2 generally works with either 2D or 3D unstructured meshes. Models are solved using either a finite element or a finite volume method. The software has been validated on a lot of applications, showing very accurate results compared to experimental data. The interested reader is referred to the article by Palacios et al. which describes the structure and applications of SU2 in much more detail [90].

Faggiano et al. select the Euler model because of its accuracy in estimating wave drag. Wave drag forms a significant component of the total drag when flying at higher Mach numbers [9]. Compared to RANS methods, the Euler model comes at a limited computational cost by neglecting viscosity. However, since the Euler model is inviscid, Faggiano et al. require a separate viscous module to estimate profile drag. This viscous module is elaborated upon in Section 4.2.2. For the study of Faggiano et al. on the Flying-V, a SU2 run costs 20 minutes on a computer with an Intel i7 processor with 2.4GHz and 16Gb ram DD3 1600 Mhz (stopped after 100 iterations because aerodynamic coefficients are within a 0.5% error with respect to the converged solution to save computational time). SU2 offers the aerodynamic designer a variety of possibilities, but that also

means that a deep understanding of the different available models is required to use this solver reliably. As Peerlings notes, some studies showed that "the choice of turbulence model or numerical scheme was shown to impact the results" ([91], p. 66).

Panel Methods

Panel methods allow the modelling of thick geometries and are very comparable to vortex lattice methods. The geometry is completely covered by panels and a singularity is imposed on every panel, solving the complete system of equations to find the singularity strengths at all panels. The ParaPy framework includes two 3D panel methods: FlightStream[1] and VSAERO[2]. Of these two models, FlightStream is the most recent and user-friendly and is therefore considered as a validation model. Note that XFLR5, which is discussed in Section 4.2.1, also includes a panel method.

FlightStream is a relatively new computational fluid dynamics solver, mainly developed by Ahuja and Hartfield following on the PhD thesis of Ahuja [92]. Ahuja and Hartfield identified the need for a flow solver with low computational cost to aid in MDO design routines, especially in unconventional aircraft configuration design. Many MDO environments use potential flow solvers which have a limited computational cost and are simple to run, requiring only surface meshes to model a complete 3D structure. These solvers are often based on solving for pressure rather than for vorticity in three-dimensional applications, since vorticity-based solvers require structured meshes or thin-surface models as in VLMs. In pressure-based solvers, strong curvatures need to be modelled by a high number of cells to accurately resemble the high local pressure gradients. Vorticity-based solvers are rather different, being unable to yield accurate pressure results but evaluating circulation around the given geometry [93]. Ahuja and Hartfield made an effort to use unstructured meshes in a vorticity-based solver, due to its large advantages in limited memory requirements compared to structured meshes and its simple generation. Circulation is integrated around the geometry cross-sections to find the aerodynamic loads on the body. A fundamental underpinning of this methodology is the lifting line theory of Prandtl which describes the relationship between induced circulation, lift and drag forces [94]. It is important to note that the potential flow solution is inviscid and that a separate lift-effectiveness factor is applied to account for viscous effects based on surface vorticity [95], which is also seen in AVL using empirical corrections to a potential-flow analysis. Note that the number of cells can be relatively low, since FlightStream solves vorticity on surface panels and does not need a closed geometry with high numbers of cells in complex high-curvature locations. VLMs are relatively accurate for conventional aircraft configurations with moderately thin high aspect ratio wings, but are less suitable for e.g. blended wing-bodies of larger thickness. FlightStream employs the Kutta condition and can automatically determine the trailing edges where this condition should be applied.

FlightStream automatically selects one out of two wake propagation models. A prescribed wake means that the wake strands convect downstream with the free-stream velocity without being influenced by any vorticity of panels or by other wake strands, whereas free wake propagation means that the strands are influenced by the solution's vorticity. Naturally, the prescribed wake solution is less computationally expensive [95]. Johnson et al. provide an indication of the runtime of the free-wake solver, which is approximately 60 seconds on a three-core processor for every angle of attack [96]. Amongst others, Sandoz et al. describe the benefits of FlightStream as being "substantially more robust and stable compared to pressure-based potential-flow solvers and less sensitive to surface perturbations" ([97], p. 5). FlightStream has been shown to closely follow experimental results on small propeller aircraft [97] [96]. Some studies also use FlightStream on larger transport aircraft [95] or fighter aircraft [93]. Other noteworthy examples are the application on a distributed electric propulsion aircraft and on a hybrid airship [98], a VTOL and an energy-efficient transport (AR12) aircraft [99]. Most of these studies were at very limited Mach numbers in the subsonic regime; FlightStream has not (often) been applied in the transonic regime. Chakraborty et al. mention the fact that FlightStream also has a Stability & Control Toolbox which calculates stability derivatives [100].

FlightStream does not require a deep understanding of turbulence models or numerical schemes from the user, and its limited number of settings makes it therefore an interesting choice for validation purposes in this study. Additionally, its user-friendly interface and features such as its stability and control toolbox allow the designer to quickly achieve relevant results on both aerodynamics and stability. Since this research does not focus on aerodynamic optimisation but only uses the aerodynamic model as part of a larger fuel burn and family design model, FlightStream is selected as validation model.

[1] https://www.darcorp.com/flightstream-aerodynamics-software/ [cited on 24-10-2020]
[2] https://starkaerospace.com/products-services/ami/software/ [cited on 24-10-2020]

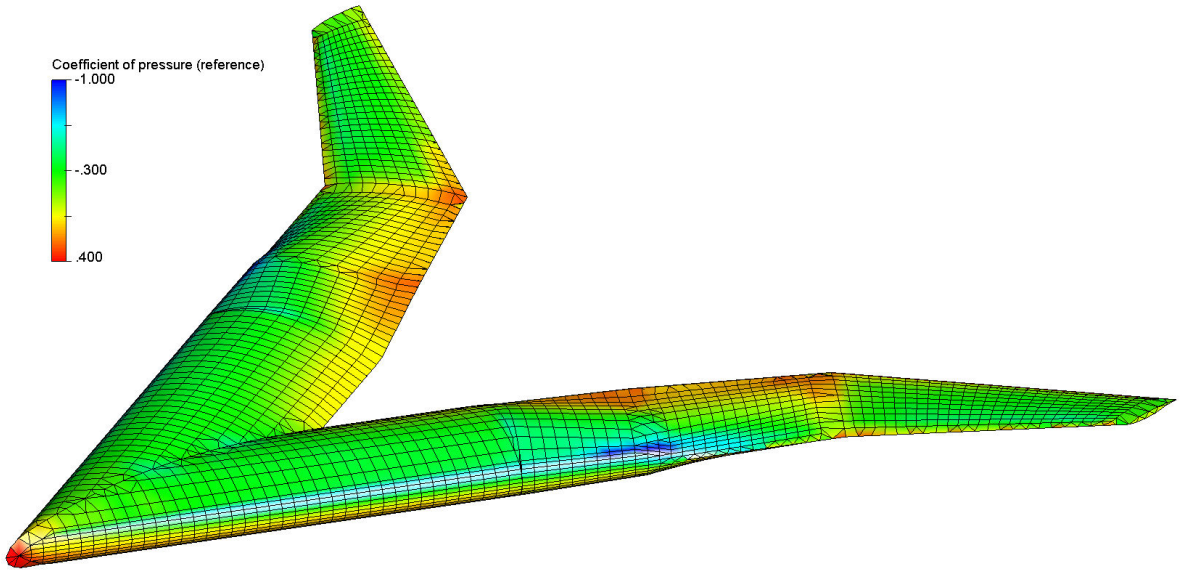

Figure 5.1: Pressure coefficient with respect to the reference velocity of 250.8 m/s at 4 degrees angle of attack modelled in FlightStream.

5.1.2. Results and Discussion

In this section, the aerodynamic characteristics of a Flying-V design approximating the design of Faggiano [9] are assessed. This design differs with respect to the design described in Chapter 3. Altered variables including the design variables are presented in Table 5.1.

Table 5.1: Fixed and design variables for the approximation of Faggiano's Flying-V geometry. Fixed variables are further explained in Table 3.8.

Variable	Value	Unit
L_4	m	10.96
w_{H_1}	m	5.97
w_{H_3}	m	3.3
H_{2_1}	m	2.1
H_{2_3}	m	1.8
H_{arm_3}	m	0.05
L_1	m	21.54
L_3	m	7.0
b_{outer}	m	15.325
λ	-	0.15
c_1'	-	1.25
c_3'	-	1.8
H_{1_1}	m	0.6
H_{1_3}	m	0.3
H_{3_1}	m	0.7
H_{3_3}	m	0.3

Both AVL and FlightStream are run in the subsonic incompressible regime for the described aircraft. Three aspects of the aerodynamic model are to be validated, being the lift-to-drag ratio, spanwise lift distribution and stability derivatives. Figure 5.1 visualises the pressure coefficient for the aircraft in FlightStream.

Lift-to-drag Ratio

Figure 5.2 visualises the results in terms of lift, drag and moment polar. The results indicate a very similar lift coefficient between FlightStream and AVL, whereas drag lift polar is somewhat different at higher angles of attack. This results in a different lift-drag polar for both analyses, with larger differences towards higher

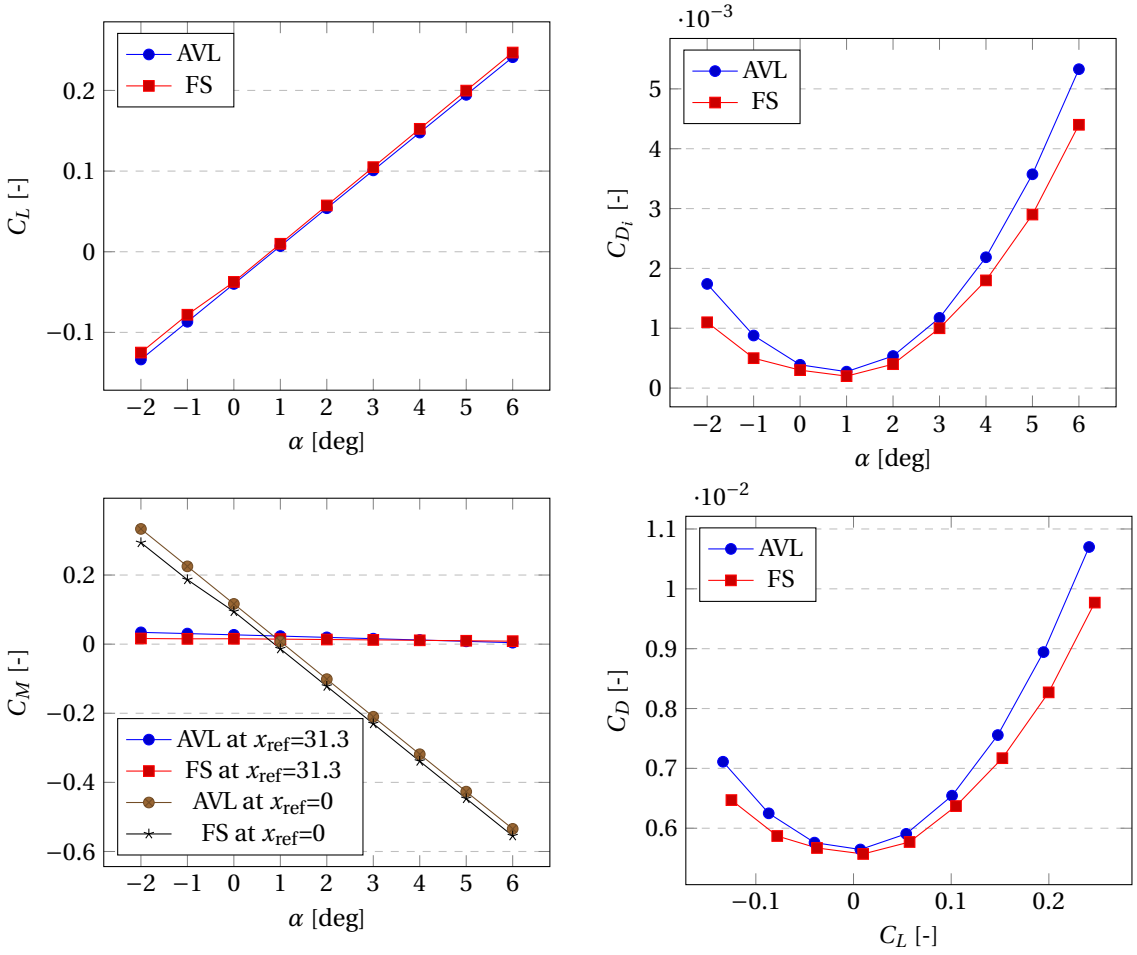

Figure 5.2: Validation results for an approximation of the Flying-V geometry of Faggiano [9] using AVL and FlightStream (FS).

lift coefficients. A difference in drag coefficient is not completely unexpected, since AVL is a vortex-lattice method neglecting thickness, whereas FlightStream is a 3D panel method. The pitching moment coefficient is very similar between both analyses, indicating a similar pitching moment coefficient slope C_{m_α}.

Since the result in terms of lift-drag polar is not completely conclusive, an extra validation step is made to ensure the validity of the model in terms of lift-to-drag ratio, which is a key input to the fuel burn method. Figure 5.3 shows the drag coefficient and lift-to-drag ratio for a range of lift coefficients. Clearly, the AVL model closely resembles the results of Faggiano which were obtained using SU2. The lift-to-drag ratio of FlightStream gets larger than 25, which is really high for large passenger aircraft and higher than the initial studies on the Flying-V such as by Benad and Faggiano [2, 3]. Since AVL closely follows the results of Faggiano, the lift-to-drag ratio is considered to be validated.

Lift Distribution

The spanwise lift distribution is an important input to the weight estimation method. At the design lift coefficient, the spanwise lift distribution is assessed using AVL and FlightStream and compared to the results of Faggiano et al. [9], as shown in Figure 5.4. The untrimmed results of AVL show the lift to be too far outboard. The trimmed results of AVL are obtained by trimming the aircraft at the same pitching moment coefficient as Faggiano et al., resulting in a similar lift distribution. The unstable results of FlightStream are caused by the abrupt changes in trailing edge sweep and trailing edge panel size between the tapered and untapered cabin part and between the inner and outer wing.

Static Stability Derivatives

The static stability of the validation aircraft design has been assessed both using FlightStream and using AVL. The results obtained for a reference point placed at the centre of gravity are provided in Table 5.2. Clearly,

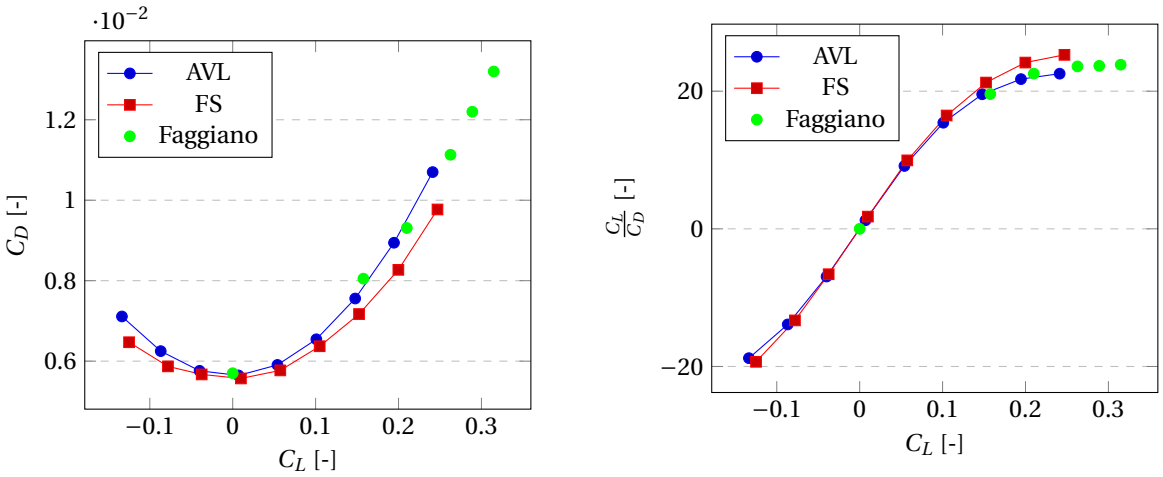

Figure 5.3: Validation of the lift-to-drag ratio resulting from AVL with FlightStream (FS) and the results of Faggiano et al. [9].

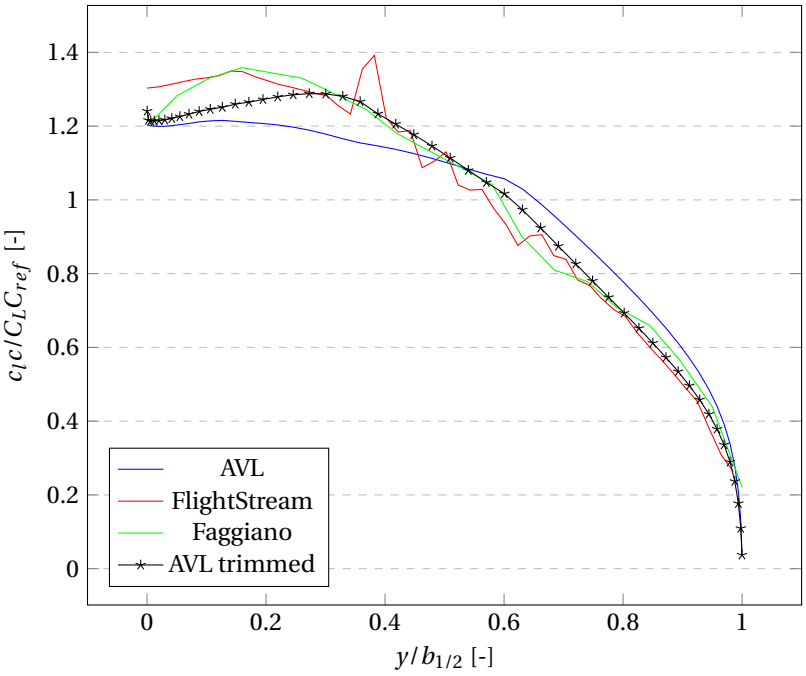

Figure 5.4: Spanwise lift distribution at the design lift coefficient. The trimmed results of AVL are obtained by trimming the aircraft at the same pitching moment coefficient as Faggiano et al. [9].

the results in C_{m_α} and C_{L_α} are very similar, which confirms the comparison in lift and pitching moment coefficient earlier in this section. C_{n_β} and C_{l_β} differ to a larger extent. The main difference between the models in FlightStream and AVL is the fact that AVL assumes a thin wing, whereas FlightStream is a 3D panel method. As such, there can be differences in drag force especially at sideslip conditions, such that a difference in these stability derivatives can be expected. The difference in drag coefficient earlier in this section confirms this thought. The stability derivatives do have the same sign, indicating a directionally and laterally stable aircraft. However, a more sophisticated model should be used in subsequent research to fully validate the stability of the aircraft. In this research, requirements on the static stability derivatives are not found to be driving and therefore the accuracy of their magnitude has no effect on the Flying-V family design.

Table 5.2: Stability derivatives for two angles of attack obtained using AVL and FlightStream (FS), reference point at the centre of gravity.

α	Solver	C_{L_α}	C_{m_α}	$C_{m_\alpha}@nose$	C_{n_β}	C_{l_β}
2	AVL	2.69	-0.22	-6.24	0.0013	-0.035
3	AVL	2.69	-0.22	-6.23	0.0018	-0.052
2	FS	2.66	-0.24	-6.21	0.0026	-0.085
3	FS	2.65	-0.21	-6.20	0.0005	-0.094

5.2. Weight Estimation

Building upon the verification and validation of the aerodynamic analysis, the weight estimation method can be verified and its results validated. Before diving into the verification and validation of the weight estimation method, it should be noted that parts of the model are already considered verified and validated. First of all, the method of Schmidt to estimate the weight of an oval fuselage is already extensively validated by Schmidt [80] and is further elaborated upon by subsequent studies such as by Elmendorp [78]. The loads acting on the oval fuselage consist of the weight of the different elements, which are validated in this section, and the aerodynamic loads which are validated in Chapter 4.2. The empirical relations by Torenbeek form the basis of many aircraft design studies and do not require a very extensive validation. Finally, EMWET is considered to be verified and validated, both by the initial study of Elham and by multiple studies employing this model [78, 79].

Verification and validation of the weight estimation method is performed in two ways. First of all, the A350 reference aircraft has been modelled and the resulting weights are compared to earlier studies on the Flying-V and where possible to existing information from Airbus. Secondly, the Flying-V component group weights are compared to the results by Claeys [12] and the landing gear location, engine placement and centre of gravity are compared to earlier studies. Performing these two subsequent steps ensures a complete validation of the method, validating the method including the described oval fuselage weight estimation method both on an existing conventional aircraft with a circular fuselage and on the Flying-V with its oval fuselage. The oval fuselage weight estimation method has been verified by unit testing all load determination and sizing procedures, comparing the results to the oval fuselage weight estimation of Schmidt [80] where possible.

5.2.1. Reference Aircraft

The reference aircraft design has been described in Section 4.4. In this section, the weight estimation results are validated. First, the loads along the fuselage beam are investigated. Then, the component group weights are validated.

Load Distribution

For the reference aircraft, the loads along the fuselage beam are analysed for three main load cases in Figure 5.5 and Figure 5.6. The shear force diagram shows a large increase in shear force at the location of the wing, and equillibrium of forces is validated since the shear force is zero at both ends of the fuselage beam. The bending moment should be zero both at the start and end of the fuselage beam, which is almost the case. The small non-zero bending moment at the end of the fuselage beam can be the result of a small difference in pitching moment of the wing or horizontal tail, which have been assumed to act at the average location of their respective spars whereas in reality this would be a more complex distributed bending moment. Note that the torsion is not depicted since it is zero.

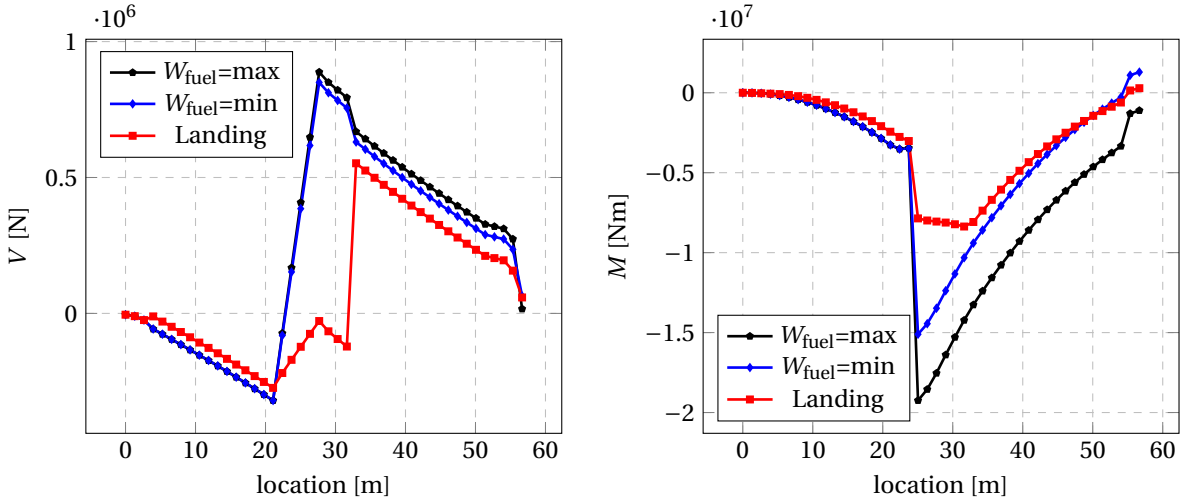

Figure 5.5: Shear force and bending moment along the fuselage beam for the A350-900, results for 44 sections.

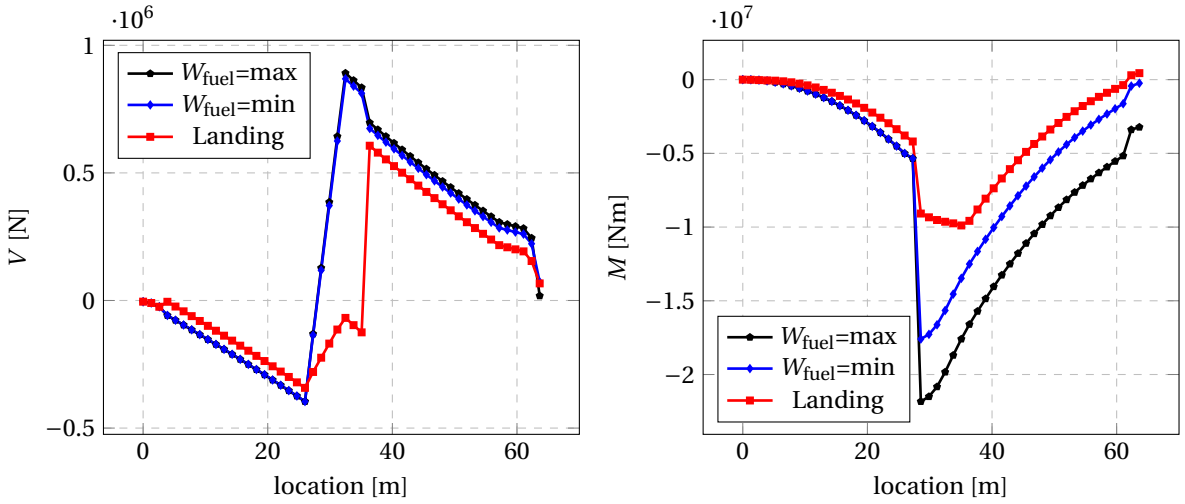

Figure 5.6: Shear force and bending moment along the fuselage beam for the A350-1000, results for 50 sections.

Component Group Weights

The component group weights are validated using data from Roskam on existing aircraft, as shown in Figure 5.7 [10]. Note that the fuel weight is more extensively verified and validated in Section 5.3, where the payload-range diagrams of the reference aircraft are compared to data given by Airbus. The assumption on the furnishing weight reduction factor described in Section 4.3.5 is considered validated, with a furnishing weight that is very comparable to reference aircraft.

A version of the reference aircraft is also modelled by Claeys, modelling a version with a smaller takeoff weight to compare to a Flying-V (FV) with the same takeoff weight [12]. Since the results of Claeys are confidential, component group weights as a fraction of the operating empty weight (OEW) are compared in Table 5.3. The largest differences in weights are found in the landing gear and fuselage weight, which can be explained by the lower design takeoff weight of Claeys. Additionally, Claeys uses a very high payload weight compared to the structural weight of the reference aircraft, which does not resemble the ratio between payload and OEW reported by Airbus [5]. Furthermore, the empennage weight in the modelled reference aircraft is higher than the results of Claeys, with a very low empennage weight for the study of Claeys. The ratio between weight and surface area of the modelled empennage is 5.1 lbs/m^2. A comparison with data from Roskam as in Figure 5.7 shows that the modelled empennage weight is already low compared to reference aircraft [10]. Hence, the result of this research is deemed more realistic.

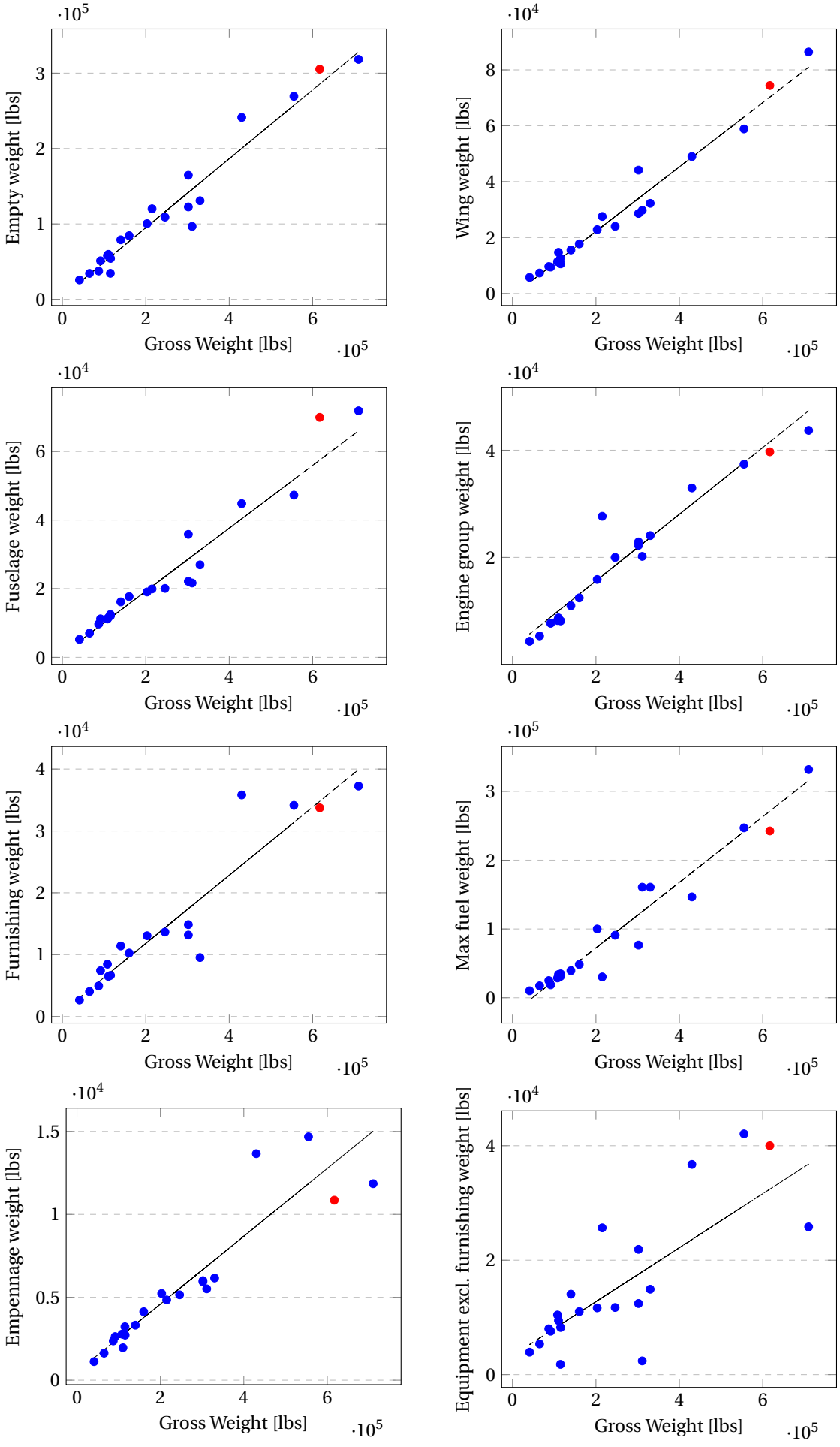

Figure 5.7: Component group weight validation for the reference aircraft, data from Roskam [10]. Results are shown in red, data of Roskam in blue.

Table 5.3: Component weight groups as fraction of the operating empty weight compared to the results of Claeys [12]. All results are for the -900 aircraft variant. Landing gear is abbreviated as LG.

	LG	Propulsion	Operational items and furniture	Systems	Wing	Fuselage	Empennage
	$\frac{W_{LG}}{W_{OEW}}$	$\frac{W_{propulsion}}{W_{OEW}}$	$\frac{W_{oper\,items}+W_{furniture}}{W_{OEW}}$	$\frac{W_{systems}}{W_{OEW}}$	$\frac{W_{wing}}{W_{OEW}}$	$\frac{W_{fuselage}}{W_{OEW}}$	$\frac{W_{empennage}}{W_{OEW}}$
A350 Claeys	0.12	0.18	0.15	0.12	0.23	0.18	0.02
A350 Model	0.08	0.17	0.15	0.09	0.24	0.23	0.04
FV Claeys	0.12	0.19	0.15	0.12		0.43	
FV Model	0.08	0.17	0.17	0.10		0.47	

5.2.2. Flying-V

In this section, the results for the Flying-V validation model are described. The starting point for this verification and validation is a Flying-V (FV) design which is largely based on the FV-900 design of Hillen [55]. Table 5.4 describes the design variables of this Flying-V.

Table 5.4: Design variables for the weight estimation verification and validation.

Variable	Value	Unit
L_1	m	23.75
L_3	m	11.1
b_{outer}	m	14.85
λ	-	0.15
c_1'	-	1.16
c_3'	-	1.21
H_{1_1}	m	0.6
H_{1_3}	m	0.6
H_{3_1}	m	0.7
H_{3_3}	m	0.6

Load and Mass Distribution

For the Flying-V, the loads along the fuselage beam are analysed for three main load cases in Figure 5.8. The shear force diagram shows that at the maximum fuel weight the loads are distributed more or less equalling the lift force at the inner part of the fuselage beam, whereas a large shear load is present on the outer part. The large increase in absolute shear force is the result of the landing gear and engine which are positioned at this location, at approximately 23 m. During landing, less upward force is generated by the wing due to the loads on the landing gear, resulting in an increase in shear force along the fuselage beam till the location of the landing gear. The bending moment and torsion are non-zero both at the start and end of the fuselage beam due to the clamped condition at the root and the loads on the outer wing respectively.

The mass and thickness distribution along the fuselage beam are shown in Figure 5.9. The total mass of the fuselage is largest at its clamped root, decreasing towards the end of the fuselage beam. This decrease in mass is mainly caused by a decrease in stringer mass. First of all, this is the result of the decrease in absolute bending moment and torsion along the fuselage beam as indicated in Figure 5.8. At the most outer sections of the fuselage beam, the thickness and hence mass increase again since the absolute bending moment increases again. Furthermore, the decrease in thickness and mass towards the outer sections of the fuselage beam can be explained by a decrease in pressure loads. The radii in the oval fuselage section decrease in the tapered part of the fuselage, since the cabin height decreases for the outer section whereas the keel and crown height are equal to the inner section.

The thickness distribution of the oval fuselage and inner wing structure can be compared to the result of Claeys, which unfortunately are confidential [12]. Claeys indicates a more or less constant mass distribution over the inner wing, which confirms the result of this study. The smeared thicknesses for the inner wing structural components of Claeys are in the range of 3 to 6 mm, which resembles the result of this study. Unfortunately, Claeys provides only figures with a colour scale indicating the thickness distribution, without

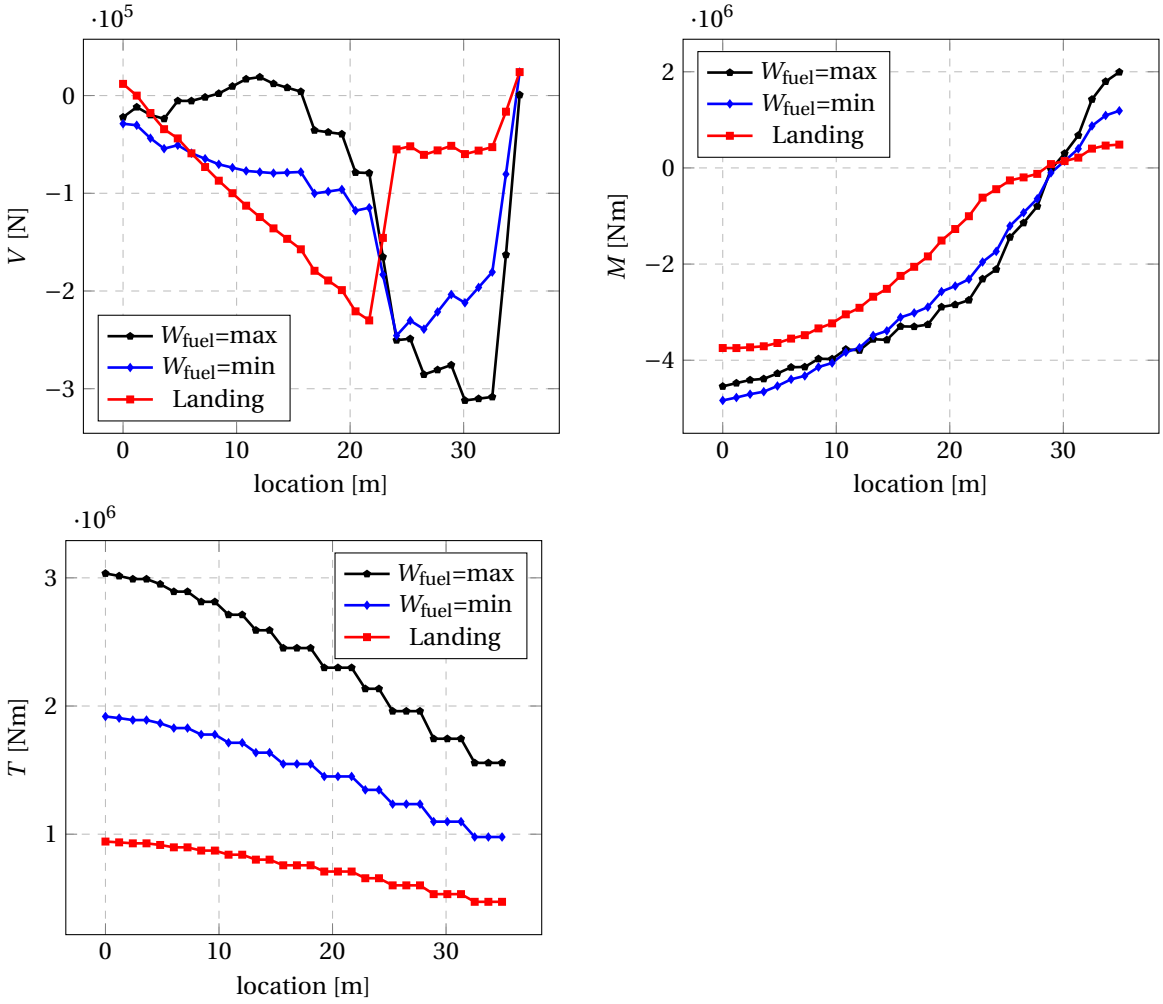

Figure 5.8: Shear force, bending moment and torsion along the fuselage beam for the FV-900, results for 30 sections.

a specification of thicknesses per component or clear structured data which can be compared to the results of this study. As such, component weight groups are compared to the result of Claeys in the following section.

Component Group Weights

The component group weights of the Flying-V are validated by comparing them to both the reference aircraft and the results of Claeys [12]. Table 5.3 shows that the component group weights as a fraction of the operating empty weight are rather similar between this research and the study of Claeys. The largest difference for these component group weights is the landing gear weight, which is the result of a lower maximum takeoff weight in this research for the Flying-V such that the landing gear weight can be reduced. The same line of reasoning applies to the weight of the propulsion group. Claeys does not capture this effect and uses the same landing gear and propulsion group on the reference and Flying-V aircraft.

The landing gear of the Flying-V is relatively long compared to reference aircraft [31] and therefore the validity of the empirical relation used to estimate this weight deserves further attention. Bourget studied the landing gear of the Flying-V, considering several options for landing gear design and location [31]. The weight of the landing gear is at $10.0 \cdot 10^3$ kg for the FV-900 to $11.6 \cdot 10^3$ kg for the FV-1000 close to the values of Bourget, who obtains $9.7 \cdot 10^3$ kg to $10.2 \cdot 10^3$ kg for a $260 \cdot 10^3$ kg MTOW aircraft. However, the study of Bourget suggests a landing gear weight of $10.8 \cdot 10^3$ kg for the A350-900, whereas the relation used in this research results in $11.7 \cdot 10^3$ kg. Probably, the use of more lightweight materials in modern aircraft explains this difference, such that the relation by Torenbeek overestimates the landing gear weight. For the Flying-V the relation could be more applicable, compensating for the relatively long landing gear. The landing gear weight of Bourget was estimated using a relation of Raymer, which was found to underestimate the gear weight [31]. In this study,

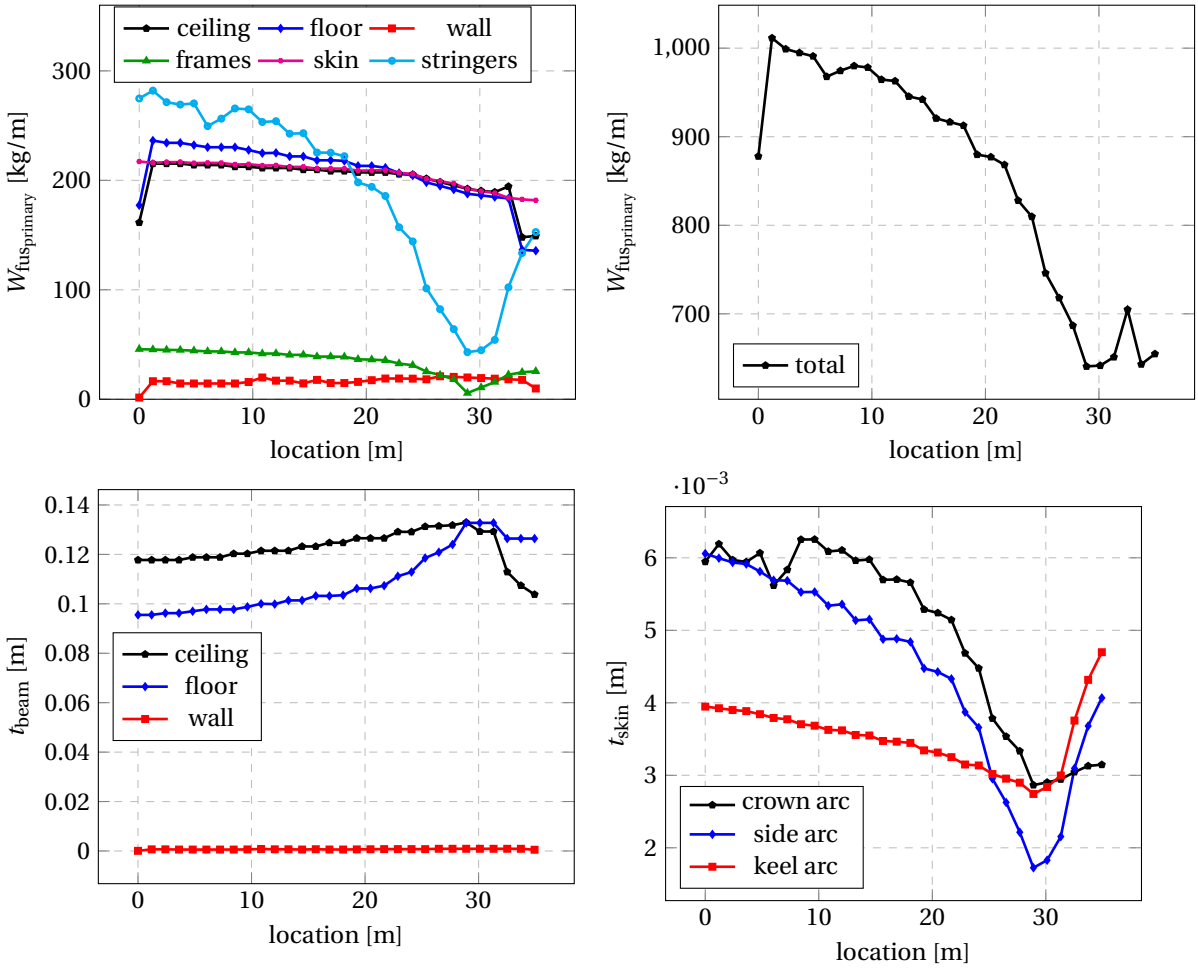

Figure 5.9: Mass and thickness distribution along the fuselage beam for the FV-900. Mass is provided in kg/m by dividing the weight at each longitudinal section by the longitudinal section width.

the relation of Torenbeek is still applied since mixing multiple weight estimation methods is not favourable to ensure that all aircraft components are included exactly once. The applicability of the Torenbeek landing gear weight estimation to modern passenger aircraft might be the subject of future research.

Claeys shows a 17% reduction in primary structural weight between the Flying-V and the A350 [12]. Since EMWET is used to size both the outer wing of the Flying-V and the main wing of the A350 in this study and does not separately output primary and secondary weights, it is not possible to separate the results of this study into primary and secondary weights. The total structural weight (including secondary weights) is reduced by 16% in this research, which is very close to the primary structural weight reduction of Claeys. Since secondary weights are largely dependent on the primary weight applying an empirical relation linearly relating the two weights (described in Section 4.3.5) the comparison with Claeys is still considered relevant.

Landing Gear and Engine Placement

As has been described in Section 4.3.4, the landing gear and engine location are closely related. In this section, the results for the location of the landing gear and engine are validated. Rubio Pascual determined the optimal engine location to be at 4.7 m of the aircraft's centre axis in span-wise direction, using the aircraft design of Faggiano with a span of 65 m. The engine location of the baseline Flying-V design in this study is at 4.2 m for a span of 60.4 m. Dividing by the span, Rubio Pascual places the engine at 14% of the span, and this study results in 14% of the span as well.

Bourget puts the main landing gear due to a tilt of 10 degrees at approximately 32.8 metres for the design of Faggiano and the nose gear at 7.11 m, which is at 58.0% and 12.6% of the aircraft length measured from the nose respectively. In this study, the location of the nose and main landing gear for the FV-900 is found to be at 8.9 m and 30.6 m respectively, which is at 16.8% and 58.0% respectively. The location of the main gear

exactly equals the design of Bourget, but the location of the nose gear differs. The nose gear could easily be placed more forward, but is currently set at the root of the fuselage centre beam. Since the location of the nose gear follows from the location of the main gear and the desired loading on the nose gear, this location might in reality differ from the location used in this research. Since the fuselage beam already includes the assumption to place all weights on its elastic axis, the assumption to place the landing gear placement on this axis does not introduce an additional assumption.

Centre of Gravity

The centre of gravity has been investigated in multiple earlier studies on the Flying-V. The initial aerodynamic study by Faggiano and the preliminary design of Benad assumed the centre of gravity to be ahead of the neutral point by 6% of the MAC at the design condition [3, 13]. Palermo, who studied the longitudinal static stability and control of the 4.6% scaled Flying-V model, determined the aerodynamic centre to move between 1.32 and 1.42 m from the nose of the scaled aircraft model for angles of attack between -10 and 20 degrees [26]. Palermo determines the optimal centre of gravity location based on maximising the trimmed lift coefficient whilst ensuring trimability for this entire range of angle of attacks. The study concludes that the optimal centre of gravity location would be at 1.336 m on the scale model. For the reference aircraft, Palermo assumes the centre of gravity of the A350-900 aircraft to be at 25% of the MAC. Viet finds the centre of gravity based on trim limitations to be bound between 1.345 and 1.425 m behind the nose of the scale model [27]. The neutral point was determined to be at approximately 1.430 m from the nose, and the optimal centre of gravity location is set at 1.365 m. This yields a static margin of approximately 9% of the MAC. Ruiz Garcia includes thrust in the analysis to determine the optimal centre of gravity location [28]. This study concludes that the centre of gravity is bound between 1.32 and 1.40 m. The optimal centre of gravity location is set at the middle of this range, at 1.36 m. All results of these earlier studies are summarised in Table 5.5

Table 5.5: Centre of gravity (x_{cg}) location for earlier studies on the Flying-V and this study.

x_{cg} (m)	% of aircraft length w.r.t. nose	Source
1.336	52.4	Palermo [26]
1.345-1.425	52.8-55.9	trim limitations Viet [27]
1.365	53.6	optimal according to Viet [27]
1.32-1.40	51.8-55.0	Ruiz Garcia [28]
27.93	52.8	this study

The FV-900 model in this research results in the centre of gravity at 27.9 m at the design maximum takeoff weight condition, which is at 52.8 % of the aircraft length measured from the nose of the aircraft. This is very similar to the aforementioned earlier studies on the Flying-V scale model. The most aft location is found at 29.1 m, which is far from the aerodynamic centre at 31.1 m, resulting in a large static margin of 11% of the MAC. For the design mission, the most aft and most forward locations are at 27.9 m and at 24.7 m respectively, which means that the centre of gravity shifts approximately 3.2 m during a flight. This centre of gravity shift is rather large and will be further discussed after optimisation in Chapter 6. Since the centre of gravity location at the design condition closely resembles earlier studies on the scaled model of the Flying-V, the approach to calculate the centre of gravity is considered to be validated.

5.3. Fuel Burn Analysis

Verification and validation of the fuel burn analysis is performed in two ways. First of all, the payload-range diagram of the reference aircraft is compared to the official data provided by Airbus and the fuel burn for the Flying-V is compared to the reference aircraft and to the studies of Faggiano et al. [9] and Benad [2]. Secondly, a sensitivity analysis on several key input parameters is performed.

The reference aircraft model is entirely based on the dimensions provided by Airbus [5]. The total wetted area of the baseline model is 2302 m^2, which is within 3% of the total cleaning area provided by Airbus of 2242 m^2 [5]. The larger -1000 variant has a total wetted area of 2434 m^2, which is within 2% of the provided total cleaning area of 2392 m^2.

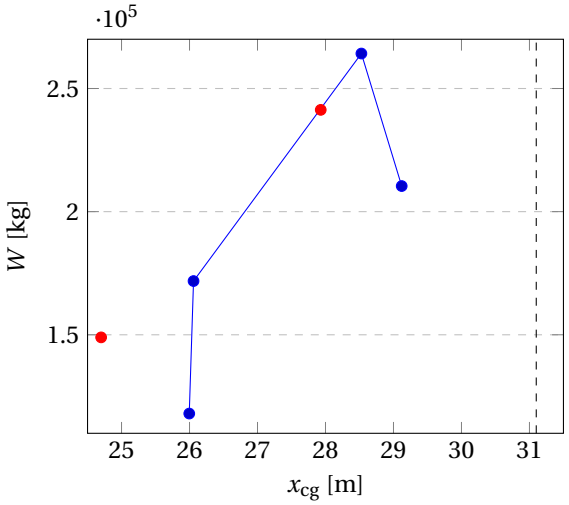

Figure 5.10: Longitudinal centre of gravity location at different maximum and minimum loading points (blue) and the most forward and aft location at the design condition (red). The dashed black line indicates the position of the aerodynamic centre.

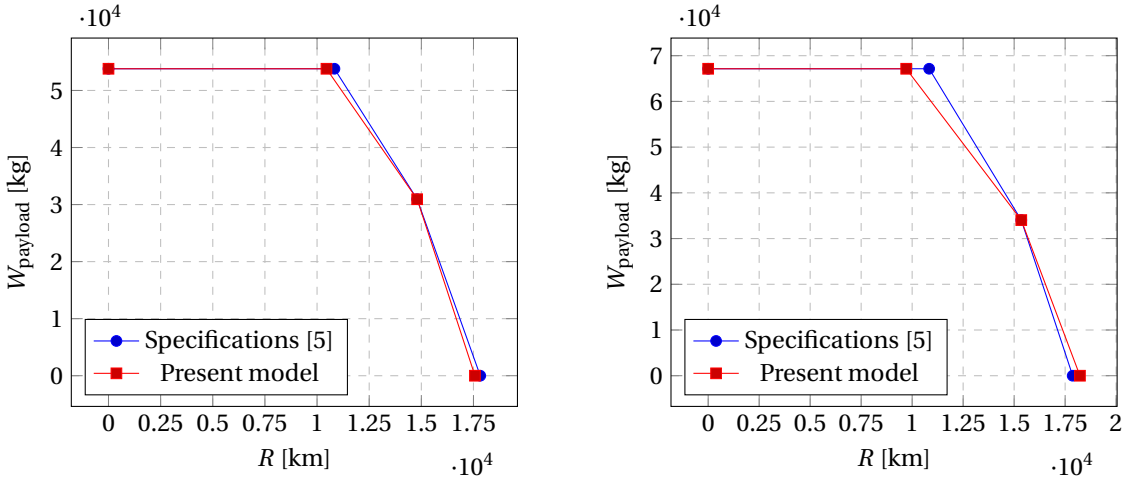

Figure 5.11: Payload range diagram of the -900 and -1000 aircraft family members. A350 specifications data from Airbus [5].

5.3.1. Payload-Range Performance

Airbus provides the payload-range diagrams of the A350-900 and -1000 reference aircraft, which are compared to the result of this study in Figure 5.11 [5]. Since the design mission is at the maximum range with a fully filled aircraft in terms of passengers, these points exactly correlate for all aircraft. It should be noted that these results are for individual aircraft without a commonality constraint applied. Clearly, the modelled reference aircraft closely follow the payload-range specification of Airbus. The harmonic range of the modelled A350-1000 aircraft is slightly smaller due to a slightly lower maximum takeoff weight. As such, the ferry range for the modelled A350-1000 aircraft is slightly larger than specified.

5.3.2. Fuel Burn

The studies of Benad and Faggiano et al. suggest a fuel burn reduction of 20% based on a lift-to-drag ratio improvement of 10% with respect to the reference aircraft or 25% with respect to the NASA Common Research Model [2, 9]. An estimation of this fuel burn performance is made using the FV-900 design of Hillen for the Flying-V [55] as described in Section 5.2.2. Both the Flying-V design and reference aircraft model do not incorporate commonality constraints. The fuel burn of the FV-900 and A350-900 for the design mission are estimated at 92.6 $\cdot 10^3$ kg and 111.7 $\cdot 10^3$ kg respectively. Hence, the modelled difference in fuel burn performance between the Flying-V and A350-900 is 17.1%, which is close to the estimations of Benad and Faggiano et al. The difference in fuel burn reduction is probably mainly the result of the differences in Flying-V design between the design of Hillen and the design of Faggiano, especially due to a sudden change in thickness be-

tween the inner and outer wing. In Section 6.2.1 this problem is discussed, leading to several design changes on the Flying-V. Finally, optimisation of the Flying-V presented in Chapter chapter 6 should lead to the larger fuel burn reduction predicted by earlier studies.

5.3.3. Sensitivity Analysis

The sensitivity of the fuel burn model to several key inputs is assessed to ensure the model reacts to inputs in a logical way. First of all, the number of sections used to define the fuselage of a Flying-V aircraft is increased as shown in Figure 5.12a. The fuel burn is found to be stabilising at an increasing number of sections, which is as expected. This analysis additionally shows that when the number of sections is chosen too small, the resulting fuel burn will probably be too high such that a rather conservative design results.

Figure 5.12b visualises the sensitivity of the fuel burn to the rib spacing on the outer wing, s_{rib}. The effect of changing the rib spacing is very small, especially around the rib spacing of 0.6 m used in this research.

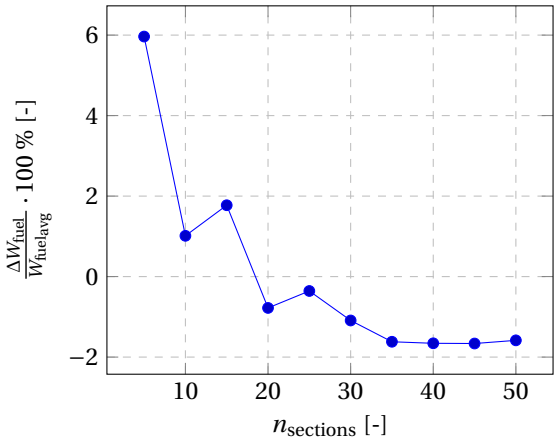

(a) Sensitivity analysis on the number of sections describing the aircraft along its fuselage centre axis.

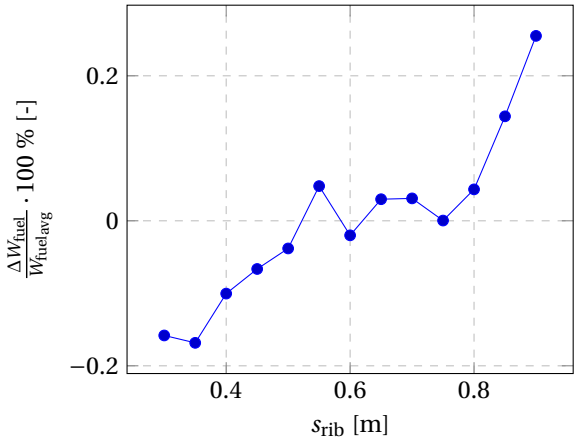

(b) Sensitivity analysis on the outer wing rib spacing.

An increase in the differential pressure in the cabin, Δp_{cruise}, leads to a higher fuel burn, as shown in Figure 5.13a. This result is not surprising, since a higher differential pressure means that the structure should withstand larger loads and hence will be heavier. The sensitivity of the fuel burn to the fuselage frame spacing is depicted in Figure 5.13b. At a larger frame spacing, the structural members between the frames require more stiffening and as such will be heavier. The frame spacing of 0.635 m of the reference aircraft is used for both aircraft families as explained in Section 4.3.2. A smaller frame spacing might yield a lower fuel weight, but the frame spacing is often dictated by the window spacing.

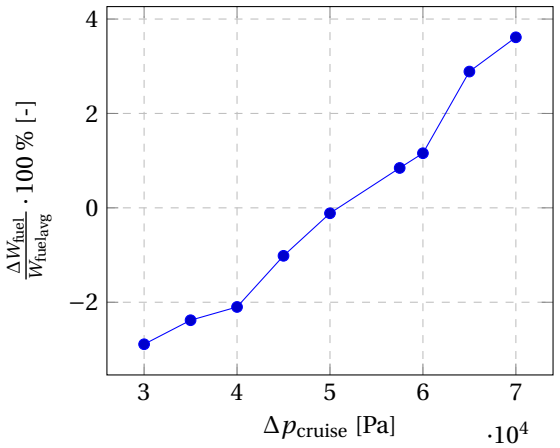

(a) Sensitivity analysis on the pressure difference between the cabin and the atmosphere at cruise conditions.

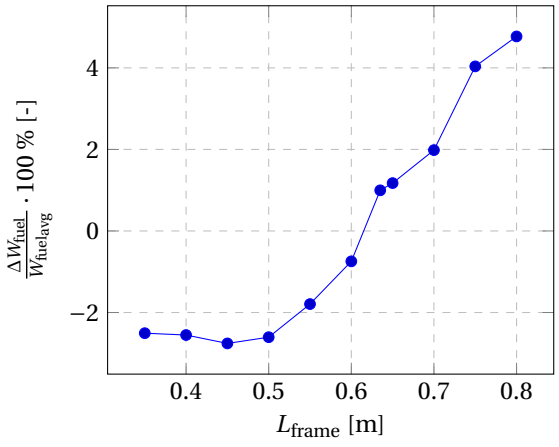

(b) Sensitivity analysis on the fuselage frame spacing. The frame spacing used in this study is 0.635 m.

6

Results and Discussion

In this chapter, the results of the Flying-V aircraft family design are presented and discussed. First, the reference aircraft family is investigated, followed by the Flying-V family. The Flying-V family is compared to the reference aircraft family, both in terms of performance and regarding driving requirements in family design. Finally, a sensitivity analysis of the results to the design variables is performed and the optimal Flying-V family design is shown.

6.1. Reference Aircraft Family

For the reference aircraft family, the effect of commonality is determined by applying the same family design principles as for the Flying-V aircraft family. The wing and empennage are already identical between both family members, such that only the thickness of the structural members of the fuselage should be set equal to find the cost of commonality. Note that the landing gear of both aircraft is not assumed to be identical, since this is not the case for the real Airbus A350 either [5]. To form the -1000 version of the aircraft from the -900 version, 7 frames are inserted between the nose and wing and 4 frames are inserted aft of the wing.

The resulting penalty in component group weight and fuel burn is presented in Table 6.1. The results indicate a fuel burn penalty of 0.4% for the smallest aircraft variant and 0.7% for the largest variant. These results show that the penalty resulting from commonality is not necessarily larger for the smallest aircraft variant. For instance, for the A350-900 the thickest structural members are close to the wing, whereas these are moved away from the wing by inserting plugs on the -1000. As such, these components are sized by the -900 variant and increase the weight on the -1000 variant.

A penalty of 0.4% to 0.7% in terms of fuel burn and 0.4% to 0.8% in terms of maximum takeoff weight seems rather small. However, this result only captures a part of the effect of including commonality on the A350 aircraft family. Looking at the two types of penalties due to commonality described in Section 3.3.3, only part of the first penalty is captured. Firstly, not the complete first penalty due to commonality can be determined because the impact of including the same wing or empennage in terms of weight cannot be captured, since these are not separately designed for both reference aircraft in the current model. Secondly, the second penalty due to commonality is not estimated at all, since no single optimised aircraft have been modelled for the reference aircraft family.

Now that the reference aircraft family has been designed with a commonality constraint applied, its fuel burn and maximum takeoff weight can be compared to the specifications stated by Airbus [5]. The results are shown in Table 6.2, indicating an accurate model of the reference aircraft both in terms of fuel burn and in terms of MTOW.

Payload-range performance of the reference aircraft is shown in Figure 6.2. Due to the very small penalty in terms of fuel burn and maximum takeoff weight resulting from commonality the results do not differ much from the results presented in Section 5.3.1. Additional results on the reference aircraft family are presented and discussed in Section 6.3.

6.2. Flying-V Family

In this section, the Flying-V family is designed. First of all, a baseline aircraft family is presented, serving as a starting point for optimisation of the aircraft family. Then, optimised designs are compared and the effect

Table 6.1: Component group weight penalties due to commonality for the reference aircraft, all in 10^3 kg.

Weight group	A350-900	%	A350-1000	%
Payload	-	-	-	-
Fuel	0.46	0.4	0.94	0.7
Landing gear	0.06	0.5	0.11	0.9
Propulsion	-	-	-	-
Operational items	-	-	-	-
Furniture	-	-	-	-
Structure	0.64	0.9	1.24	1.7
Systems	0.02	0.2	0.04	0.3
OEW	0.7	0.5	1.4	0.9
MTOW	1.2	0.4	2.3	0.8

Table 6.2: Fuel burn and MTOW for the reference aircraft, specification data from Airbus [5].

		A350 specifications [5]	A350 family model	Difference %
W_{fuel} [10^3 kg]	-900	113.2	112.2	-0.9
	-1000	127.7	128.4	0.5
MTOW [10^3 kg]	-900	280.0	281.2	0.4
	-1000	316.0	312.3	-1.2

of enforcing commonality is investigated, identifying driving requirements in Flying-V family design and its effect on fuel burn performance.

6.2.1. Baseline Aircraft Family Design

A baseline aircraft family is designed as a starting point for the optimisation procedure. The design of the FV-900 of Hillen serves as a starting point for the baseline aircraft family in this research [55]. For the -800 and -1000 version of the Flying-V, only the length of the untapered cabin is scaled to ensure commonality between the family members. With respect to this original design by Hillen, some small design changes are made. Especially the structure connecting the outer and inner wing deserves attention, since this part of the wing is not considered aerodynamically efficient due to an abrupt change in thickness. The following design changes are made with respect to the original starting point of Hillen:

- decrease the height of the cargo compartment, H_{2_3}, to 1.22 m, using 45" containers when normal-sized LD-4 containers do not fit anymore;
- increase the connecting structure between the inner and outer wing, L_4, to 1.5 m;
- decrease the outer wingspan to 14.85 m due to the maximum wingspan constraint.

The family design variables for the baseline aircraft family are shown in Table 6.5. The component weight groups and key characteristics for this baseline aircraft family are presented in Table 6.3 and Table 6.4. These results indicate a large centre of gravity shift for all aircraft family members, a large static margin for especially the FV-1000 and too large fuel tanks for the largest two aircraft variants. Note that the design range of the FV-800 is determined based on its available tank volume, as explained in Section 3.4, such that its fuel tanks are completely filled.

6.2.2. Optimisation Results

All Flying-V aircraft have been optimised both as part of the aircraft family and individually. The design variables of the baseline aircraft and single and family optimisation results are presented in Table 6.5. Table 6.6 and Table 6.7 present the results of both the single aircraft optimisation (SO), family of aircraft optimisation (FO-F) and the results for a single aircraft without the commonality constraint using the design vector of the optimised family of aircraft (FO-S).

Principal differences between the baseline aircraft and the optimised aircraft are the reduced taper ratio, reduced outer cabin chord length c_3' and reduced outer cabin crown and keel height H_{1_3} and H_{3_3}. These changes move more wing area inboard, bringing the aerodynamic centre forward such that the static margin

Table 6.3: Component group weights of the baseline Flying-V aircraft, all in 10^3 kg.

Weight group	FV-800		FV-900		FV-1000	
	B	F	B	F	B	F
Payload	27.6	27.6	30.9	30.9	34.0	34.0
Fuel	74.4	74.4	92.6	92.8	110	109
Landing gear	8.0	11.6	9.9	11.6	11.5	11.6
Propulsion	16.1	16.1	19.6	19.6	21.9	21.9
Operational items	5.2	5.2	5.8	5.8	6.4	6.4
Furniture	12.2	12.2	14.3	14.3	16.7	16.7
Structure	44.2	48.9	55.6	56.5	61.1	64.3
Systems	10.9	11.1	12.3	12.4	13.5	13.6
OEW	96.6	105	118	120	131	134
MTOW	199	207	241	244	275	278

Table 6.4: Key characteristics of the baseline Flying-V aircraft.

	Unit	FV-800		FV-900		FV-1000	
		B	F	B	F	B	F
Outer wing weight	10^3 kg	7.2	7.5	7.1	7.5	6.1	7.5
Static margin	m	2.0	2.0	3.4	3.0	4.1	3.7
Fuel tank volume available	m^3	92	92	129	129	156	156
Fuel tank volume required	m^3	92	92	115	115	137	136
Span	m	56.4	56.4	60.7	60.7	65.0	65.0
Approach speed	m/s	66.4	67.9	68.7	69.2	69.7	70.0
Lift-to-drag ratio	-	21.0	21.0	20.7	21.1	20.3	20.6
CG shift design mission	m	3.2	3.2	2.9	3.0	3.4	3.0
Design range	10^3 km	14.5	13.6	14.8	14.8	15.4	15.4

of the aircraft is reduced, which has a beneficial effect on fuel burn performance. Additionally, these changes move the fuel tank volume inboard, such that the fuel is located closer to the centre of gravity which reduces the centre of gravity shift during flight. A smaller taper ratio would have the same effect, but the taper ratio is set to a minimum value of 0.1 to ensure structural feasibility and sufficient fin area. The outer cabin crown and keel height H_{1_3} and H_{3_3} are set at 0.45 m, which is the result of a trade-off. On the one hand, the crown and keel height should not be too small to limit the radius of the oval cabin and hence limit stresses in the pressurised cabin. On the other hand, a larger keel or crown height would increase the abrupt change in thickness between the inner and outer wing with possibly negative aerodynamic effects such as flow separation.

Especially for the FV-800, the shift in centre of gravity during flight for the design mission has been reduced significantly compared to the baseline design presented in Section 6.2.1. When including centre of gravity locations at maximum and minimum payload and maximum and minimum fuel weight, Figure 6.1 results. Between design missions, the centre of gravity shift can still be very large. The main reason for this is the fact that the passengers are located towards the front of the cabin, whereas the cargo containers are placed aft of the cabin, shifting the centre of gravity aft quite significantly. The static margin is relatively large in all cases, with the aerodynamic centre indicated by the dashed lines in the figures.

The fins resulting from this optimised aircraft family have a maximum height of 5.0 m, which means that the maximum tail height constraint is easily met. The track width of the largest aircraft variant is set at 12.2 m following from the study of Bourget [31], such that the constraint on track width is not active either.

The payload-range diagrams of the optimised Flying-V aircraft family members are compared to the reference aircraft family in Figure 6.2. The FV-800 does not have a reference aircraft family member. The FV-800 has a relatively low harmonic payload or a relatively high design payload. The FV-900 and FV-1000 have a lower empty weight and maximum takeoff weight than their competitor such that the harmonic range is smaller and the ferry range is larger.

The length of all plugs is given in Table 6.8. The lengths of the plugs are not an exact multiple of the frame pitch because the variables describing the Flying-V were defined to be continuous. In reality, the lengths of

Table 6.5: Design variables for the baseline aircraft (B), single optimisation (SO) and family optimisation (FO) results.

		FV-800			FV-900			FV-1000		
Variable	Unit	B	SO	FO	B	SO	FO	B	SO	FO
L_1	m	18.75	17.5	18.0	23.75	19.1	24.0	28.75	21.0	29.0
L_3	m	11.1	12.0	11.0	11.1	16.6	11.0	11.1	20.0	11.0
b_{outer}	m	14.85	15.5	14.75	14.85	16.0	14.75	14.85	14.2	14.75
λ	-	0.15	0.10	0.10	0.15	0.10	0.10	0.15	0.10	0.10
c_1'	-	1.16	1.07	1.11	1.16	1.12	1.11	1.16	1.14	1.11
c_3'	-	1.21	1.12	1.13	1.21	1.12	1.13	1.21	1.13	1.13
H_{1_1}	m	0.6	0.63	0.68	0.6	0.65	0.68	0.6	0.65	0.68
H_{1_3}	m	0.6	0.45	0.45	0.6	0.45	0.45	0.6	0.45	0.45
H_{3_1}	m	0.7	0.64	0.68	0.7	0.65	0.68	0.7	0.65	0.68
H_{3_3}	m	0.6	0.45	0.45	0.6	0.45	0.45	0.6	0.45	0.45

Table 6.6: Component group weights for the single optimisation (SO) and family optimisation without (FO-S) and with (FO-F) commonality constraint, all in 10^3 kg.

	FV-800			FV-900			FV-1000		
Weight group	SO	FO-S	FO-F	SO	FO-S	FO-F	SO	FO-S	FO-F
Payload	27.6	27.6	27.6	30.9	30.9	30.9	34.0	34.0	34.0
Fuel	53.3	54.0	58.0	81.6	86.7	87.5	98.6	105	103
Landing gear	6.8	6.8	11.1	9.2	9.4	11.1	10.7	11.1	11.1
Propulsion	16.1	16.1	16.1	19.6	19.6	19.6	21.9	21.9	21.9
Operational items	5.2	5.2	5.2	5.8	5.8	5.8	6.4	6.4	6.4
Furniture	12.1	12.1	12.2	14.3	14.3	14.3	16.6	16.7	16.7
Structure	39.2	38.4	43.8	51.1	51.0	52.4	57.4	55.6	60.0
Systems	10.4	10.3	10.7	12.2	12.2	12.3	13.5	13.3	13.4
OEW	89.9	89.0	99.9	112	112	115	127	125	129
MTOW	171	171	185	225	230	234	259	264	266

the plugs should be a multiple of the frame pitch, which is largely determined by the window pitch of the aircraft.

The mass and thickness distribution of the oval fuselage structural members for the optimised FV-900 as part of the aircraft family is visualised in Figure 6.3. Results for the FV-800 and FV-1000 aircraft family members are presented in Appendix C. The results do not differ much from the results for a single aircraft presented in Section 5.2.2. Except for the stringers, the weight of the oval fuselage structural members is almost constant over the length of the fuselage. This underlines the structural efficiency of a Flying-V, which distributes payload and fuel over the lifting surface by integrating the fuselage into the wing. The decrease and increase of the stringer weight towards the end of the fuselage is caused by an increase and decrease in absolute bending moment as explained in Section 5.2.2. The weight of the wall is very small, suggesting the application of separate struts at different locations rather than a complete sandwich panel. Note that no load case including cargo was included, such that possibly strengthening is required towards the end of the fuselage to withstand this increase in payload weight. However, since at a larger payload weight the fuel weight would decrease due to the maximum takeoff weight of the aircraft, this effect could possibly be very limited. The bending moment, shear force and torsion diagrams for all optimised aircraft family members are included in Appendix C.

A comparison between single optimised aircraft and the aircraft family design is made in Section 6.2.4.

6.2.3. Driving Requirements in Flying-V Family Design

There are several driving requirements in the optimised Flying-V family. Naturally, the most important active constraint is the commonality in design variables and components between the different aircraft variants. Several other top-level requirements are discussed in this section.

As expected, requirements on the volume and floor area of the payload are driving. Sufficient floor area for the passengers should be available with a minimum cabin height towards the back of the cabin of 1.9 m.

Table 6.7: Key characteristics for the single optimisation (SO) and family optimisation without (FO-S) and with (FO-F) commonality constraint.

		FV-800			FV-900			FV-1000		
		SO	FO-S	FO-F	SO	FO-S	FO-F	SO	FO-S	FO-F
Outer wing weight	kg	5.7	5.4	6.6	7.2	6.3	6.6	5.3	4.8	6.6
Static margin	m	2.3	2.2	1.9	2.3	3.0	2.6	2.7	3.7	3.3
Fuel tank volume available	m^3	67	72	72	101	109	109	124	133	133
Fuel tank volume required	m^3	66	67	72	101	109	109	123	133	128
Span	m	57.1	55.5	55.5	63.2	60.7	60.7	65.0	65.0	65.0
Approach speed	m/s	64.4	64.7	67.2	67.9	69.5	70.1	69.3	70.8	70.7
Lift-to-drag ratio	-	21.1	20.7	20.9	22.5	21.3	21.6	21.7	20.4	21.2
CG shift design mission	m	2.4	2.4	2.5	2.8	2.9	3.0	2.9	3.4	3.0

Table 6.8: Length of fuselage plugs to build a family of Flying-V aircraft.

plug		frames	length (m)
-900	front	4	2.67
	aft	5	3.33
-1000	front	3	1.88
	aft	5	3.12

Since the length of the tapered cabin is set at a maximum of 11 m by the smallest aircraft, the minimum cabin height is not an active constraint. The total floor area of the cargo, passengers, lavatories, galleys and free space for aisles is an active constraint in all family members. The fuel volume is also an active constraint in the optimised aircraft family, in which only the fuel tank of the largest aircraft variant is not completely filled.

The constraint on the span is also active during the optimisation. The maximum wingspan of 65 m means that the outer wing can have a maximum length of 14.75 m following from the span constraint on the largest aircraft variant. As such, the smaller aircraft variants have a limited total wingspan whereas the individual aircraft optimisations showed a somewhat larger wingspan is preferable for these variants. Naturally, removing the commonality constraint on the outer wing would allow for unique outer wingspans between aircraft variants.

The centre of gravity shift during flight is a driving requirement in the optimisation of the aircraft family. As explained in Section 3.2, a constraint on the centre of gravity shift is hard to define, and hence it was included implicitly in the optimisation procedure.

Constraints that are not active are the constraints on the approach speed, tail height, main gear track width and directional and lateral static stability. The constraint on approach speed entails an assumption on the maximum lift coefficient during approach, which was defined at 0.73 in Section 3.2. Further research is required to check the validity of this assumption, but since the approach speed of the optimised Flying-V family is very low, a small decrease in maximum lift coefficient would still not activate the approach speed requirement. The constraint on tail height is also easily met, allowing an increase in tail height of approximately 3 m with respect to the optimised family design and earlier Flying-V designs. The main gear track width follows from the study of Bourget and the centre of gravity location as explained in Section 4.3.4. At 12.2 m, a margin of 1.8 is present with respect to the maximum track width of 14 m. AVL suggests that the aircraft are all directionally and laterally stable. A more sophisticated aerodynamic model should be used to verify these stability derivatives in later design phases.

Since the height of the tapered cabin is only 1.22 m, the minimum height of the cabin is an active constraint in single aircraft optimisation with the optimiser maximising the part of the cabin which is tapered.

6.2.4. Cost of Commonality

As has been explained in Section 3.3.3, the cost of commonality can be separated into two components. The first penalty, related to the direct penalty in terms of structural weight when selecting common components between family members, is easily obtained by comparing an aircraft design with the same design subject to commonality constraints on component weights and structural member thicknesses. The second penalty, related to the optimisation in common variables instead of unique variables, is obtained by comparing indi-

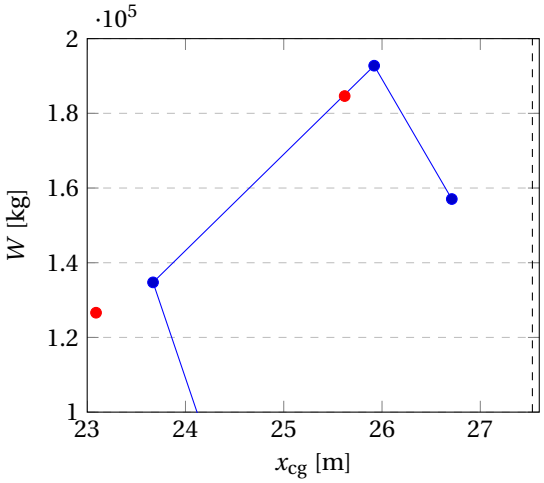

(a) Flying-V 800.

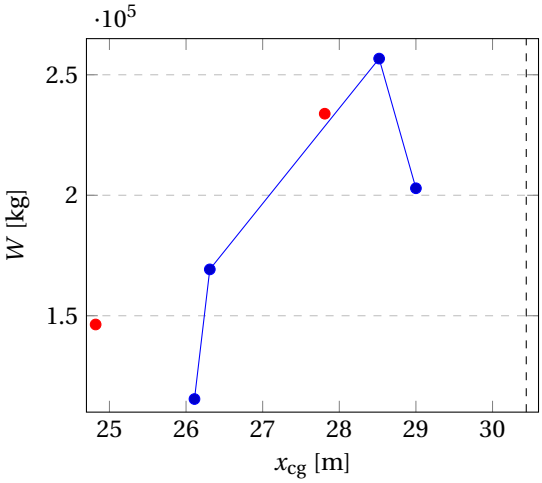

(b) Flying-V 900.

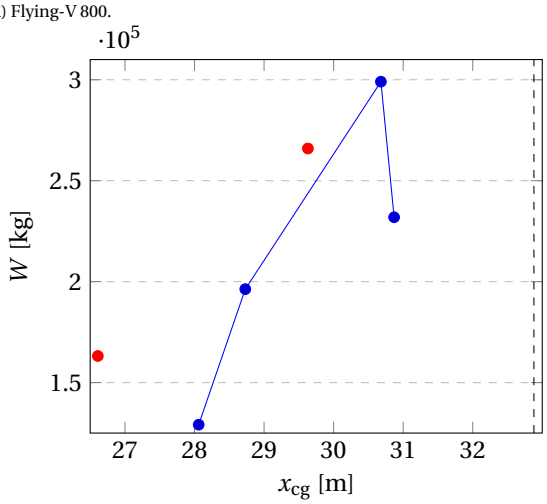

(c) Flying-V 1000.

Figure 6.1: Longitudinal centre of gravity location for the optimised aircraft family at different maximum and minimum loading points (blue) and the most forward and aft location at the design condition (red). The dashed black lines indicate the position of the aerodynamic centre. All distances are with respect to the nose of the aircraft.

vidually optimised aircraft to designs obtained with a family optimisation routine. For the reference aircraft, only the first part can be obtained since no data on single optimised aircraft exists and developing a model to find these aircraft is considered beyond the scope of this research. The results for the reference aircraft are shown in Section 6.1. In this section, the results on both penalties for the Flying-V aircraft family is presented and the impact of including the FV-800 on the aircraft family is discussed. The total fuel burn penalty due to commonality is 8.9% for the FV-800, 7.1% for the FV-900 and 4.2% for the FV-1000.

Component Commonality Penalties

A comparison between the results for a single aircraft with and without the commonality constraint (FO-F and FO-S) using the design vector of the optimised family of aircraft yields the component commonality penalty. The penalty in fuel burn is approximately 7.3%, 0.9% and -2.4% for the -800, -900 and -1000 respectively. The increase in takeoff weight is 8.2%, 1.8% and 0.7% respectively, almost exclusively the result of a larger structural weight and landing gear weight. The landing gear weight increases significantly for the -800 and -900 version by 62% and 18% respectively. The large increase in fuel weight for the -800 aircraft can be mainly explained by this large increase in landing gear weight which comes with an increase in structural weight. The reduction in fuel weight for the -1000 version can be explained by a large reduction in static margin, as shown in Table 6.7. This reduction in static margin is caused by a shift in centre of gravity (CG) location due to a larger structural weight.

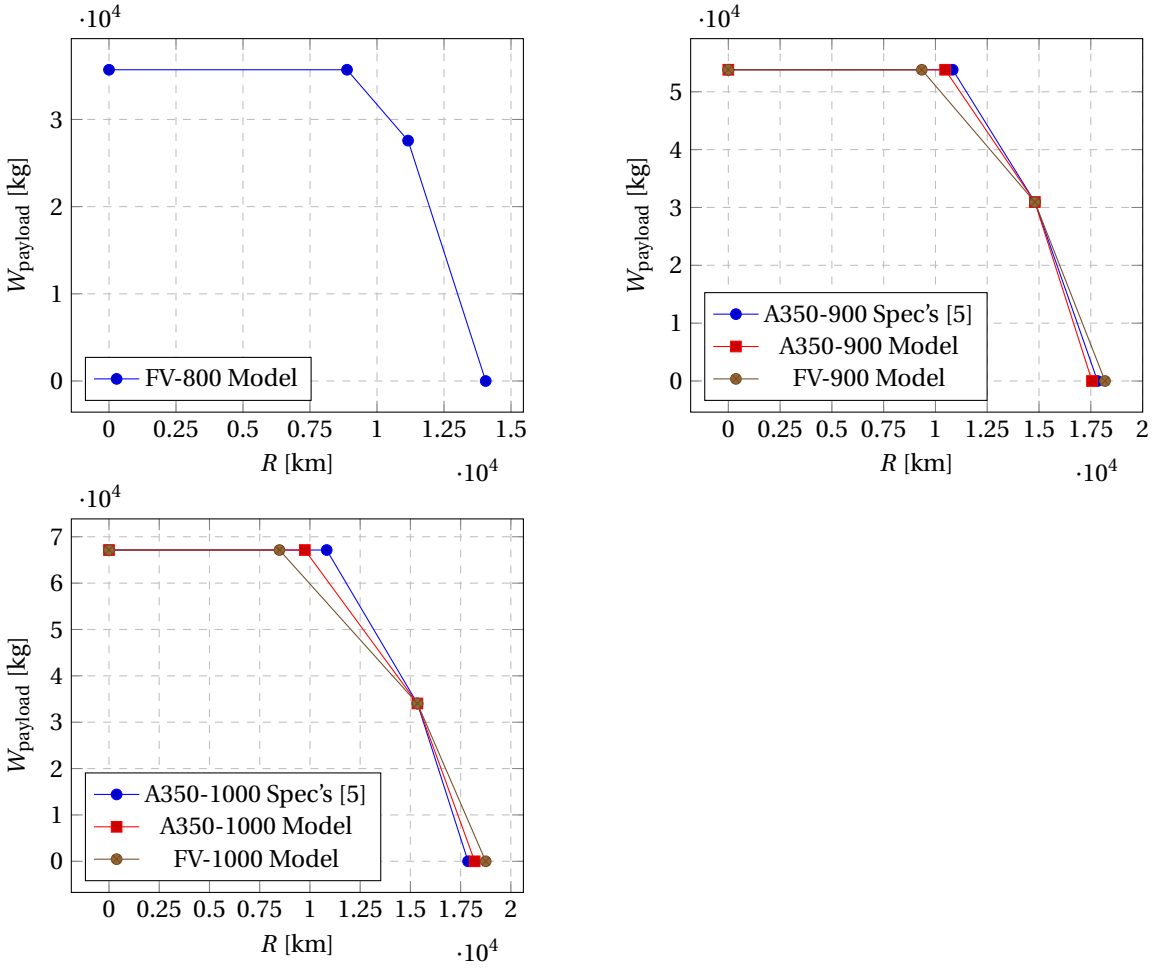

Figure 6.2: Payload range diagram of the -800, -900 and -1000 aircraft family members. A350 specifications (spec's) data from Airbus [5].

The outer wing weight is increased on all aircraft families, which is a direct result of the commonality constraint on this component. Furthermore, due to the increase in operating empty weight the approach speed of the FV-800 and FV-900 increases.

Common Design Variable Penalties

Comparing the penalty due to common design variables, the optimised single aircraft (SO) results are compared with the optimised family aircraft without the commonality constraint (FO-S). Clearly, the commonality constraint has a large influence on the fuel burn performance of the individual aircraft. The increase in fuel burn is 1.4%, 6.2% and 6.7% for the -800, -900 and -1000 respectively. The increase in takeoff weight is 0.1%, 2.3% and 1.9% respectively. The increase in fuel burn for the FV-900 and FV-1000 is primarily caused by an increase in static margin caused by a shift in the centre of gravity location. An increase in static margin has a negative effect on the lift-to-drag ratio, resulting from larger elevon deflections to trim the aircraft. The centre of gravity is shifted forward in the family-optimised aircraft mainly due to the more forward location of the fuel and increased fuel weight. The fuel is located more forward due to the constraint on the length of the tapered cabin part. Note that this centre of gravity location is at the design weight with full fuel tanks. During flight the centre of gravity can be shifted aft by pumping fuel aft.

The outer wing weight decreases for all aircraft variants, which is mainly due to the larger fuel weight being placed in the outer wing resulting in a bending moment relief. Due to the increased operating empty weight, the approach speed of all aircraft increases. The centre of gravity shift during flight is also slightly increased.

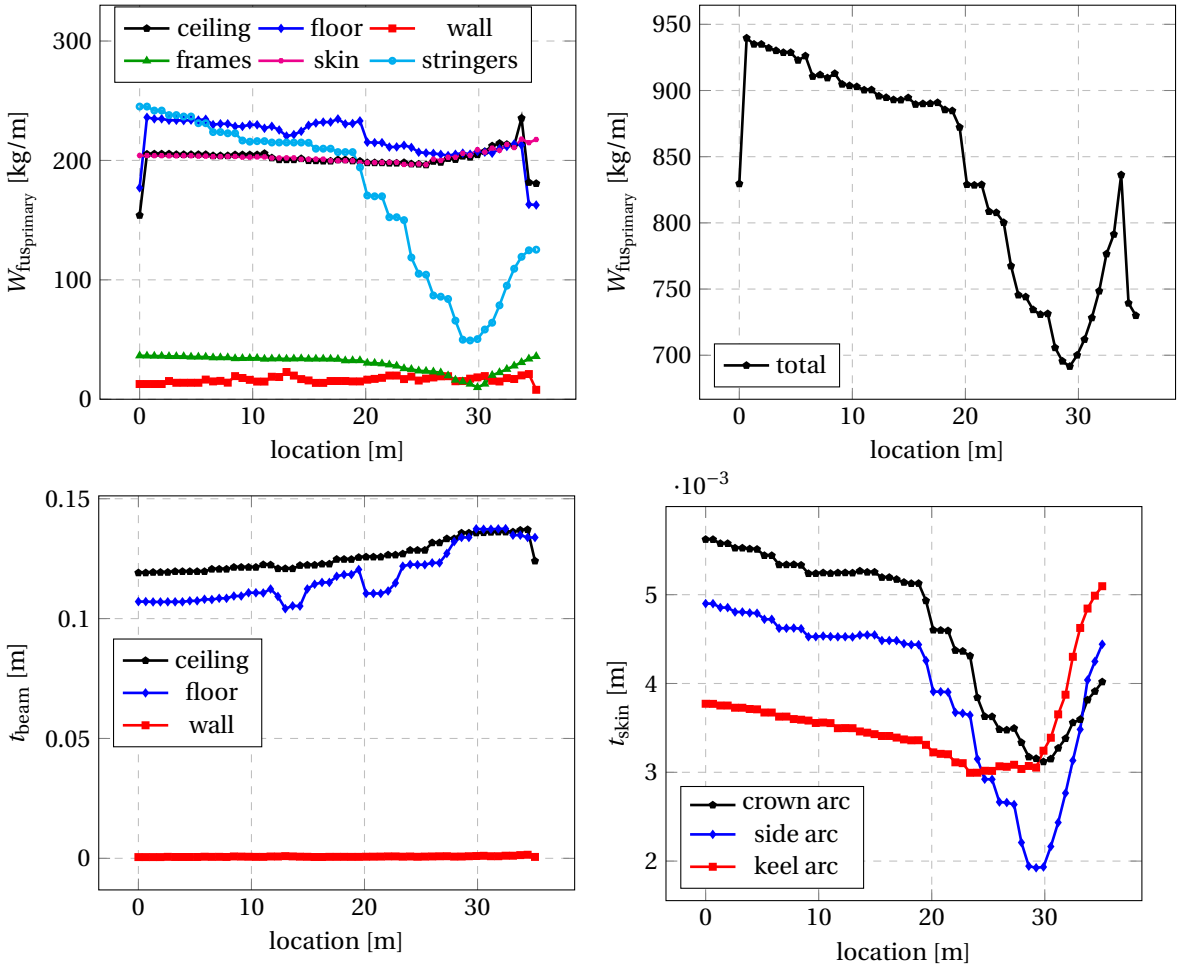

Figure 6.3: Mass and thickness distribution along the fuselage length for the FV-900, results for 55 sections. Mass is provided in kg/m by dividing the weight at each longitudinal section by the longitudinal section width.

Penalty due to the FV-800

The impact of including the smallest aircraft variant is possibly rather large. A principal difference between the single optimised aircraft and family optimised aircraft is the division between the tapered and untapered cabin length, which is constrained by the smallest aircraft variant at approximately 11 m as explained in Section 3.3.3.

A rough investigation of a two-member aircraft family results in a fuel burn of 85.5 $\cdot 10^3$ kg and 101 $\cdot 10^3$ kg for the FV-900 and FV-1000 respectively. Note that this two-member family is not fully optimised. The principal difference with respect to the three-member family is the length of the tapered cabin, which can be increased to approximately 14.5 m for a two-member family. The total fuel burn penalties due to commonality with respect to the single optimised aircraft become 4.8% and 2.5% for the FV-900 and FV-1000 respectively. Comparing these penalties to the penalties of a three-member family of 7.1% and 4.2%, the option of leaving out the smallest aircraft family member seems worth considering. The benefit could be even larger, since the two-member aircraft family was not fully optimised.

6.3. Comparing the Flying-V and Reference Aircraft Families

The fuel burn of the reference aircraft family following from the model and as specified by Airbus was already presented in Table 6.2. Comparing these data to the fuel burn of the optimised Flying-V aircraft family results in the estimated fuel burn benefit for the Flying-V aircraft family as presented in Table 6.9. Clearly, the Flying-V aircraft family is still a very viable aircraft concept in terms of fuel burn performance with a reduction of 19.9% to 22.0% with respect to the reference aircraft family.

Payload-range performance of the aircraft is compared with the Payload Range Efficiency (PRE) using

Equation 6.1 [101].

$$\text{PRE} = \frac{W_{\text{payload}} \cdot R}{W_{\text{fuel}}} \tag{6.1}$$

The payload-range efficiency of the Flying-V and reference aircraft is assessed at the harmonic range and design range. For the ferry range, the payload weight is zero and hence the PRE will also be zero, such that the ratio between the range and fuel weight, $R_{\text{ferry}}/W_{\text{fuel}}$, is assessed. Clearly, the payload-range efficiency of the Flying-V is higher than the reference aircraft, especially at the design mission. Naturally, this difference can be mainly explained by the higher aerodynamic efficiency in terms of the lift-to-drag ratio of the Flying-V. The harmonic range of the Flying-V is somewhat limited due to its relatively low maximum takeoff weight, such that the difference in PRE is less pronounced at the harmonic mission. The wing loading of the Flying-V, W/S, is much lower than the reference aircraft due to its very large wing area and lower takeoff weight. This directly affects the approach speed of the aircraft, such that the approach speed of the Flying-V is lower than for the reference aircraft. The low wing loading is in general the case for flying wing or BWB configurations as described in Section 2.1.

An obvious additional benefit of the Flying-V aircraft family is the automatic scaling of the wing surface area and fuel tank volume with an increase in cabin size. This results in a more constant wing loading between the aircraft family members, such that the approach speed potentially does not differ as much between aircraft variants as for conventional aircraft. Table 6.9 shows a relatively small difference in approach speed between the FV-900 and FV-1000, confirming a proportional growth of wing area with landing weight. In conventional aircraft families such as the reference Airbus A350 the wing loading increases for the larger aircraft variants, assuming roughly the same wing is used on all aircraft variants. Hence, a proportional growth of wing area with takeoff weight can be described as a benefit of the Flying-V configuration, indicating that smaller aircraft variants are not designed with an oversized wing area or weight.

It should be noted that the reference aircraft family, despite earlier plans of Airbus, only consists of two family members. It is not known what the impact of the undeveloped smallest aircraft variant has been on the larger aircraft, but possibly a comparison between two two-member aircraft families would be fairer and would result in an even larger fuel burn performance benefit for the Flying-V, as touched upon in Section 6.2.4.

Table 6.9: Performance characteristics for the reference aircraft family and optimised Flying-V family, Airbus A350 approach speed data from Airbus [5].

	Unit	FV-800	FV-900	A350-900	FV-1000	A350-1000
$W_{\text{fuel}_{\text{des}}}$	10^3 kg	58.0	87.5	112	103	128
$\text{PRE}_{\text{harmonic}}$	10^3 km	5.47	5.75	5.02	5.54	5.10
$\text{PRE}_{\text{design}}$	10^3 km	5.30	5.23	4.08	5.09	4.07
$R_{\text{ferry}}/W_{\text{fuel}}$	km/kg	0.24	0.21	0.16	0.18	0.14
$(C_L/C_D)_{\text{des}}$	-	20.9	21.6	19.7	21.2	19.5
MTOW	10^3 kg	185	234	281	266	312
W/S	kg/m^2	271	295	636	300	673
V_{app}	kts	131	136	140	137	147

Comparing the driving requirements in Flying-V family design with conventional aircraft configurations, it should be noted that the Flying-V copes with difficulties in terms of centre of gravity shift during flight and static margin to a higher extent than is expected for a conventional aircraft family. The centre of gravity shift for the reference aircraft is described by Bourget as 20% of the MAC, with a 9.1 m MAC, which means a shift of 1.82 m. a 20% MAC shift of the centre of gravity is also indicated by the Flight Deck and Systems Briefing for Pilots by Airbus[1]. Clearly, this shift in centre of gravity is much lower than the current FV-900 design. Since fuel tanks of a conventional aircraft are located mainly in the wing, the increase in fuel volume for a larger aircraft family member is mainly centred around the centre of gravity. In addition, the aerodynamic centre and centre of gravity of a conventional aircraft are relatively close, such that the static margin is generally limited. Furthermore, the addition of extra payload for larger family members can be spread around the centre of gravity and the aerodynamic centre such that effects on the static margin and centre of gravity shift

[1] http://www.smartcockpit.com/docs/a350-900-flight-deck-and-systems-briefing-for-pilots.pdf [cited on 6-9-2020]

can be limited. Finally, the shift in centre of gravity during flight can be kept small when fuel is stored in the wing. For the Flying-V, placing the fuel around the centre of gravity means that the fuel is stored mainly along the cabin, whereas the outer wing should not contain a lot of fuel due to its large moment arm with respect to the centre of gravity. The presence of the outer wing also entails an aerodynamic centre which is aft of the centre of gravity, such that the outer wing area should be limited to avoid a very large static margin and associated trim drag. This leads to a potentially unused part of the outer wing in terms of fuel tank volume, which also means a smaller bending moment relief on the outer wing.

6.4. Sensitivity Analysis

The optimal family design vector for the -900 and -1000 aircraft combined was run 55 times and yielded in 98% of the cases a fuel burn objective within +/- 0.1% of the average result. The only outlier had a fuel burn objective 0.16% higher than the average result. This shows that inaccuracies due to the convergence of the fuel burn and family design method do not largely affect the results.

The sensitivity of the optimised family design is assessed as a means of validation of the optimality of the obtained design. This sensitivity analysis also functions as an extra check on the design process checking whether the output changes as expected with changing design variables. Equation 6.2 is used to assess the sensitivity S_i of an objective function f to changes in a design variable x_i. This sensitivity can be described as a partial derivative of the objective function to a normalised change in a design variable.

$$S_i = \frac{f(x_i + \Delta x) - f(x_i)}{f(x_i)} \frac{x_i}{\Delta x}. \tag{6.2}$$

Figure 6.4 visualises the sensitivity of the fuel burn performance of the optimised aircraft family to its design variables. Clearly, variables describing the planform have a relatively large impact on the fuel burn performance. The impact of the chord length c' is interesting to note and was already noted during the optimisation process. Since a change in the chord length does not affect the floor area of the cabin, it has no effect on the weight distribution of the payload, furnishing or systems. However, it does have a large effect on the size of the fuel tanks and on the aerodynamic loads. The fuel burn performance of the Flying-V family could be improved by decreasing L_1 and L_3, but these are actively constrained by the cabin floor area. In addition, decreasing the length of the cabin would violate the fuel tank volume constraint and moving the fuel outboard increases the centre of gravity shift during flight. A decrease in chord length, c', is not possible due to the constraint on fuel tank volume. Likewise, decreasing the keel height for the untapered cabin H_{3_1} or the normalised chord length c' would hit the fuel tank volume constraint on one or more of the aircraft family members.

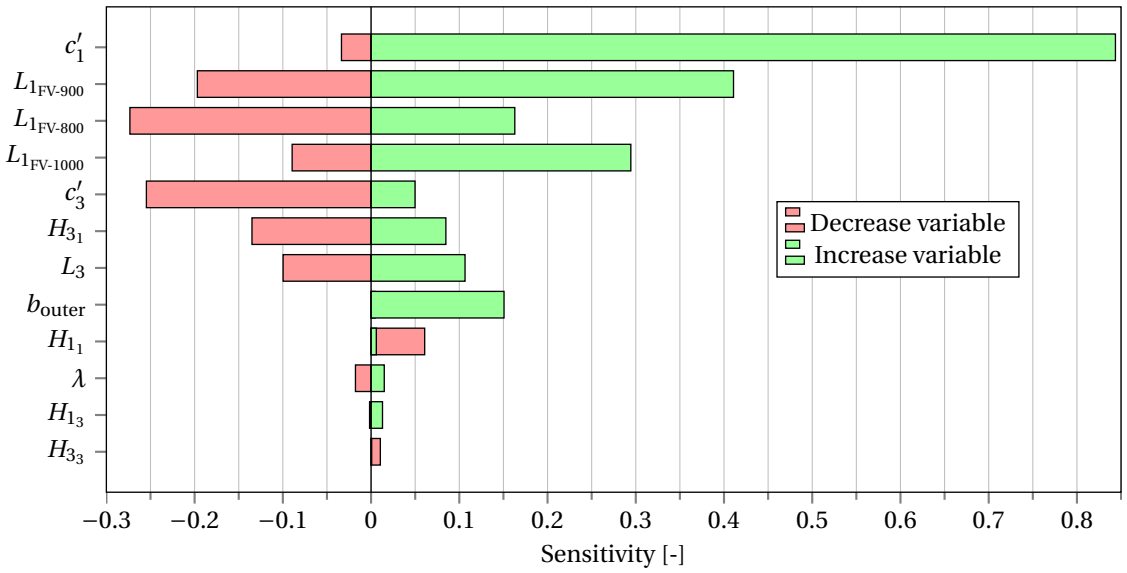

Figure 6.4: Tornado diagram visualising the sensitivity of the optimised aircraft family fuel burn performance to its principal design variables.

6.5. Flying-V Family Floor Plan

The final design of the largest Flying-V family member is shown in Figure 6.5. This figure includes a visualisation of the fuselage plugs which are inserted to form this largest family member from smaller family members. The floor plan shows that the constraint on floor area is sufficient and can lead to a realistic aircraft configuration, fitting the required payload, aisles and furnishing. Floor plans of all aircraft family members are shown in Appendix B. The total number of economy class passengers on the floor plan is slightly higher than the top-level aircraft requirements, indicating a small overestimate of the required floor area for the payload, aisles and furnishing. Design principles that were followed to construct the floor plans include the following:

- separate the business class and the economy class, placing the business class towards the front of the aircraft;
- place lavatories and emergency exits not in removable fuselage plugs to maximise commonality;
- place emergency exits at a distance of maximum 18.3 m (60 ft) apart along the longitudinal axis of the aircraft as specified in CS25.807;
- place two emergency exits at the main aisle connecting the two swept cabins, allowing evacuation through one side of the aircraft within 90 seconds as specified in CS25.803;
- place one attendant seat at every door as specified by the EASA [102] and ICAO[2];
- reserve room for a wall between the passenger cabin and the cargo compartment and for the cargo net;
- place a structural shell wall at the aft side of the connection between the two swept cabins for structural rigidity;
- place a structural wall on the symmetry plane for rigidity;
- use the floor space of the galleys as cross-aisle;
- use a minimal seat rotation to allow for simple seat belts, with a maximum of 18 deg as specified in CS25.785.

For all aircraft, the division between business class and economy class could be reconsidered. Airlines might want to have a clear separation by an aisle between these two classes, such that the current floor plan or the number of seats per class is not optimal. Furthermore, the FV-800 floor plan includes four doors per side of the aircraft with a width of the large type-A door, whereas this number of passengers does not require four type-A doors. Doors could be changed to a type-C door, or one door per side could be removed. Finally, the total number of economy class passengers placed in the FV-900 and FV-1000 are 18 and 17 more than required, which is possibly the result of the reservation of too much floor area for emergency exits and aisles. The weight of these extra passengers is not included during the design of the Flying-V, such that the weight of more passengers should be included in further research, the floor plan could be changed by e.g. including more space for aisles or the total floor area of the FV-900 and FV-1000 could be slightly reduced.

[2]https://www.icao.int/safety/airnavigation/OPS/CabinSafety/Pages/Minimum-Cabin-Crew-Requirements.aspx [cited on 16-3-2021]

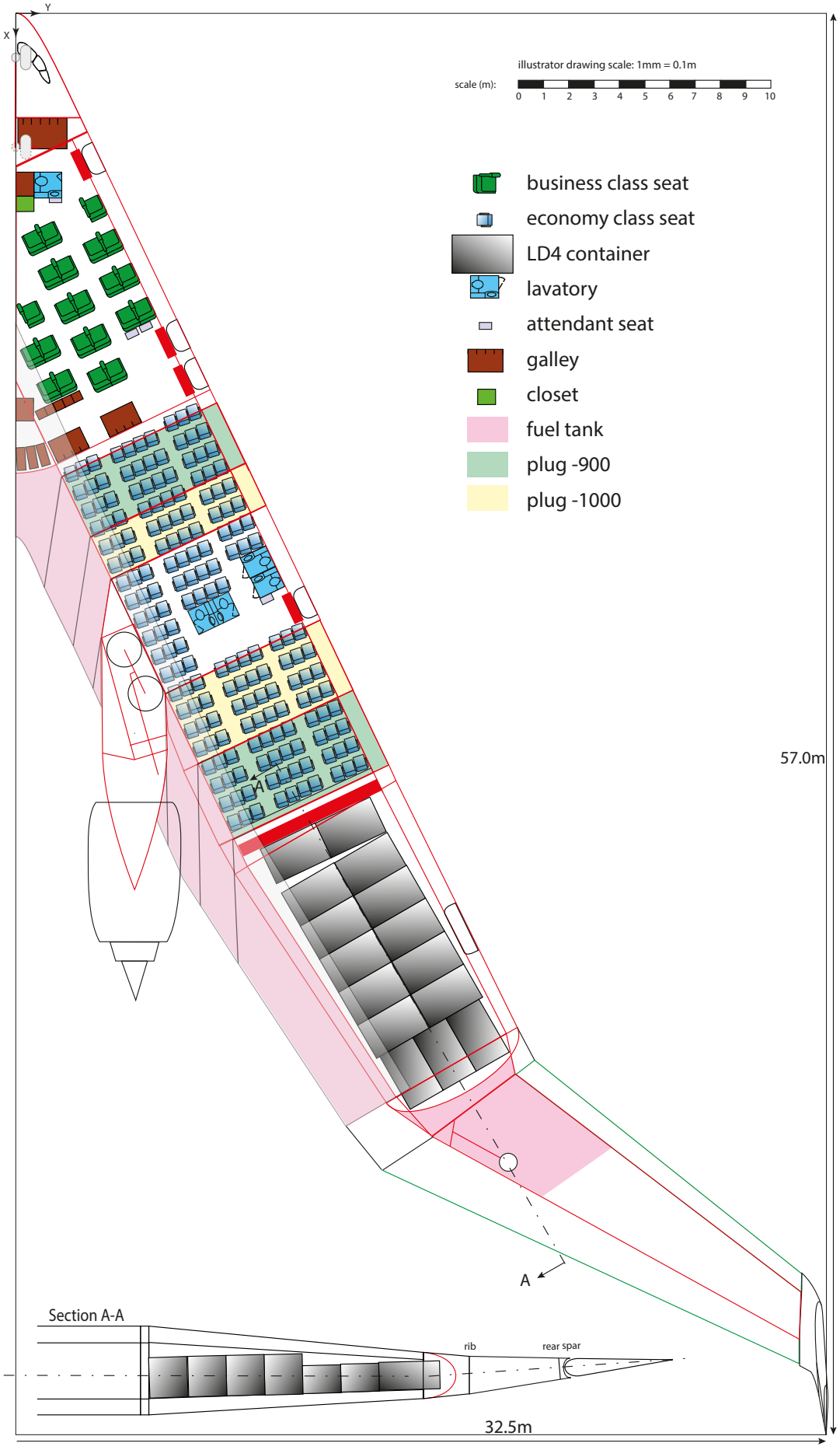

Figure 6.5: Floor plan of the FV-1000 aircraft, visualising the plugs to form a FV-800 or FV-900 variant. Modified from R. Vos.

7

Conclusion and Recommendations

Conclusions from this research and recommendations for further research are described in this chapter.

7.1. Conclusion

The Flying-V is a promising concept regarding reduced fuel consumption and opportunities for novel cabin interior design. Up till now, research on the Flying-V has focused on single aircraft optimisation as a competitor to the A350-900 aircraft. No research has been performed into family design of a Flying-V aircraft. The goal of this research is to study the design of a family of Flying-V aircraft and to compare its fuel burn and driving requirements to a conventional reference aircraft family.

Estimating the fuel burn of the Flying-V sparked the development of a computationally efficient and accurate weight estimation method including a method to estimate the weight of a swept oval fuselage subject to structural and aerodynamic loads. The resulting fuel burn method can be considered a major result of this research. The modelled fuel burn for the reference A350-900 and A350-1000 aircraft differs 0.9% and 0.5% respectively from the fuel burn specified by Airbus.

An optimisation procedure results in a Flying-V aircraft family of three members, fulfilling top-level aircraft requirements on payload, range, cruise speed and altitude, low-speed performance, stability and control and airport regulations. Commonality between aircraft family members is ensured by defining common variables and by using common components and structural thicknesses between family members. The optimised aircraft family members are compared to individually optimised aircraft. The penalty in fuel burn due to common components and commonality in design variables between family members is 8.9%, 7.1% and 4.2% for the FV-800, FV-900 and FV-1000 respectively. The fuel burn of the optimised FV-900 and FV-1000 are 20% and 22% lower than their respective Airbus A350 reference aircraft. The takeoff mass of the Flying-V family members is $185{\cdot}10^3$ kg, $234{\cdot}10^3$ kg and $266{\cdot}10^3$ kg respectively. With respect to the modelled A350 family, this is a reduction of 17% and 15% for the -900 and -1000 variant. The design ranges of the Flying-V family members at maximum passenger capacity are $11.2{\cdot}10^3$ km, $14.8{\cdot}10^3$ km and $15.4{\cdot}10^3$ km. The range of the FV-800 is smaller than the other two aircraft family members because no requirement was imposed on this range, determining the range implicitly from the available fuel volume resulting from optimisation of a two-member aircraft family.

Driving requirements, besides the volume and floor area of the payload and the family commonality constraint, are the centre of gravity shift during flight, the wingspan of 65 m and the fuel tank volume. The larger aircraft family members can be formed by inserting plugs before and aft of the structural component with the engine and landing gear attached, inserting 4 and 5 frames for the -900 and 3 and 5 frames for the -1000 respectively. A sensitivity analysis validates the optimality of the design. The feasibility of the aircraft design is demonstrated by a study on the floor plan of all aircraft family members, including the furnishing, payload, aisles and (emergency) exits. Wing loading of the Flying-V is much lower than for the reference aircraft and is almost constant between the FV-900 and FV-1000, resulting in an estimated approach speed of 136 and 137 kts, much lower than the approach speed of 140 and 147 kts of the reference aircraft family.

This study forms another crucial step in the development of the Flying-V aircraft, proving that a family of Flying-V aircraft can be developed whilst ensuring competitiveness with reference conventional aircraft in terms of fuel burn performance. This research can form a basis for further analyses of Flying-V family

members, including studies on the floor plan and furnishing of the aircraft or its ability for a quick evacuation. The developed fuel burn method including an elaborate weight estimation method can serve any future study on the Flying-V requiring a computationally efficient and accurate estimation of the weight or fuel burn of the Flying-V. This research is one of the few focusing on family design of an unconventional aircraft configuration in the conceptual design phase, and might be the start of more research into this interesting and crucial aspect of aircraft design.

7.2. Recommendations

Whilst this study shows that a family design of Flying-V aircraft can result in a competitive aircraft family compared to reference tube-and-wing aircraft, several aspects need further attention in future research.

First of all, an investigation into the centre of gravity location and shift and the static margin is required. The results of this research indicate a centre of gravity shift for the design mission of 2.5 m, 3.0 m and 3.0 m for the FV-800, FV-900 and FV-1000 respectively. For the A350 aircraft family, the shift in centre of gravity is not much larger than 2 m, such that the centre of shift for the Flying-V family design deserves further attention. The current parametrisation of the Flying-V does not really enable a detailed description of the location and size of the fuel tanks, whereas for instance it might prove beneficial to enlarge the fuel tanks towards the root of the wing-fuselage structure. Furthermore, the weight of various components was smeared out over the length of the structure or cabin, whereas in reality this will not be the case. A detailed study into the centre of gravity can also entail a study into the structural implications of including the majority of the fuel weight between the aft spar and trailing edge of the inner wing. Possible means to limit the centre of gravity shift during flight or to reduce the static margin could be the inclusion of fuel tanks under the cabin floor or the inclusion of fuel trim tanks.

Secondly, the location and structure of a combined landing gear and engine fuselage component deserves further attention, especially coupled with the ground stability of the aircraft and the aerodynamic efficiency of the proposed engine location. In this research, the main landing gear was placed at an angle with respect to the most aft centre of gravity and the nose landing gear location can be determined based on this location and the minimum load on the nose gear. When a new analysis of the centre of gravity position and shift is made, the location of the landing gear therefore needs to be updated. Furthermore, the landing gear length can probably decrease for smaller aircraft variants, for instance applying a semi-levered gear on the largest aircraft variant to effectively increase its length when required. Additionally, the structure connecting the landing gear and engine needs to be studied in more detail; in this research, the engine was assumed to be positioned at a fixed position from the landing gear. Engine installation effects on the lift-to-drag ratio have been studied for the baseline Flying-V earlier, but the optimal location for smaller or larger aircraft variants is not yet known and could affect the location of the landing gear.

Thirdly, the aerodynamic design of the Flying-V family should be studied with higher accuracy than the vortex-lattice method in the incompressible regime employed in this research. The outer shape and centre of gravity location of the aircraft have been changed during the optimisation for a Flying-V family, both as a result of designing a family of aircraft and due to concerns on the centre of gravity location and shift resulting in an updated fuel tank design. Additionally, the shape between the inner and outer wing of the aircraft is aerodynamically rather interesting, with a relatively large change in wing thickness. A more sophisticated aerodynamic study of the Flying-V family members will provide more accurate stability derivatives and hence an updated design of the fins.

In the fourth place, in the current family design optimisation process some assumptions were made which could be changed in more detailed future analyses. For example, the current optimisation varies one unique design variable per aircraft and nine common variables for the aircraft family. Other design variables, such as the width or height of the cabin, have not been varied and could be optimised for the Flying-V family as a whole rather than for the baseline Flying-V -900 aircraft. More detailed design studies could also include more load cases than the ten load cases which were considered in this study.

Finally, it will be interesting to study the market prospects of the different Flying-V family members. During the development of the reference Airbus A350 family, development of the A350-800 was stopped due to a lack of interest of potential buyers, being positioned at a probably relatively small niche in-between the A350-900 and the A330 family. Possibly, the same line of reasoning should be followed for the smallest Flying-V family member, which would have a beneficial effect on the fuel burn performance of the larger aircraft variants. Alternatively, the competitiveness of the smallest aircraft family member could be increased by reducing commonality with the larger aircraft variants, for instance by designing a less heavy landing gear.

Bibliography

[1] R. H. Liebeck. Design of the Blended Wing Body Subsonic Transport. *Journal of Aircraft*, 41(1):10–25, 2004. ISSN 00218669. doi: 10.2514/1.9084.

[2] J. Benad. the Flying V - a New Aircraft Configuration for Commercial Passenger Transport. In *Deutscher Luft- und Raumfahrtkongress*, pages 1–8, 2015.

[3] F. Faggiano. Aerodynamic design of a flying V aircraft. Master's thesis, Delft University of Technology, 2017.

[4] A.S.J. Van Heerden, M.D. Guenov, A. Molina-Cristóbal, and A. Riaz. Enhancing the exploration of aircraft changeability during conceptual design. *30th Congress of the International Council of the Aeronautical Sciences, ICAS 2016*, pages 1–12, 2016.

[5] Airbus. A350 Aircraft Characteristics Airport and Maintenance Planning. Technical Report Revision No. 8 - May 01/20, Airbus, 2020.

[6] D. Raymer. *Aircraft Design: A Conceptual Approach, Second Edition.* American Institute of Aeronautics and Astronautics, Inc., 1998. ISBN 0-930403-51-7.

[7] E. Torenbeek. *Advanced Aircraft Design.* John Wiley & Sons, 2013. ISBN 9781118568118. doi: 10.1002/9781118568101.

[8] J. J. Bertin and R.M. Cummings. *Aerodynamics for Engineers.* Pearson Education Limited, 2014. ISBN 10: 0-273-79327-6.

[9] F. Faggiano, R. Vos, M. Baan, and R. Van Dijk. Aerodynamic design of a flying V aircraft. In *17th AIAA Aviation Technology, Integration, and Operations Conference: 5-9 June 2017, Denver, Colorado [AIAA 2017-3589] AIAA*, 2017. ISBN 9781624105081. doi: 10.2514/6.2017-3589.

[10] J. Roskam. *Airplane Design Part V - Component Weight Estimation.* Design, Analysis and Research Corporation, Lawrence, Kansas, 1985.

[11] J. Roskam. *Airplane Design Part I - Preliminary Sizing Of Airplanes.* Design, Analysis and Research Corporation, Lawrence, Kansas, 1985.

[12] M.B.P. Claeys. Flying V and Reference Aircraft Structural Analysis and Mass Comparison. Master's thesis, Delft University of Technology, 2018.

[13] J. Benad. Design of a commercial aircraft for high-subsonic speed as a flying wing configuration. Master's thesis, Technical University of Berlin, 2015.

[14] R. H. Liebeck. Blended Wing Body design challenges. In *AIAA\ICAS International Air and Space Symposium and Exposition: The Next 100 Years*, pages 1–13, 2003. doi: 10.2514/6.2003-2659.

[15] P. Okonkwo and H. Smith. Review of evolving trends in blended wing body aircraft design. *Progress in Aerospace Sciences*, 82:1–23, 2016. ISSN 03760421. doi: 10.1016/j.paerosci.2015.12.002.

[16] Z. Chen, M. Zhang, Y. Chen, W. Sang, Z. Tan, D. Li, and B. Zhang. Assessment on critical technologies for conceptual design of blended-wing-body civil aircraft. *Chinese Journal of Aeronautics*, 32(8):1797–1827, 2019. ISSN 1000-9361. doi: 10.1016/j.cja.2019.06.006.

[17] A. Velicki and P. Thrash. Blended Wing Body Structural Concept Development. *Aeronautical Journal*, 114:513–519, 08 2010. doi: 10.1017/S0001924000004000.

[18] N. Qin, A. Vavalle, A. Le Moigne, M. Laban, K. Hackett, and P. Weinerfelt. Aerodynamic studies for blended wing body aircraft. In *9th AIAA/ISSMO Symposium on Multidisciplinary Analysis and Optimization*, pages 1–12, 2002. doi: 10.2514/6.2002-5448.

[19] M.F.M. Hoogreef. The Oval Fuselage - A New Structural Design Concept for Blended Wing Body Cabins. Master's thesis, Delft University of Technology, 2012.

[20] L. Prandtl and A. Betz. Vier Abhandlungen der Hydrodynamik und Aerodynamik, Göttingen: Selbstverlag des Kaiser Wilhelm Instituts für Strömungsforschung, 1927.

[21] B.M. Kulfan. Universal Parametric Geometry Representation Method. *Journal of Aircraft*, 45(1):142–158, 2008. doi: 10.2514/1.29958.

[22] R. Vos, F.J.J.M.M. Geuskens, and M.F.M. Hoogreef. A new structural design concept for blended wing body cabins. In *53rd AIAA/ASME/ASCE/AHS/ASC Structures, Structural Dynamics and Materials Conference*. American Institute of Aeronautics and Astronautics (AIAA), 2012. doi: 10.2514/6.2012-1998.

[23] L.A. Van Der Schaft. Development, Model Generation and Analysis of a Flying V Structure Concept. Master's thesis, Delft University of Technology, 2017.

[24] B. Rubio Pascual. Engine-Airframe Integration for the Flying V. Master's thesis, Delft University of Technology, 2018.

[25] I. Chung. Cabin Interior Design of the Flying-V. Master's thesis, Delft University of Technology, 2018.

[26] M. Palermo. The Longitudinal Static Stability and Control Characteristics of a Flying V Scaled Model. Master's thesis, Delft University of Technology, 2019.

[27] R.A. Viet. Analysis of the flight characteristics of a highly swept cranked flying wing by means of an experimental test. Master's thesis, Delft University of Technology, 2019.

[28] A. Ruiz Garcia. Aerodynamic Model Identification of the Flying-V using Wind Tunnel Data. Master's thesis, Delft University of Technology, 2019.

[29] T. Cappuyns. Handling Qualities of a Flying V Configuration. Master's thesis, Delft University of Technology, 2019.

[30] A.J. Santosh. Numerical Investigation of the Influence of Ground Effect on the Flying V Aircraft. Master's thesis, Delft University of Technology, 2020.

[31] G. Bourget. The effect of landing gear implementation on Flying V aerodynamics , stability and controllability by. Master's thesis, Delft University of Technology, 2020.

[32] R. Van der Pluijm. Cockpit Design and Integration into the Flying V. Master's thesis, Delft University of Technology, 2021.

[33] T.W. Simpson, Z. Pirmoradi, and G. Wang. A Review of Recent Literature in Product Family Design and Platform-Based Product Development. In *Advances in Product Family and Product Platform Design, Methods and Applications*. Springer, 2014. ISBN 9781461479376. doi: 10.1007/978-1-4614-7937-6.

[34] T.W. Simpson, Z. Siddique, and J. Jiao. *Product Platform and Product Family Design*. Springer Science and Business Media, Inc, 2006. ISBN 9780387291970.

[35] J. Jiao, T.W. Simpson, and Z. Siddique. Product family design and platform-based product development: A state-of-the-art review. *Journal of Intelligent Manufacturing*, 18(1):5–29, 2007. ISSN 09565515. doi: 10.1007/s10845-007-0003-2.

[36] A.S.J. van Heerden. *Computational Techniques for Aircraft Evolvability Exploration during Conceptual Design*. PhD thesis, Cranfield University, 2019.

[37] D.P.M.D. Bador, W.J. Seering, and E.S. Rebentisch. Measuring the efficiency of commonality implementation: Application to commercial aircraft cockpits. In *ICED 2007, the 16th International Conference on Engineering Design*, pages 1–12, 2007. ISBN 1904670024.

[38] R.C. Boas. *Commonality in complex product families: Implication of divergence and lifecycle offsets*. PhD thesis, Massachusetts institute of technology, 2008.

[39] R. Birrenbach. Regional aircraft family design. In *World Aviation Conference*, 2000. doi: 10.2514/6.2000-5547.

[40] R.C. Boas and E.F. Crawley. Parallel and sequential development of complex platform-based product families. In *IEEE International Engineering Management Conference*, pages 151–157, 2007. ISBN 9781424421466. doi: 10.1109/IEMC.2007.5235080.

[41] A. Messac, M.P. Martinez, and T.W. Simpson. Introduction of a product family penalty function using physical programming. In *8th Symposium on Multidisciplinary Analysis and Optimization*, 2000. doi: 10.2514/6.2000-4838.

[42] K. Willcox and S. Wakayama. Simultaneous optimization of a multiple-aircraft family. *Journal of Aircraft*, 40(4):616–622, 2003. ISSN 00218669. doi: 10.2514/2.3156.

[43] A. Riaz. *A Set-Based Approach to Passenger Aircraft Family Design*. Phd thesis, Cranfield University, 2015.

[44] M.D. Guenov, M. Nunez, A. Molina-Cristóbal, V.C. Datta, and A. Riaz. Aircadia -an interactive tool for the composition and exploration of aircraft computational studies at early design stage. In *29th Congress of the International Council of the Aeronautical Sciences, ICAS 2014*, pages 1–12, 2014. ISBN 3932182804.

[45] Q.P.D. Van Keymeulen. Design of a Modular Fuselage for Commercial Aircraft: To Cope with Seasonal Variation in Passenger Demand. Master's thesis, Delft University of Technology, 2015.

[46] A. Riaz, M.D. Guenov, and A. Molina-Cristobal. Set-based approach to passenger aircraft family design. *Journal of Aircraft*, 54(1):310–326, 2017. ISSN 00218669. doi: 10.2514/1.C033747.

[47] A.S.J. van Heerden, M.D. Guenov, and A. Molina-Cristóbal. Evolvability and design reuse in civil jet transport aircraft. *Progress in Aerospace Sciences*, 108(May):121–155, 2019. ISSN 03760421. doi: 10.1016/j.paerosci.2019.01.006.

[48] M. Kingsley-Jones. A350-800 'shrink' move gains range and -900 commonality. *Flight International*, 177(5223):7, January 2010.

[49] M. Kingsley-Jones. Analysis: Why Boeing's 787-9 is More Than Just a Stretch. *Flight International*, July 2014.

[50] S. Trimble. Analysis: Boeing 787-10 technical description and cutaway. *Flight International*, 193(5629): 32–34, Mar 2018.

[51] G. La Rocca. Advanced Engineering Informatics Knowledge based engineering: Between AI and CAD. Review of a language based technology to support engineering design. *Advanced Engineering Informatics*, 26(2):159–179, 2012. ISSN 1474-0346. doi: 10.1016/j.aei.2012.02.002.

[52] EASA. Type-Certificate Data Sheet Airbus A350. Technical Report No. EASA.A.151, EASA, November 2019.

[53] J.D. Anderson. *Fundamentals of Aerodynamics*. McGraw-Hill Education, 2017. ISBN 978-1-259-25134-4.

[54] B.N. Pamadi. Static Stability and Control. In *Performance, Stability, Dynamics and Control of Airplanes*, chapter 3. American Institute of Aeronautics and Astronautics (AIAA), 2000. ISBN 9781600860997.

[55] M. Hillen. Parametrisation of the Flying-V Outer Mould Line. Master's thesis, Delft University of Technology, 2020.

[56] R. Storn and K. Price. Differential Evolution - A Simple and Efficient Heuristic for Global Optimization over Continuous Spaces. *Journal of Global Optimization*, 11:341–359, 01 1997. doi: 10.1023/A:1008202821328.

[57] EASA. ICAO Aircraft Engine Emissions Databank, August 2020.

[58] G.J.J. Ruijgrok. *Elements of Airplane Performance*. Delft University Press, 2009. ISBN 978-90-6562-203-7.

[59] B. Rubio Pascual and R. Vos. The Effect of Engine Location on the Aerodynamic Efficiency of a Flying-V Aircraft. In *AIAA Scitech 2020 Forum*, 2020. doi: 10.2514/6.2020-1954.

[60] M. Drela. Integrated Simulation Model for Preliminary Aerodynamic, Structural, and Control-law Design of Aircraft. In *40th AIAA/ASME/ASCE/AHS/ASC Structures, Structural Dynamics, and Materials Conference and Exhibit*, 1999. doi: 10.2514/6.1999-1394.

[61] M. Drela. Aerodynamics of Aircraft in Maneuver. In *Flight Vehicle Aerodynamics*, chapter 6, pages 123–142. MIT Press Ltd, 2014.

[62] B. Mialon, A. Khrabrov, S.B. Khelil, A. Huebner, A. Da Ronch, K. Badcock, L. Cavagna, P. Eliasson, M. Zhang, S. Ricci, J.C. Jouhaud, G. Rogé, S. Hitzel, and M. Lahuta. Validation of numerical prediction of dynamic derivatives: The DLR-F12 and the Transcruiser test cases. *Progress in Aerospace Sciences*, 47 (8):674–694, 2011. ISSN 03760421. doi: 10.1016/j.paerosci.2011.08.010.

[63] E.M. Cárdenas, P.J. Boschetti, and A. Amerio. Stability and Flying Qualities of an Unmanned Airplane Using the Vortex-Lattice Method. *Journal of Aircraft*, 46(4):1461–1464, 2009. doi: 10.2514/1.44306.

[64] P.R. Thomas, T.S. Richardson, and A.K. Cooke. Estimation of Stability and Control Derivatives for a Piper Cub J-3 Remotely Piloted Vehicle. In *AIAA Modeling and Simulation Technologies Conference*, 2012. doi: 10.2514/6.2012-5013.

[65] P.J. Boschetti, E.M. Cárdenas, and A. Amerio. Stability and Performance of a Light Unmanned Airplane in Ground Effect. In *48th AIAA Aerospace Sciences Meeting*, 2010.

[66] J. Mariens, A. Elham, and M.J.L. Van Tooren. Quasi-three-dimensional aerodynamic solver for multidisciplinary design optimization of lifting surfaces. *Journal of Aircraft*, 51(2):547–558, 2014. ISSN 00218669. doi: 10.2514/1.C032261.

[67] M. Drela. XFOIL: An Analysis and Design System for Low Reynolds Number Airfoils. In *Conference on Low Reynolds Number Airfoil Aerodynamics*, 1989.

[68] Ed Obert. *Aerodynamic Design of Transport Aircraft*. IOS Press BV, Amsterdam, 2009. ISBN 9781586039707.

[69] E. Torenbeek. *Synthesis of Subsonic Airplane Design*. Delft University Press, 1982. ISBN 90-247-2724-3.

[70] M.H. Sadraey. Design of control surfaces. In *Aircraft Design: A Systems Engineering Approach*, chapter 12, pages 631–753. John Wiley & Sons, 2013. doi: 10.1002/9781118352700.

[71] D. Decloedt. Investigation into the Effect of Relaxed Static Stability on a Business Jet's Preliminary Design. Master's thesis, Delft University of Technology, 2016.

[72] R. Vos and M. Hoogreef. Semi-analytical weight estimation method for fuselages with oval cross-section. *54th AIAA/ASME/ASCE/AHS/ASC Structures, Structural Dynamics, and Materials Conference*, pages 1–15, 2013. doi: 10.2514/6.2013-1719.

[73] M. Roelofs and R. Vos. Semi-analytical composite oval fuselage mass estimation. In *AIAA SciTech Forum - 55th AIAA Aerospace Sciences Meeting*, 2017. ISBN 9781624104473. doi: 10.2514/6.2017-0466.

[74] D. Howe. Blended wing body airframe mass prediction. In *Proceedings of the Institution of Mechanical Engineers, Part G: Journal of Aerospace Engineering*, volume 215, pages 319–331, 2001. doi: 10.1243/0954410011533329.

[75] P. Okonkwo. *Conceptual design framework for Blended Wing Body aircraft*. PhD thesis, Cranfield University, 2016.

[76] M. Brown and R. Vos. Conceptual design and evaluation of blended-wing-body aircraft. In *AIAA Aerospace Sciences Meeting (210059 ed.). [AIAA 2018-0522] AIAA*, 2018. doi: 10.2514/6.2018-0522.

[77] R.K. Schmidt and R. Vos. A semi-analytical weight estimation method for oval fuselages in conventional and novel aircraft. In *AIAA SciTech Forum - 52nd Aerospace Sciences Meeting*, 2014. ISBN 9781624102561. doi: 10.2514/6.2014-0026.

[78] R. Elmendorp, R. Vos, and G. La Rocca. A conceptual design and analysis method for conventional and unconventional airplanes. In *29th Congress of the International Council of the Aeronautical Sciences, ICAS 2014*, pages 1–12, 2014. ISBN 3932182804.

[79] A. Elham, G. La Rocca, and M.J.L. Van Tooren. Development and implementation of an advanced, design-sensitive method for wing weight estimation. *Aerospace Science and Technology*, 29(1):100–113, 2013. ISSN 12709638. doi: 10.1016/j.ast.2013.01.012.

[80] R.K. Schmidt. A Semi-Analytical Weight Estimation Method for Oval Fuselages in Novel Aircraft Configurations. Master's thesis, Delft University of Technology, 2013.

[81] T.H.G. Megson. *Aircraft Structures for Engineering Students*. Aerospace Engineering. Elsevier Science, 2013. ISBN 9780080969053.

[82] Z. Mikulik and P. Haase. CODAMEIN - Composite Damage Metrics and Inspection (high energy blunt impact threat. Technical Report EASA.2010/2, EASA, 2012.

[83] E. Torenbeek. Development and Application of a Comprehensive Design-sensitive Weight Prediction Method for Wing Structures of Transport Category Aircraft. Technical report, Delft University of Technology, Delft, 1992.

[84] P. Haase and Z. Mikulik. Composite damage metrics and inspection. Technical report, EASA, 2012.

[85] M. Sensmeier and J. Samareh. A Study of Vehicle Structural Layouts in Post-WWII Aircraft. In *45th AIAA/ASME/ASCE/AHS/ASC Structures, Structural Dynamics and Materials Conference*, 2004. doi: 10.2514/6.2004-1624.

[86] M. Droegkamp. Finite element model weight estimation. Technical Report 2089, SAWE, 1992.

[87] A. Elham and M.J.L. Van Tooren. Effect of wing-box structure on the optimum wing outer shape. *The Aeronautical Journal*, 118(1199):1–30, 2014. ISSN 00019240. doi: 10.1017/S0001924000008903.

[88] A. Elham. *Weight Indexing for Multidisciplinary Design Optimization of Lifting Surfaces*. PhD thesis, Delft University of Technology, 2012.

[89] C. Soutis. Fibre reinforced composites in aircraft construction. *Progress in Aerospace Sciences*, 41(2):143–151, 2005. ISSN 03760421. doi: 10.1016/j.paerosci.2005.02.004.

[90] F. Palacios, M.R. Colonno, A.C. Aranake, A. Campos, S.R. Copeland, T.D. Economon, A.K. Lonkar, T.W. Lukaczyk, T.W.R. Taylor, and J.J. Alonso. Stanford University Unstructured (SU2): An open-source integrated computational environment for multi-physics simulation and design. In *51st AIAA Aerospace Sciences Meeting including the New Horizons Forum and Aerospace Exposition*, 2013. ISBN 9781624101816. doi: 10.2514/6.2013-287.

[91] B. Peerlings. A review of aerodynamic flow models, solution methods and solvers and their applicability to aircraft conceptual design, 2018.

[92] V. Ahuja. *Aerodynamic Loads over Arbitrary Bodies by Method of Integrated Circulation*. PhD thesis, Auburn University, 2013.

[93] V. Ahuja and R.J. Hartfield. Aerodynamic loads over arbitrary bodies by method of integrated circulation. *Journal of Aircraft*, 53(6):1719–1730, 2016. ISSN 15333868. doi: 10.2514/1.C033619.

[94] L. Prandtl. Applications of Modern Hydrodynamics to Aeronautics. Technical report, Göttingen University, 1923.

[95] E.D. Olson and C.W. Albertson. Aircraft high-lift aerodynamic analysis using a surface-vorticity solver. In *54th AIAA Aerospace Sciences Meeting*, 2016. ISBN 9781624103933. doi: 10.2514/6.2016-0779.

[96] S. Johnson, D. van Dommelen, V. Ahuja, and R. Harfield. Investigation of the static longitudinal characteristics of a full-scale light single-engine airplane using a surface vorticity solver. In *AIAA Aerospace Sciences Meeting*, 2018. ISBN 9781624105241. doi: 10.2514/6.2018-1259.

[97] B. Sandoz, V. Ahuja, and R.J. Harfield. Longitudinal aerodynamic characteristics of a v/stol tilt-wing four-propeller transport model using a surface vorticity flow solver. In *AIAA Aerospace Sciences Meeting*, 2018. ISBN 9781624105241. doi: 10.2514/6.2018-2070.

[98] I. Chakraborty, R.J. Hartfield, and V. Ahuja. Energy-Based Sizing and Mission Performance Analysis Approach for Novel Flight Vehicle Concepts. In *AIAA Aviation Forum*, 2019. doi: 10.2514/6.2019-2801.

[99] V. Ahuja, I. Chakraborty, and R.J. Hartfield. Aero-Propulsive Analysis for Contemporary Conceptual Design. In *AIAA Aviation Forum*, 2019. doi: 10.2514/6.2019-3019.

[100] I. Chakraborty, V. Ahuja, A. Comer, and O. Mulekar. Development of a Modeling, Flight Simulation, and Control Analysis Capability for Novel Vehicle Configurations. In *AIAA Aviation Forum*, 2019. doi: 10.2514/6.2019-3112.

[101] R.K. Nangia. Efficiency parameters for modern commercial aircraft. *Aeronautical Journal*, 110(1110): 495–510, 2006. ISSN 00019240. doi: 10.1017/S0001924000001391.

[102] EASA. Large Aeroplane Evacuation Certification Requirements – Cabin Crew Members Assumed to be On Board. Technical Report Proposed CM–CS-008 Issue 01, EASA, September 2015.

[103] D. Scholz. An Optional APU for Passenger Aircraft. In *5th CEAS Air and Space Conference*, 2015.

A

Empirical Weight Estimation Relations

All empirical relations in this appendix follow from Torenbeek's method [69].

Landing Gear
The weight of the landing gear is calculated using Equation A.1. In this equation, k_{uc} is 1.0 for low-wing aircraft and 1.08 for high-wing aircraft. The Flying-V cannot be placed in any category and the reference aircraft is a low-wing aircraft. For both aircraft, the low-wing factor is applied.

$$W_{LG} = k_{uc}\left[A + B \cdot W_{TO}^{3/4} + C \cdot W_{TO} + D \cdot W_{TO}^{3/2}\right] \tag{A.1}$$

Factors A, B, C and D are based on reference aircraft data. For retractable landing gears on civil aircraft, the main gear factors are 18.1, 0.131, 0.019 and $2.23 \cdot 10^{-5}$ respectively. The nose gear factors are 9.1, 0.082, 0 and $2.97 \cdot 10^{-6}$ respectively.

Propulsion System
The propulsion group weight is described in Equation A.2.

$$W_{propulsion} = W_n + W_e + W_{ai} + W_{fs} + W_p \tag{A.2}$$

The nacelle weight for high bypass ratio engines is described in Equation A.3, which includes thrust reversers. Note that this relation is only valid for high bypass turbofans.

$$W_n = 0.065 T_{TO} \tag{A.3}$$

W_e is the dry engine weight, which is described in Section 4.1.1. The air induction system weight W_{ai} is included in the nacelle weight for podded engines [69]. The fuel system weight for integral fuel tanks is given in Equation A.4. Note that the number of fuel tanks n_{ft} should at least be equal to the number of engines n_e for airworthiness [69] and is assumed to be 4.

$$W_{fs} = 36.3(n_e + n_{ft} - 1) + 4.366\sqrt{n_{ft}}V_{ft}^{0.333} \tag{A.4}$$

Thrust reverses weigh approximately 18% of the total dry engine weight ($n_e \cdot W_e$). Starting systems, accessory drives, controls, starting and ignition systems are related to the time-derivative of the fuel weight during takeoff as described in Equation A.5. takeoff fuel flow for the Trent XWB-84 and -97 engine can be found in the ICAO Aircraft Engine Emissions Databank, which is 2.819 kg/s and 3.498 kg/s respectively [57]. For the Flying-V, this is described in more detail in Section 4.1.1.

$$W_p = 36 n_e \left(\frac{dW_f}{dt}\right)_{TO} \tag{A.5}$$

Operational Items

The weight of the operational items follows from the crew provisions, passenger cabin supplies, potable water, safety equipment, oil and residual fuel and cargo handling equipment. Crew provisions and passenger supplies are described in Equation A.7 and Equation A.8 respectively. n_{fc} is the number of flight crew members and $n_{\text{attendants}}$ the number of attendants.

$$W_{\text{oper items}} = W_{\text{crewprov}} + W_{\text{paxsup}} + W_{\text{potwater}} + W_{\text{emergency}} \tag{A.6}$$

$$W_{\text{crewprov}} = 93 n_{\text{fc}} + 68 n_{\text{attendants}} \tag{A.7}$$

$$W_{\text{paxsup}} = 8.62 n_{\text{pax}} \tag{A.8}$$

For long-range aircraft, the weight of the pot water is 90.7 kg per lavatory. n_{lav} is the total number of lavatories.

$$W_{\text{potwater}} = 90.7 n_{\text{lav}} \tag{A.9}$$

The weight of life jackets, fire axes, emergency navigational equipment for extended over-water flights and other emergency provisions is described by Equation A.10.

$$W_{\text{emergency}} = 3.4 n_{\text{pax}} \tag{A.10}$$

Furnishing

Furnishing weight can be broken down into flight deck accommodations, passenger cabin accommodations, cargo accommodations and emergency equipment. A weight reduction factor of 0.72 is used to include weight savings on modern aircraft components with respect to the time the relations of Torenbeek were established, as explained in Section 4.3.5. This factor is only included on seats and soundproofing that are components that are assumed to have reduced in weight most due to the application of modern materials in aircraft. This assumption is validated in Chapter 5.

$$W_{\text{furniture}} = 0.72 \cdot (W_{\text{fd}} + W_{\text{seats}} + W_{\text{galley}} + W_{\text{sp}}) + W_{\text{lav}} + W_{\text{floor}} + W_{\text{prov}} + W_{\text{ox}} + W_{\text{fireprov}} + W_{\text{escape}} \tag{A.11}$$

Flight deck accommodations including flight crew seats, instrument panels, control stands, soundproofing, floor covering, lighting and wiring, misc equipment. The weight of the flight deck W_{fd}, seats W_{seats}, galley structure and provisions W_{galley}, lavatory and toilet provisions W_{lav} and floor covering W_{floor} are found using the following relations. S_{cf} is the total floor area of the cabin.

$$W_{\text{fd}} = 16.5 W_{\text{DE}}^{0.285} \tag{A.12}$$

For the seats, a triple seat configuration is assumed, in which all weights are provided by Torenbeek.

$$W_{\text{seats}} = \frac{29.9}{3} n_{\text{pax}_{\text{ec}}} + \frac{35.4}{3} n_{\text{pax}_{\text{bc}}} + 8.2 n_{\text{attendants}} \tag{A.13}$$

The weight of small carts is assumed to be the average of the weight of snack pantries and coffee bars described by Torenbeek.

$$W_{\text{galley}} = 113.4 n_{\text{large carts}} + \frac{45.3 + 29.5}{2} n_{\text{small carts}} \tag{A.14}$$

$$W_{\text{lav}} = 136.0 n_{\text{toilet}} \tag{A.15}$$

$$W_{\text{floor}} = 1.25 S_{\text{cf}}^{1.15} \tag{A.16}$$

The weight of soundproofing, wall covering, screens, window shades, etc. is described in Equation A.17. V_{ch} is the total volume of the cargo hold.

$$W_{\text{sp}} = 6.17 (V_{\text{pax}} + V_{\text{ch}})^{1.07} \tag{A.17}$$

The weight of cargo restraints and handling provisions is described by Equation A.18. Container or pallet cargo handling provisions for convertible passenger/cargo versions are neglected, focusing on the design of a standard passenger aircraft.

$$W_{\text{prov}} = 1.28 V_{\text{ch}} \tag{A.18}$$

The weight of the oxygen system for long-range aircraft is estimated using Equation A.19. n_{pax} is the maximum number of passengers for certification, which could probably be higher than the design number of passengers.

$$W_{\text{ox}} = 18.1 + 1.09 n_{\text{pax}} \tag{A.19}$$

$$W_{\text{fireprov}} = 0.0012 W_{\text{TO}} \tag{A.20}$$

The weight of escape provisions such as evacuation slides and ropes is directly related to the number of passengers.

$$W_{\text{escape}} = 0.453 n_{\text{pax}} \tag{A.21}$$

Systems and Instruments

Provisions in the cabin, such as the air conditioning, are calculated for the complete fuselage by adding parameters such as the length and number of passengers of both fuselages. For the oval fuselage weight estimation methods, these total weights are then divided by two to find the loads per fuselage half.

$$W_{\text{systems}} = W_{\text{api}} + W_{\text{fc}} + W_{\text{el}} + W_{\text{iae}} + W_{\text{APU}} \tag{A.22}$$

The weight of the air conditioning, pressurisation and de-icing systems is estimated using Equation A.23 for pressurised aircraft. Note that l_{pax} is the length of the passenger cabin.

$$W_{\text{api}} = 14.0 (l_{\text{pax}})^{1.28} \tag{A.23}$$

Flight control system including hydraulic and pneumatic systems driving the flight control system. k_{sc} is 0.64 for transport aircraft for powered controls and trailing-edge high-lift devices only. When leading edge flap controls are used, 20% weight should be added. Lift dumper controls introduce another 15% weight.

$$W_{\text{fc}} = 0.64 (0.768 W_{\text{TO}})^{2/3} \tag{A.24}$$

Electrical system weight for an AC system is estimated using Equation A.25, in which V_{pax} is the passenger cabin volume.

$$W_{\text{el}} = 59.332 (V_{\text{pax}})^{0.7} \left[1 - 0.0630 (V_{\text{pax}})^{0.35}\right] \tag{A.25}$$

Instruments weight is estimated using Equation A.26 for jet transport aircraft, in which W_{DE} is the delivery empty weight of the aircraft and R_{D} the design range.

$$W_{\text{iae}} = 0.347 (W_{\text{DE}})^{5/9} (R_{\text{D}})^{1/4} \tag{A.26}$$

The A350 has two independent hydraulic systems [1]. For powered controls and a fully duplicated system, the weight of the hydraulic and pneumatic power system is given in Equation A.27.

$$W_{\text{hyd}} = 0.011 W_{\text{DE}} + 181 \tag{A.27}$$

The weight of the APU of the A380-800 is used by Vos et al., with a total weight of $2.25 \cdot 417$ kg [80]. The A350 aircraft family uses the Honeywell HGT1700 for all family members, which according to Scholz has a dry weight of 335 kg [103]. Comparing this weight to the APU weight of the A380, it is deemed reasonable and is hence used in this research.

$$W_{\text{APU}} = 0.008 W_{\text{TO}} \tag{A.28}$$

[1] http://www.smartcockpit.com/docs/a350-900-flight-deck-and-systems-briefing-for-pilots.pdf [cited on 6-9-2020]

B

Flying-V Family Floor Plans

This appendix shows floor plans of all Flying-V family members.

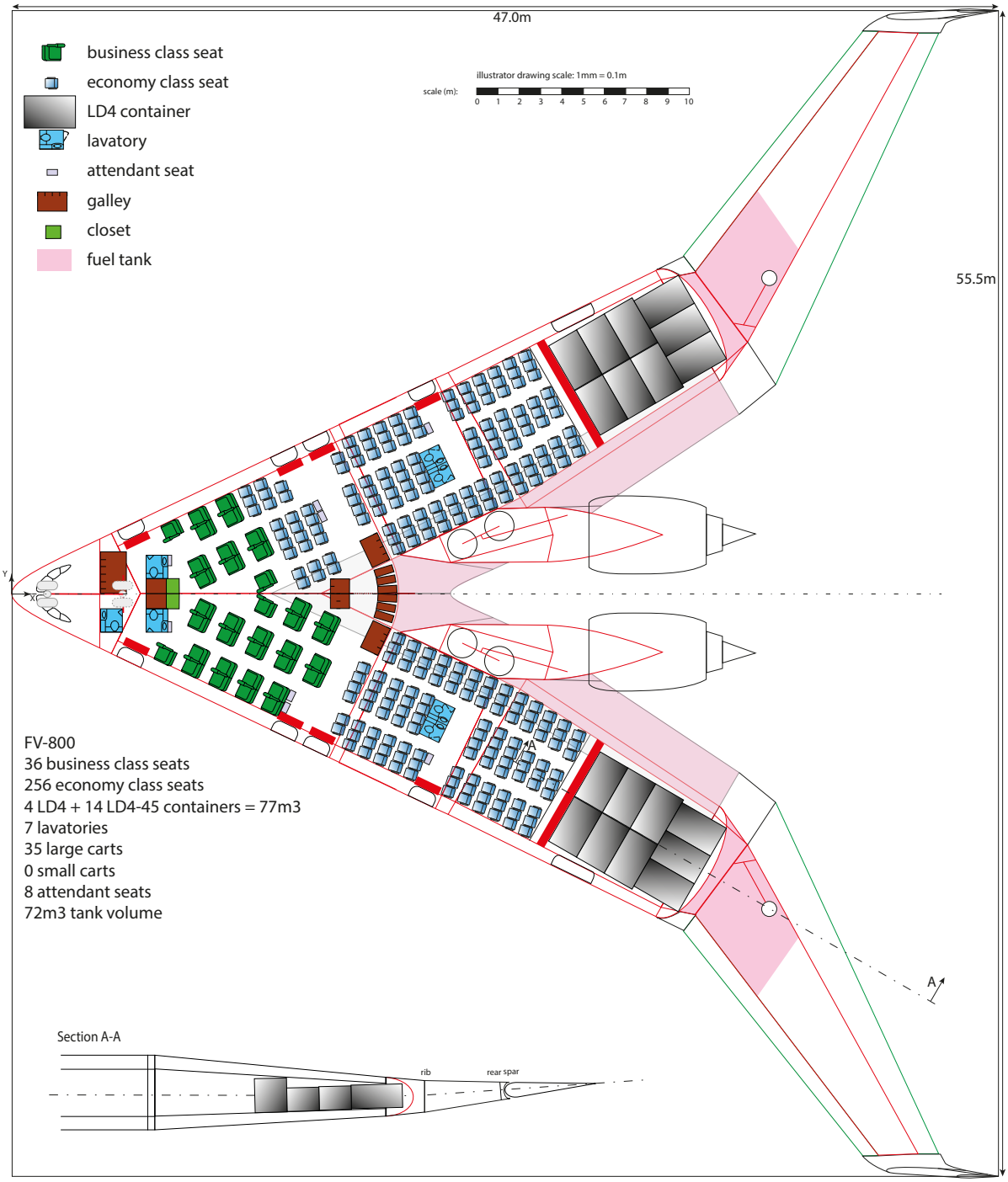

Figure B.1: Floor plan of the FV-800 aircraft. Modified from R. Vos.

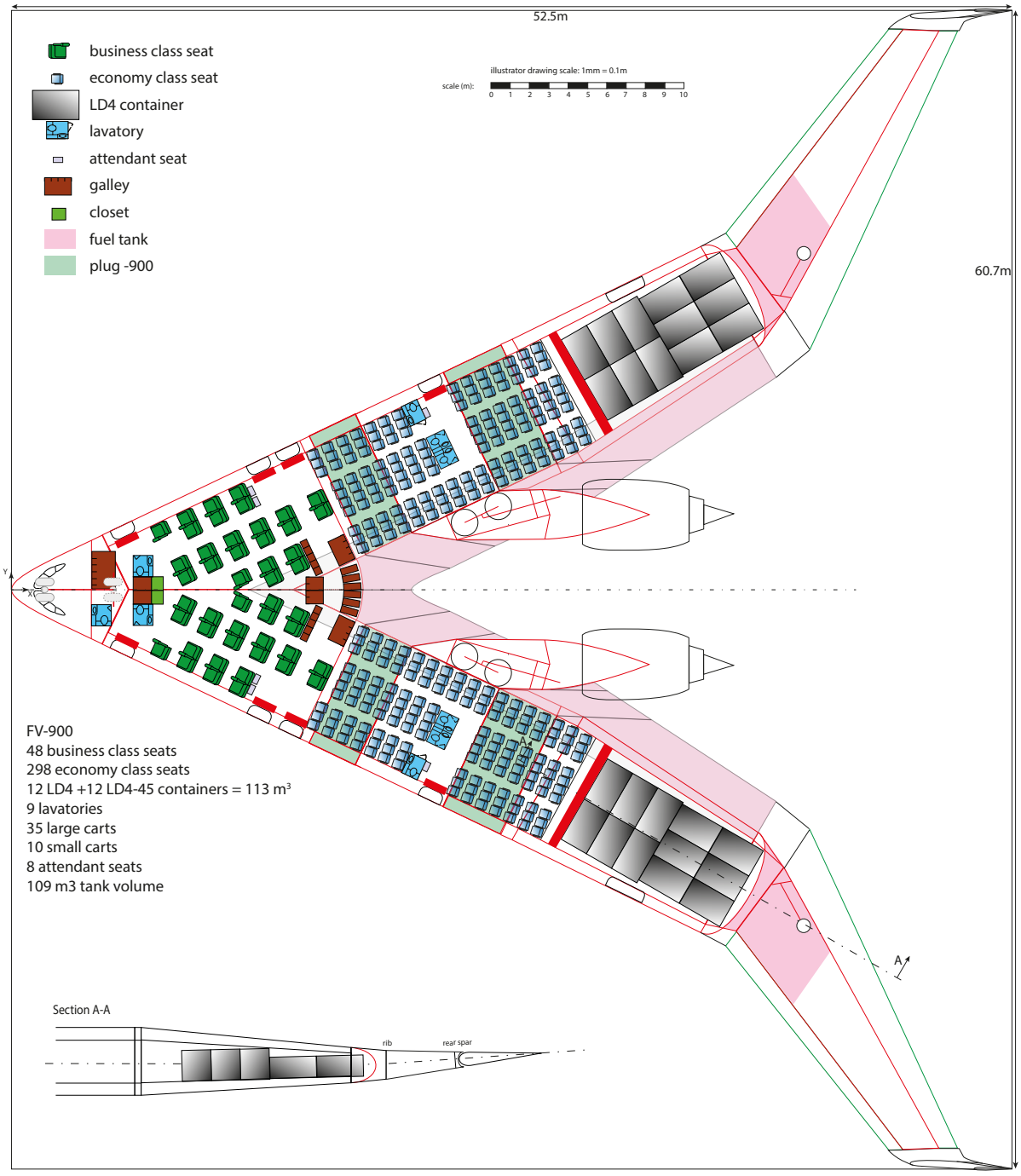

Figure B.2: Floor plan of the FV-900 aircraft, visualising the plugs to form a FV-800 variant. Modified from R. Vos.

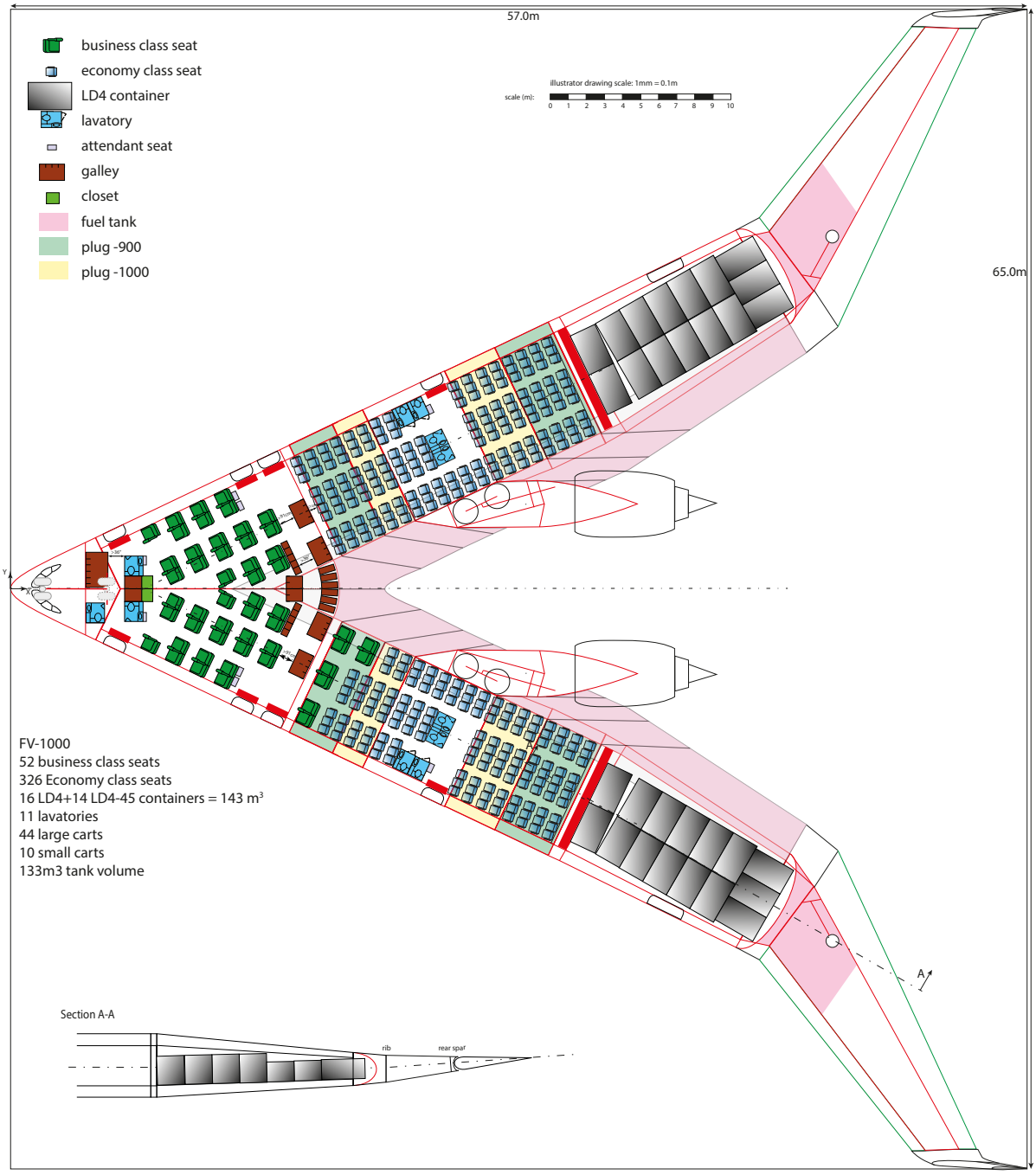

Figure B.3: Floor plan of the FV-1000 aircraft, visualising the plugs to form a FV-800 or FV-900 variant. Modified from R. Vos.

C

Flying-V Family Weight, Thickness and Loads Distribution

In this appendix, the weight distribution of structural members of the oval fuselage of the Flying-V family members is visualised. In addition, the thickness distribution of these structural members is depicted. Finally, loads acting on the fuselage beam are shown.

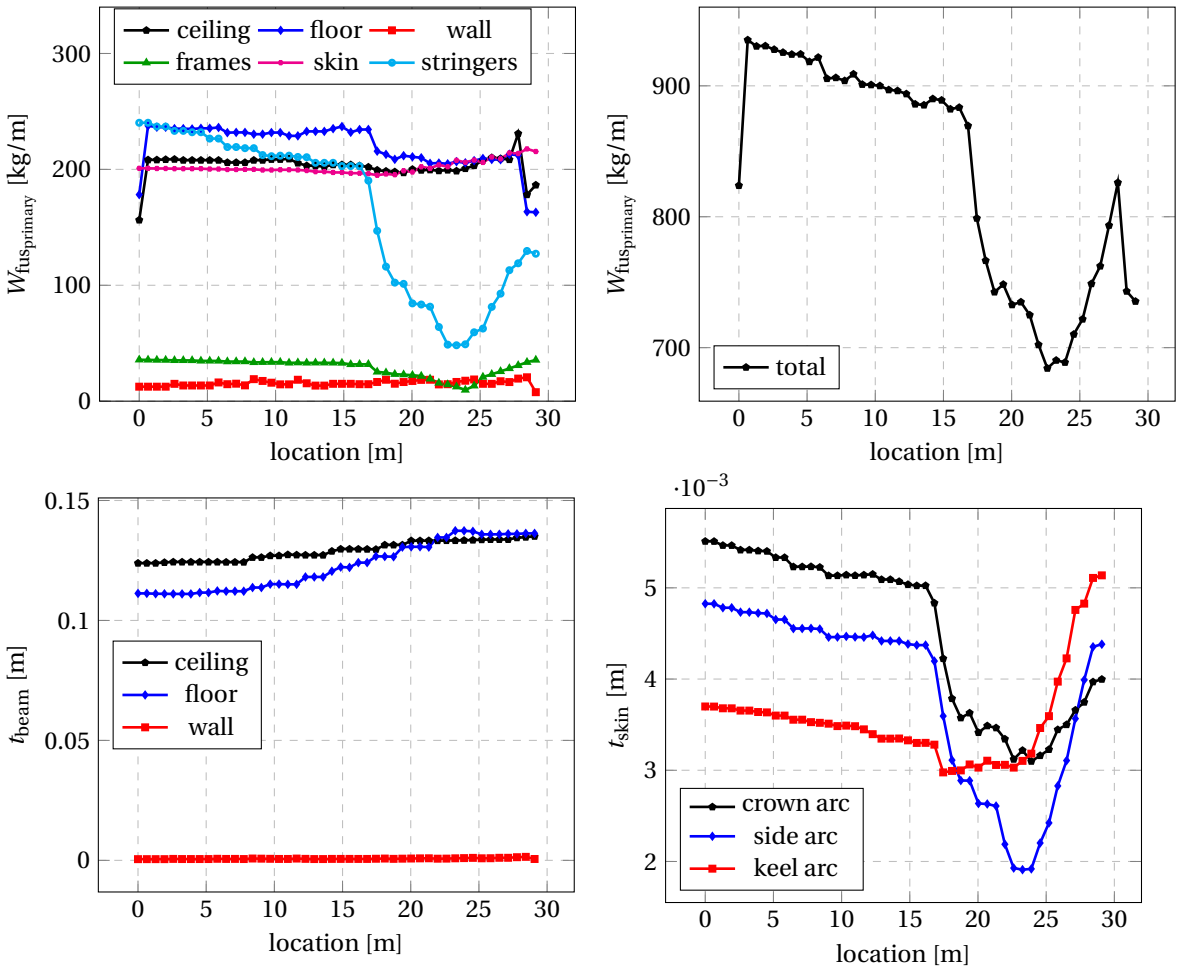

Figure C.1: Mass and thickness distribution along the fuselage length for the FV-800, results for 46 sections. Mass is provided in kg/m by dividing the weight at each longitudinal section by the longitudinal section width.

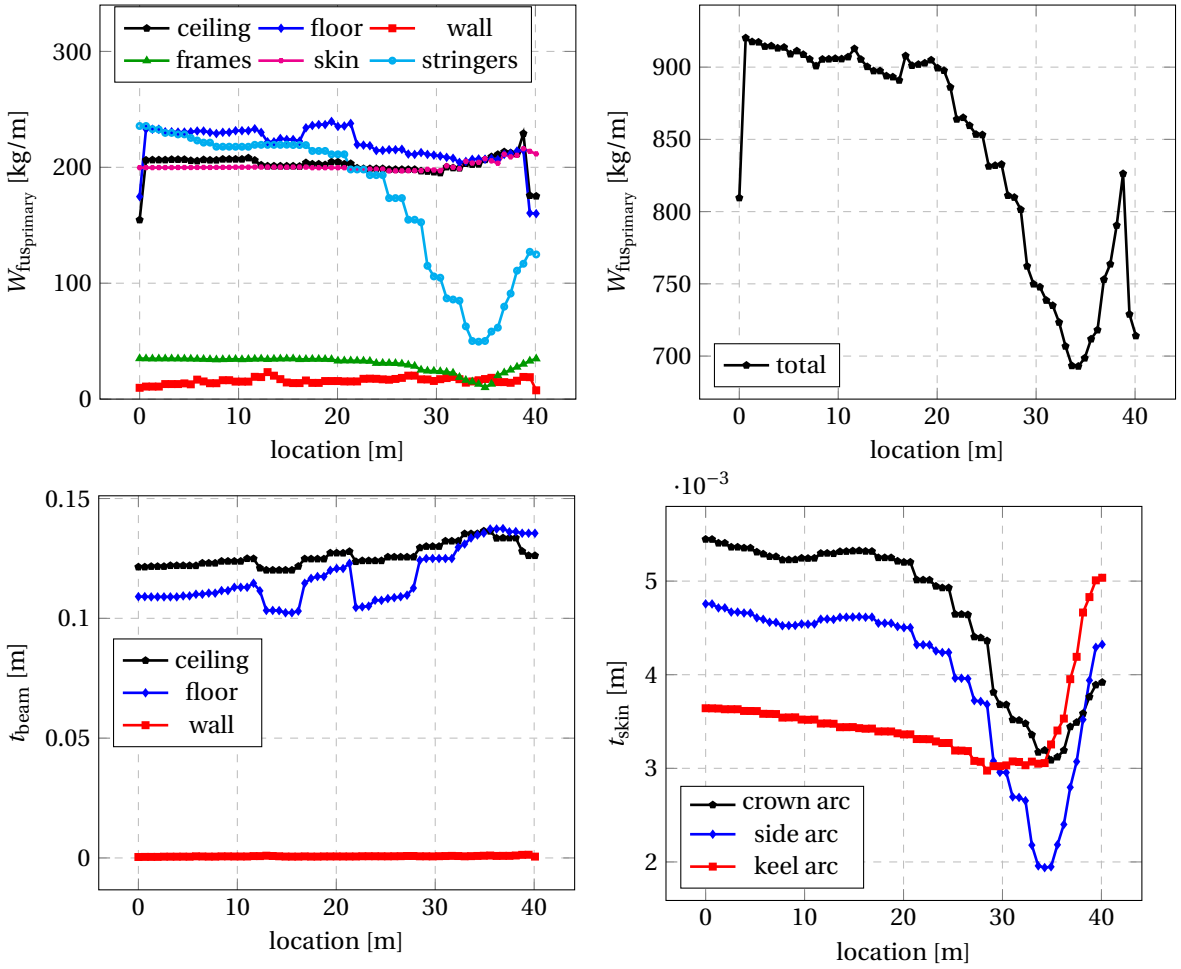

Figure C.2: Mass and thickness distribution along the fuselage length for the FV-1000, results for 63 sections. Mass is provided in kg/m by dividing the weight at each longitudinal section by the longitudinal section width.

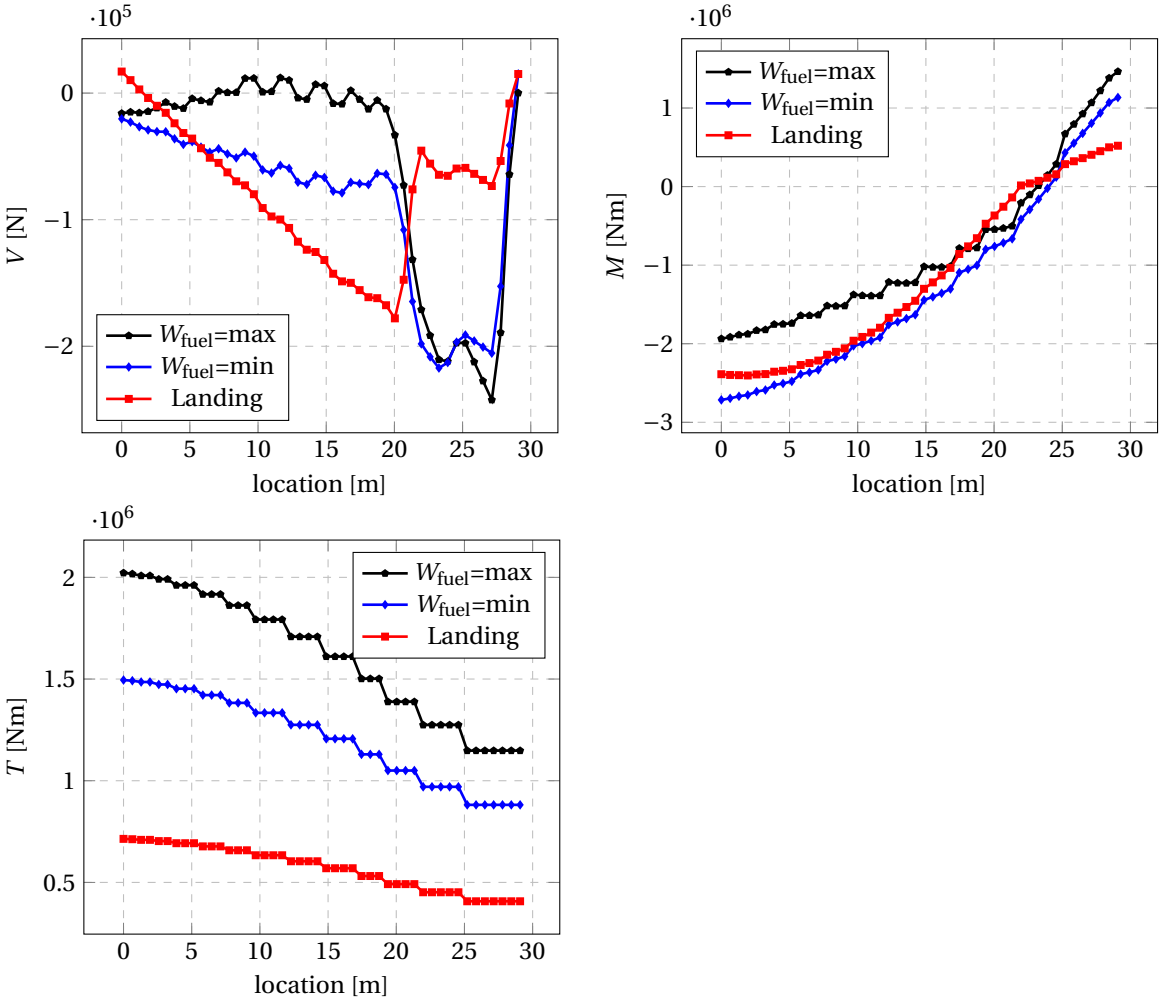

Figure C.3: Shear force, bending moment and torsion along the fuselage beam for the FV-800.

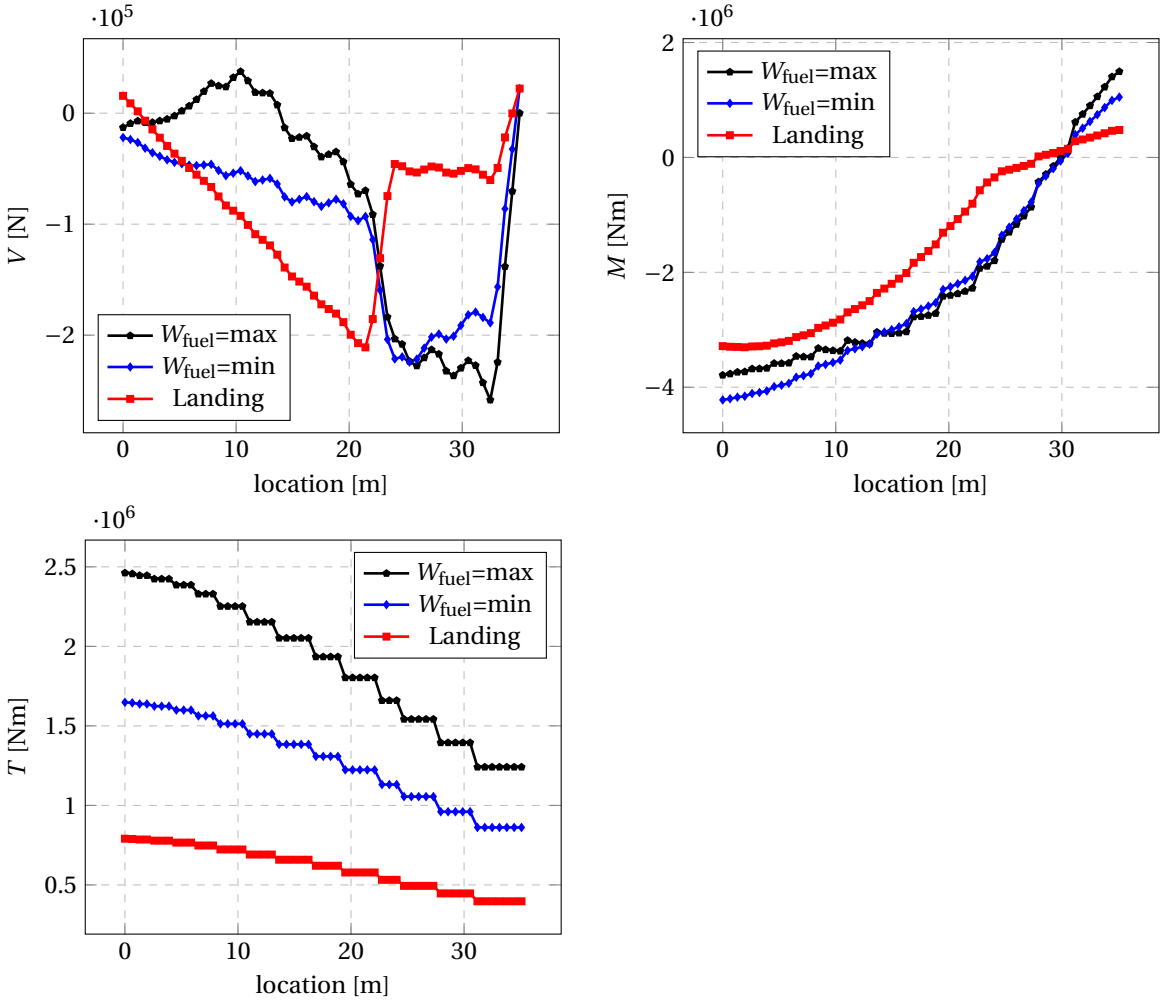

Figure C.4: Shear force, bending moment and torsion along the fuselage beam for the FV-900.

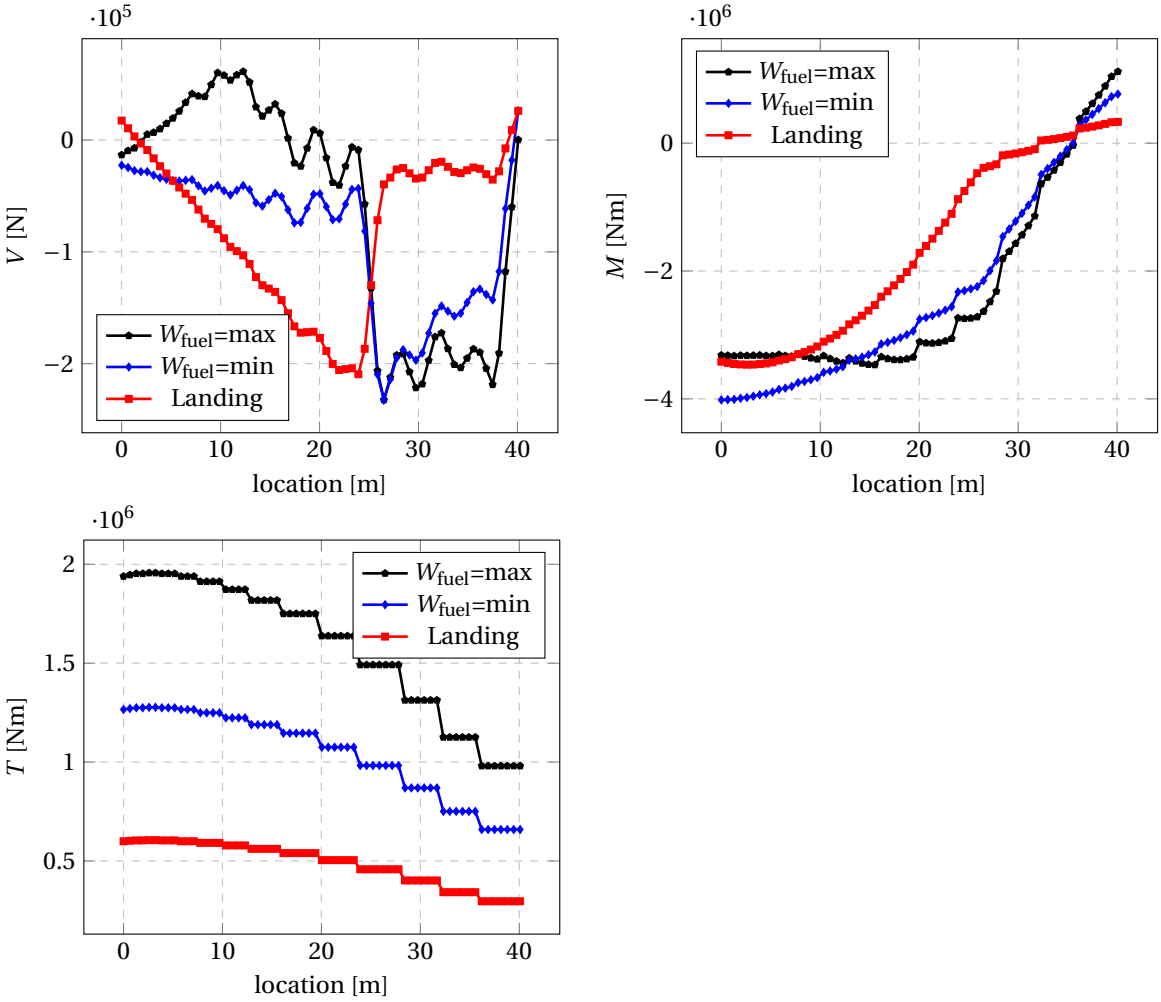

Figure C.5: Shear force, bending moment and torsion along the fuselage beam for the FV-1000.